Multi-scale modeling of fixed-bed drying of woody fuel particles

Mehran Jalili

Technische Universität Berlin
Fakultät III: Prozesswissenschaften
Institut für Energietechnik
Fachgebiet Energieverfahrenstechnik und Umwandlungstechniken regenerativer Energien

Dissertation

Multi-scale modeling of fixed-bed drying of woody fuel particles

vorgelegt von
M.Sc.
Mehran Jalili
aus Amol, Iran

von der Fakultät III - Prozesswissenschaften
der Technischen Universität Berlin
zur Erlangung des akademischen Grades

Doktor der Ingenieurwissenschaften
– Dr.-Ing. –

genehmigte Dissertation

Promotionsausschuss:

Vorsitzender: Prof. Dr.-Ing. George Tsatsaronis
Berichter: Prof. Dr. rer. nat. Frank Behrendt
Berichter: Prof. Dr.-Ing. Andreas Bück

Tag der wissenschaftlichen Aussprache: 31. March 2015

Berlin 2015
D 83

Acknowledgement

I would like to thank all those who gave me the possibility to carry out this thesis. I especially thank...

... Prof. Dr. rer. nat. Frank Behrendt, the supervisor of this work, for giving me the possibility of joining the EVUR institute to make my PhD, for the chance of scientific freedom that I had,

... Dr.-Ing. Nico Zobel, the mentor of this work and leader of the research group, for the numerous and very enlightening discussions and for being always encouraging and supportive,

... Dr.-Ing. Andrés Anca-Couce, my former colleague, for his generosity in helping the progress of my work and for his informative discussions,

... Dipl.-Ing. Alba Dieguez Alonso, whom I experienced a great group with the presence of her, Andrés and Nico, for all what I have learned from them,

... Maximilian Mehnert, for his excellent job in administrating the computer cluster of our institute, for being always available and supportive,

... Dr.-Ing. Hamid Reza Godini, my friend and a great researcher in TU Berlin, for his very useful advices during writing of this thesis,

... Dr.-Ing. York Neubauer, Dr.-Ing. Asem Hassan Mohammed, Dipl.-Ing. Omid-Henrik Elhami, Dipl.-Ing. Till Belusa, Carsten Waechtler, colleagues and former colleagues at the EVUR institute with whom I shared my stay, for helping me many times,

... My wife, Elham, and my family in Amol-Iran, especially my parents and my sisters, for their support,

Dedicated to ...

... Elham, my wife. Thank you for your love!

... Sanambar, my mother. Thank you for all you've done for me and Elham!

... Kheironesa, my mother-in-law. Thank you for all you've done for Elham and me!

Abstract

Drying is an unavoidable process before and during energy harvesting from solid fuels such as woody fuel particles which are naturally wet. Hygroscopic, anisotropic and heterogeneous nature of the wood causes the complexities in describing and predicting its drying behavior. In addition there are different time and length scales in the drying of a pile of fuel particles that must be taken into account for accurate simulation of such a complex process.

Averaging or neglecting the effect of phenomena occurring at different scales may lead to remarkable errors in predicting the drying dynamics of these materials. In this work a multi-scale approach, representative particle model (RPM), is developed to describe fixed-bed drying of hygroscopic porous particles such as wood fuel particles, at particle as well as reactor scales. A heterogeneous quasi-continuous model (HQCM) is also developed for comparing with the RPM and highlighting the benefits of this multi-scale model. At the particle scale, a comprehensive drying model is developed for coupling to the reactor scale through the RPM. This particle model captures intra-particle profiles of independent variables spatially and temporally. The intra-particle solution of the RPM and also the solution of solid phase in the HQCM are coupled to the solution of interstitial gas phase at reactor scale via two-way coupling. Heat and mass transfer in the interstitial gas phase are solved by a fractional-step algorithm. A code using parallel computing (MPI approach) is employed for solving the phenomena at reactor scale for both the RPM and the HQCM. Several cases of fixed-bed drying of wood and lignite particles under different circumstances are simulated by these models.

Using the iterative solution method for particle model and also the parallel computing at the reactor scale, the computational time of the multi-scale model reduces. It is shown that the RPM is able to describe the fixed-bed drying of hygroscopic porous particles properly; reasonably accurate and computationally efficient.

Contents

List of Figures

List of Tables

Chapter 1

Introduction

1.1 Wood fuel

During the centuries, the human kind learned how to employ different sources of energy existent in the nature. At the beginning he explored using the energy of the sun and wind, later the energy of biomass in the form of primary energies. In fact renewable energy sources (RES) were the first sort of energy which have been used by the human kind. Urbanization and industrialization increased the demand of energy so that the primary sources of renewable energies were not enough any more. On the other hand, development of knowledge and technology provided the opportunity to employ other sources of energies such as fossil fuels and nuclear energy as well as the secondary sources of renewable energy. These new forms of non-renewable energies had higher heating value and better energy efficiency so that could speed up the industrialization process. However, the consumption of non-renewable energies made two serious problems during recent decades. Firstly, the limited resources of these kinds of energies, particularly fossil fuels, decreased quickly with huge demand of big populations over the world which caused serious concern about energy supply for future. Secondly, the emissions resulting from these kinds of energy such as greenhouse gas emissions and radiations have threaded the climate, ecology and human life. These reasons made unsustainable the energy balance over the world. This forced the countries to adopt new policies in the field of production as well as consumption of non-renewable energy sources (Non-RES). In Tab. 1.1 the consumption of EU's members during one decade, from 2001 to 2011, is shown.

From 2001 to 2011, the gross inland consumption in the EU-28 fell by 4%. The consumption of renewable energy sources grew by 69% while the consumption of all other non-renewable energies including oil, gas, nuclear, coal and lignite energies declined by 8% ([1]). European energy agency (EEA) reported that the greenhouse

Table 1.1: *Gross inland consumption, by fuel, EU-28 (Mtoe), data from European Union ([1])*

	2001	2003	2005	2007	2009	2011	Change (%)
Total	1772	1808	1834	1818	1711	1706	-4
Non-RES	1671	1703	1717	1683	1557	1536	-8
RES	101	105	117	135	154	170	69

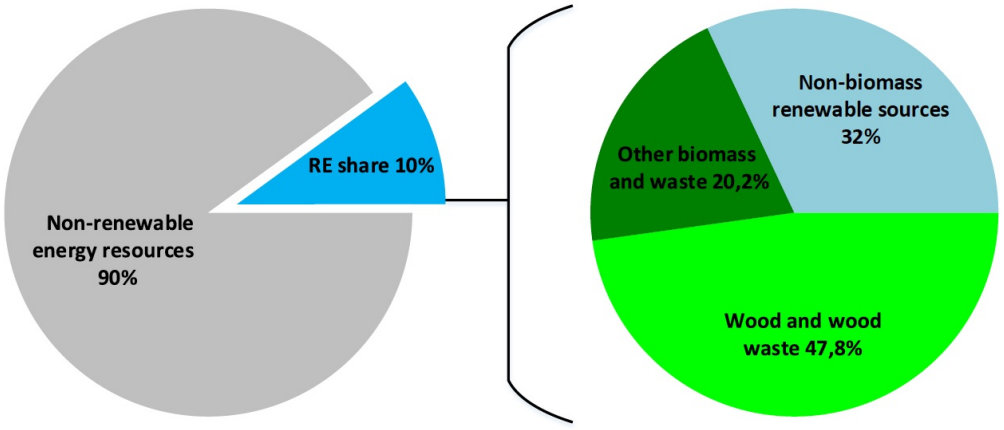

Figure 1.1: *Share of renewable energy consumption, EU-28, 2011, data from Eurostat ([2])*

gas emissions (in the EU-27) have fallen 8.11% during the years between 2001 and 2011; a net reduction of 406 million tons of CO2 equivalents. The reduction of non-renewable energy sources during that decade can be one of the important reasons for the reduction of greenhouse gas emissions. Energy from biomass is the major source of renewable energy that provides heat, electricity and transport fuels. As seen in Fig. 1.1, wood fuel including wood and wood waste had the highest share of the EU-28's gross inland consumption of renewable energy sources in 2011. The share of wood fuel is 47.8% versus to 32% the share of non-biomass renewable sources including hydropower, wind power, geothermal energy and solar energy. Wood resources used in EU-27 in 2010 shows that 42% of woody biomass (% share of total volume in m^3) was consumed for energy applications [2]. Woody biomass can be converted to the secondary energy carriers via direct combustion, biochemical conversion and thermochemical conversion.

1.2 Moisture in wood fuel

In spite of the vitality of water for plants and trees, when these biomass resources are used as solid biofuels the water existence would make some troubles from econom-

ical, environmental and technical point of views. Rather high latent heat of water makes the drying of solid biofuel particles to be intensive energy-consuming. Moisture in the solid biofuel particles causes reduction of their effective heating value as well as energy density while it increases weight of wood particles that leads to higher transportation cost. Moisture during thermochemical conversion of wet solid biofuel particles can decrease the process efficiency that may lead to higher emissions. Wood has rather low thermal conductivity and permeability. These properties along with the heterogeneous nature of wood structure make it resistant against heat and mass transfer. Resistance against heat and mass transfer may be an advantage for using wood as an insulation material in building and construction industry but for using wood as a fuel this is a limitation. During thermochemical conversion of woody biomass to biofuel, heat and mass transport play an important role in controlling of the whole process. Drying is an unavoidable process before or during thermochemical conversion of woody biomass. With respect to these all, drying is a very important stage in the processes involving energetic utilization of biomass materials. An accurate description of the drying process is required for optimal design of dryers and reactors for pyrolysis, gasification or incineration. Therefore models properly describing the drying of wood particles are of high interest for industry and research.

1.3 Problem description

When a coarse and thermally thick wet wood particle is subjected to the heat, because of above mentioned properties of wood, significant gradients of temperature, moisture and pressure appear inside the particle; as shown in Fig. 1.2. These gradients can be driving forces for heat and mass transport phenomena occurring in the particle. By interaction between these transport and phase change phenomena, the drying rate of the particle is determined. There are several mechanisms involved in heat and mass transfer in the wood particle during drying process such as convection, diffusion and conduction. The relative importance of these mechanisms determines the drying dynamics of the wood particle. The contribution of each mechanism can be different under different heating and boundary conditions. Nowadays, there are some comprehensive mathematical models that can describe important phenomena occurring during drying of a single wood particle properly. These models can present temporal temperature, moisture and pressure profiles inside the particle during drying process.

Complex phenomena occurring in the universe are mostly non-linear and non-equilibrium consisting of high degree of heterogeneity in both time and space.

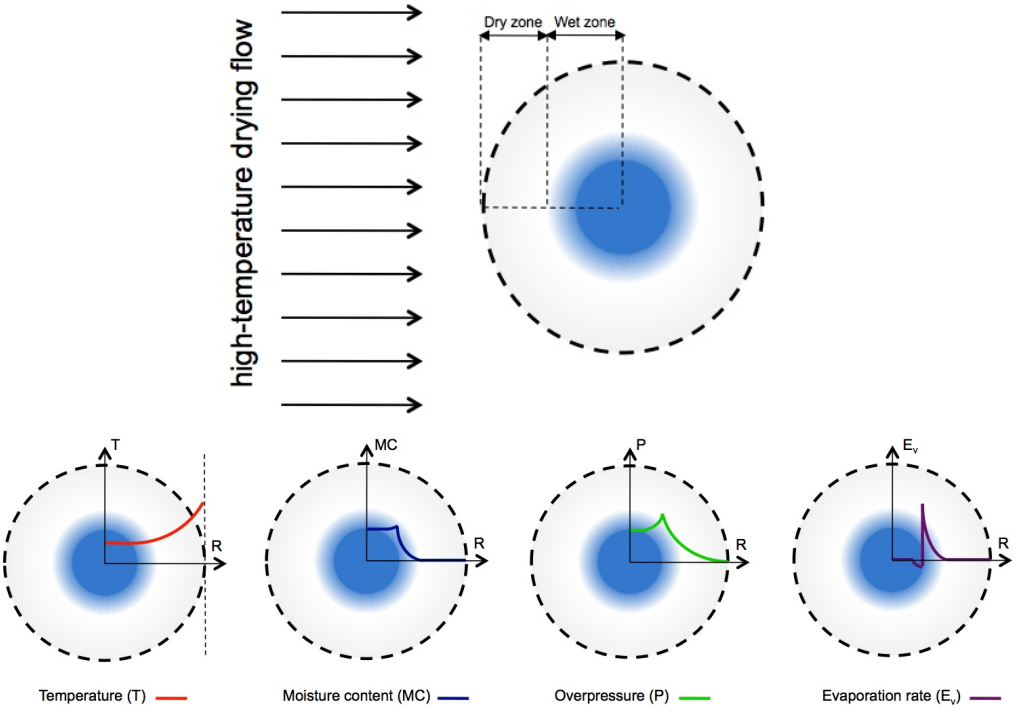

Figure 1.2: *Typical profiles of different variables inside a wet wood particle subjected to high-temperature drying flow; temperature, moisture content, pressure and evaporation rate*

For limited cases under particular conditions, it is reasonable to ignore such complexities in the phenomena and simplify them by linear, reductionism and averaging methods. Although justified assumptions and appropriate methods for simplification are necessary. In chemical engineering almost all challenging problems are categorized as the complex problems with above mentioned characterization. Fig. 1.3 shows the multi-scale nature of different levels of chemical processes [3]. For modeling this kind of problems, an understanding of different phenomena occurring at different scales is needed. Multi-scale methods can be used to correlate different scales involved in the problem [4]. In multi-scale modeling, more than one scale is involved in the modeling so that the coarser scale contains the finer scale [5].

Drying of a pile of heterogeneous porous materials like wood is one of the most complex problems in engineering field that has also a multi-scale nature. Modeling and numerical simulation of drying of a bed of wood particles is much more complicated than modeling and simulation of single wood particle drying. It is more time-consuming with higher computational cost. Knowledge about multi-phase flow in porous media with phase change phenomena is needed for modeling of drying of a pile of wood particles. Also the interaction between particles as well as liquid and gas flows in a dual-porous media must be taken into account in modeling of drying of a pile of wood particles. Moreover, the information about the structure

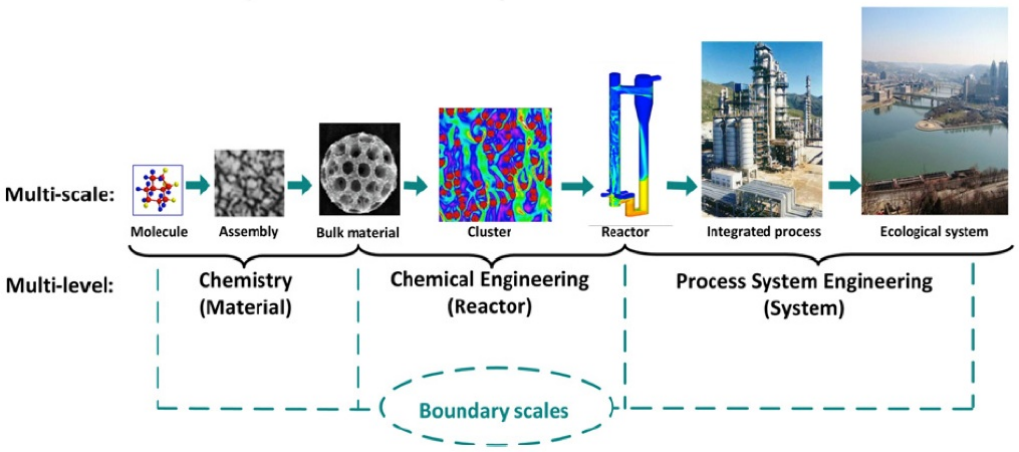

Figure 1.3: *Hierarchical multi-levels and multi-scales of phenomena in chemical processes, modified from Ge et al. ([3])*

and properties of wood particles as well as about the phenomena occurring at pore scale is needed to provide better interpretations of wood behaviors during drying. Because of these complexities the modeling of drying process of wet solid biofuel particles in a reactor is still challenging. One of the major difficulties related to the thermochemical gasification of wood in industrial practice, which is usually done in fixed-bed reactor, is the fact that the drying of the wood particles are modeled very poorly [6]. This causes inaccuracy in designing of gasifiers and low efficiency of whole process. Moisture in wood particles affects the thermochemical conversion of these particles significantly. If the size of wood particles is in cm scale or more then resulted gradients of temperature, moisture and pressure inside the particles would be remarkable and these gradients play an important role in controlling of the thermochemical conversion of these particles. A multi-scale model is required to capture these intra-particle gradients to correctly describe the processes in a fixed-bed reactor. As seen in Fig. 1.4, three scales can be considered in fixed-bed drying of thermally thick wood fuel particles; from pore scale to particle and reactor scales.

On the one hand, considering the important phenomena at different scales can lead to higher accuracy in description as well as prediction of the fixed-bed drying of solid porous particles. On the other hand, solving the equations for each particle in a reactor with enormous number of particles (between 10^5 to 10^6 particles in conventional gasifiers) is extremely time-consuming.

1.4 Objectives of the thesis

In this study, the improvement of numerical simulation of fixed-bed drying of thermally thick porous particles like wood is intended; by improving mathematical model

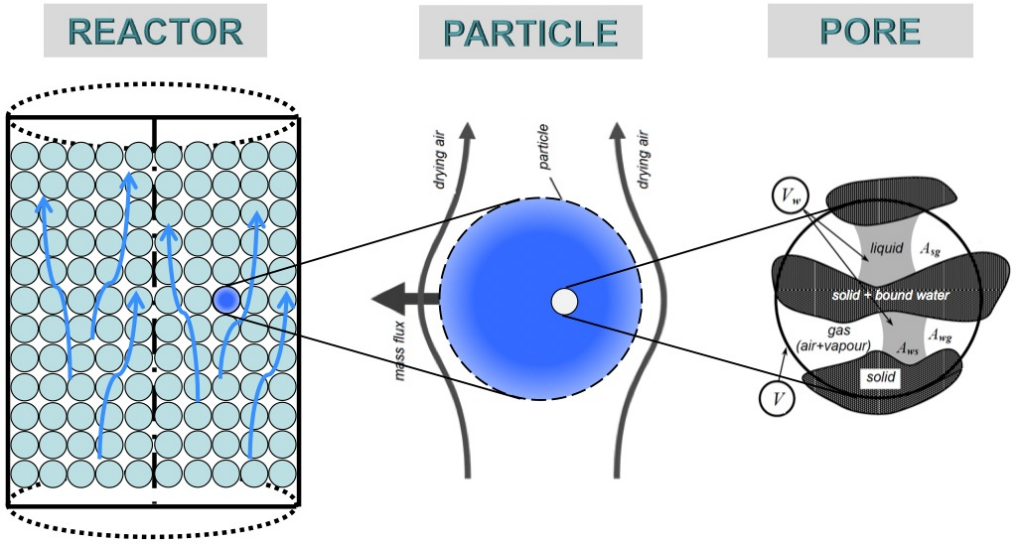

Figure 1.4: *Multi-scale nature of fixed-bed drying of solid fuel particles, partially adopted from Vu ([13])*

as well as optimization in numerical procedure. A multi-scale model titled Representative Particle Model (RPM) is implemented with the aim of achieving higher accuracy with an affordable computational cost. The optimization of the numerical solutions is performed through using an efficient iterative solution method for solving the particle model as well as employing parallelized computational code for solving the equations at the reactor scale. In addition, a heterogeneous quasi-continuous model (HQCM) is developed for fixed-bed drying to highlight the accuracy obtained by the multi-scale model. 1D+1D model, 1D in particle scale and 1D in reactor scale, is considered for the RPM and 1D model for the HQCM. Aiming at achieving reasonably accurate and computationally efficient simulation of fixed-bed drying of hygroscopic porous particles such as woody fuel particles, the objectives of the thesis include:

- Implementation of a comprehensive drying model for a hygroscopic porous particle, which is able to capture the transport phenomena and presents the intra-particle profiles spatially and temporally,
- Introducing an appropriate solution method for efficiently solving the particle model under the conditions coupling to the reactor model,
- Coupling the comprehensive particle model to the reactor scale via a multi-scale model (the RPM), to capture important phenomena during fixed-bed drying at particle as well as reactor scale,

- Implementation of a continuum model (the HQCM) for fixed-bed drying to highlight the difference between two the multi-scale and the continuum models qualitatively and quantitatively.
- Employing a parallelized computational code for solving the governing equations at reactor scale to reduce the computational time,

1.5 Structure of the thesis

The thesis is structured in 6 chapters. In chapter 1 after introduction, the problem and its multi-scale nature were explained. It was pointed out that for better description of the fixed-bed drying of woody fuel particles a multi-scale approach is needed.

Chapter 2 discusses the drying process at particle scale. At the first section, drying characterstics of a wood particle is described. Then a comprehensive mathematical model for drying of a hygroscopic porous particle is presented. The uncertainty of the coefficients of the drying model is highlighted by collecting different values of these coefficients reported in the literature.

The drying process in fixed-bed reactors are investigated in chapter 3. Initially, the phenomena involved in the fixed-bed drying are presented. Afterwards, mathematical models for the fixed-bed drying are discussed. Governing equations of heterogeneous quasi-continuous model (HQCM) as well as representative particle model (RPM) are presented in this chapter. Then, two-way coupling between the solid phase and the gas phase in these two fixed-bed drying models are described.

Chapter 4 describes the numerical methods for solving governing equations of the drying models at particle and reactor scales. Two different solution methods are introduced for solving the equations of the particle model including LIMEX solver and an iterative method. The limitation of LIMEX solver for solving the equations of the particle model under the conditions in a fixed-bed reactor is mentioned. The algorithm of the iterative solution method is presented and its adventages in coupling to the reactor solution is highlighted. Numerical procedure for fixed-bed drying models are discussed at the last part of this chapter.

The simulation results of drying of hygroscopic porous particles such as wood and lignite fuel particles are presented in chapter 5. In the first section of this chapter, at particle scale, after verification of computational performance of the particle model, the effect of variation of the model parameters on a wood drying

model is quantified, by sensitivity analysis. Then experimental data and simulation results from the literature for drying of single- wood and lignite particle are considered as case studies. Average mass loss and also intra-particle profiles of the particle is shown during the drying process by comparing with the data from the literature. In the second section of this chapter, experimental data and simulation results of the DPM from the literature for the fixed-bed drying of wood and lignite particles are considered as case studies at reactor scale. The simulation results of the HQCM and the RPM are compared with the data from the literature under different conditions of drying. Share of parallel computing in reduction of total computational time for both fixed-bed drying models are presented in this section. In chapter 6 a summary of this work, its conclusions and future works are given.

Chapter 2

Drying model at particle scale

For multi-scale modeling of fixed-bed drying, the drying process at particle scale has to be understood well. In this chapter the drying behavior of a woody biomass particle is explained in Section 2.1. Then a comprehensive single particle model describing hygroscopic particle drying is presented in Section 2.2. Different correlations and values of physical properties of wood as well as transport coefficients of the presented model is discussed in Section 2.3. Finally the concluding remarks are explained in Section 2.4.

2.1 Drying characteristics of woody biomass feedstocks

The drying process is commonly defined as thermally removing moisture to yield a solid product [7]. Drying does not only include evaporation but as pointed out by [8]: "drying is amalgamation of material science and transport phenomena". Regarding desired quality of the final production, drying process can be performed via different drying technologies. The dryers are usually classified based on the mode of operation (batch or continuous), heat or energy input-type (convection, conduction, radiation, microwave or electromagnetic fields), pressure (vacuum or atmospheric) and drying medium (air, steam or flue gases) [8]. Drying is employed in different industries from pharma to food, construction and energy industries. Operating conditions of the dryers are determined regarding the properties desired for the dried production. In food industry, the appearance, taste and aroma of the final production are the most important criteria that the operating conditions of the dryers must meet while in construction industry the dimensions and thermo-mechanical properties of the dried production are more important than the other factors.

In the conversion of biomass to biofuel, none of above mentioned criteria are limiting factors for drying of biomass particles. In thermo-chemical conversion

of biomass to biofuel, drying process is not only involved in pre-treatment stage but it is an unavoidable process in thermo-chemical conversion of biomass particles that are naturally wet. As shown in Fig. 1.2, steep gradients of temperature, moisture and gas pressure appear inside a thermally thick biomass particle exposed to an intensive heating rate during high-temperature drying or thermochemical conversion of a biomass particle. Such steep gradients are resulting from the properties and the structure of these materials resisting against heat and mass transfer under severe heating conditions that play a key role in controlling the drying process. Exact interpretation of the behavior of these materials during drying is dependent on the analysis of all involved phenomena during the process. Drying of a coarse woody fuel particle under high-temperature drying or during thermo-chemical conversion process is one of the most complex engineering problems. Woody biomass has anisotropic, heterogeneous and porous structure and its drying related properties (those will be explained later) significantly change from one tree to another and even in one tree from top to bottom. First principles study is needed to explain the transport phenomena with phase change occurring during the drying process inside a thermally thick particle. Following a common interpretation of high-temperature convective drying of a hygroscopic porous particle such as a woody biomass particle is presented [9–12].

When a coarse wood particle with high moisture content so that its cell cavities filled by water, is exposed to a high-temperature air drying flow then, after a short heating up stage, evaporation of the water located on the particle surface is started. Temperature of the particle surface reaches to wet bulb temperature and it maintains constant under constant drying conditions as long as the water exists on the particle surface. By reduction of the moisture content at the particle surface, the water existing in the cell cavities is transferred from the interior region of the particle toward the particle surface by capillary forces. This stage is called the period of constant drying rate because, under constant drying conditions, the drying rate of the particle is constant. It is assumed that the particle drying in this period is similar to the evaporation from the surface of a pool or sea so that the drying process progresses like the drying of a water body. The evaporation takes place on the particle surface that means the drying front is located there (Fig. 2.1). The drying rate is externally controlled by surrounding drying air flow. Heat and mass transfer characterizations of the drying air flow control the drying rate of the particle at this period. The heat transfer from the drying air flow to the particle and the mass transfer of the water vapor from the particle to the surrounding determine the rate of particle drying. In addition to the evaporation rate, the internal mass

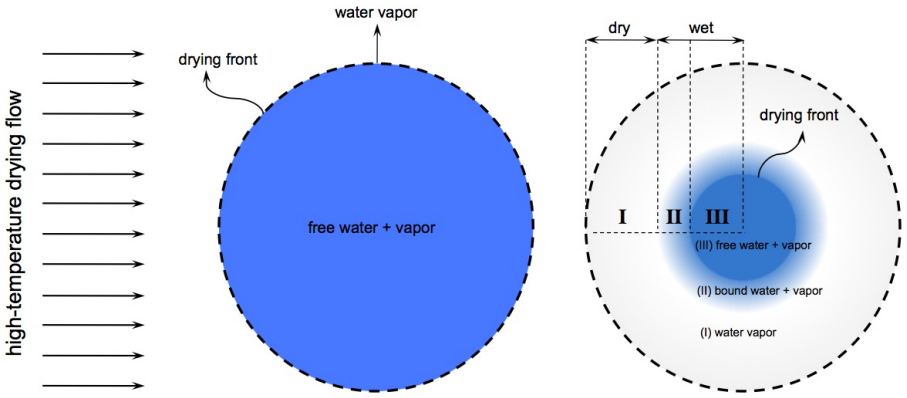

Figure 2.1: *Important phases involved in different stages of high-temperature drying of a wooden particle*

transfer that here is capillary motion of the free water determines the duration of this period.

By continuation of the drying process, the amount of water on the particle surface decreases and some dried patches appear on the particle surface. This point is the end of first period of drying and the start of second period that is called falling drying rate. The water is not sufficiently transferred from the interior region of the particle to the surface where the drying front is located. It can happen when no water remains in the cell cavities of the particle or in a case that the drying rate is higher than the rate of water flow to the particle surface. The dried patches expands so that they cover whole the surface particle and the drying front starts to advance toward to the interior region of the particle. Two regions form inside the particle: dry and wet (Fig. 2.1). The drying rate is not constant during second period of the drying process. At this period, the drying rate is not only dependent to the external flow specifications but also the interaction between internal heat and mass transfer inside the particle with phase change phenomena playing a key role in determination of the drying rate of the particle. It should be emphasized that the drying behavior of a wood particle presented in Fig. 1.2 and Fig. 2.1 are only representing a typical behavior of wood drying. Heating conditions and the properties of the wood particle can remarkably affect the drying stages as well as the property profiles inside the particle.

2.2 Mathematical models for wood drying

An appropriate drying model must be capable of providing reliable predictions for different operating conditions under which measurements are very complex and challenging with currently available techniques. Every drying model must be able to de-

scribe all relevant and effective physical and chemical phenomena occurring during the studied process.

The advances in the field of transport models for drying of porous media and also their restrictions and applications have been reviewed by Vu [13]. Fernandez & Howell [14] and Jianmin & Fangtian [15] surveyed and discussed various models dealing with the simulation of moisture migration during drying of wood. Perre [16] showed how to define a relevant model for wood drying simulations and explained the validity of the different models in different applications, including low- and high-temperature drying. The drying models established most recently can accurately describe all the physical and chemical phenomena taking place during wood drying, as stated by [17].

2.2.1 Principles of wood drying models

For a hygroscopic, anisotropic, heterogeneous and porous material such as a woody biomass fuel particle, the drying process is very complex. The wood drying process includes the multicomponent multi-phase flow in a heterogeneous porous medium with the phase change phenomena. From modeling point of view, the drying process can be categorized to transport phenomena, phase change and the parameters explaining these phenomena as well as the drying medium. For a comprehensive mathematical model of wood drying, following parameters as well as phenomena must be taken into account.

2.2.1.1 Main parameters

Temperature, mixture gas pressure and moisture content or saturation are commonly used as three independent variables in drying models. All other dynamic state variables and also the physical properties of the material (Section 2.3) are expressed based on these three independent variables. In the following, the parameters that must be considered in a mathematical drying model of a hygroscopic porous particle like wood are presented:

1. Porosity: Volume fraction of pore volumes (void space) in a porous material (medium) to the total volume of that material (medium) is the porosity. In drying model of a single woody biomass particle when there is no degradation neither shrinkage, the porosity is usually considered to be a constant value. The porosity is measured based on dry particle and it in fact represents the void space of the particle when the pores are empty of water.

2. Moisture content: Water can exist in a hygroscopic material such as wood in three forms of liquid or free water in cell cavities (the pores), hygroscopic or bound water in cell walls and water vapor in the pores. Two definitions are commonly used in the literature for the moisture content of a material; dry basis moisture content and wet basis moisture content. Mass fraction of the total mass of water to the total mass of wet particle is defined as wet basis moisture content. Dry basis moisture conetent is defined as the mass fraction of the total mass of water to the mass of dry solid particle. These two definitions by multiplying to 100, might be presented in percentage unit. Since the mass of water vapor is negligible in comparison to other forms of water therefore the total mass of water in above mentioned definitions is usually referred to the sum of the masses of free and bound water. In this thesis, the moisture content is considered based on dry basis.

3. Maximum hygroscopic range: In hygroscopic materials, free water moisture content and bound water moisture content are separated by the maximum hygroscopic range. For woody materials, this is referred as fiber saturation point (FSP). Upper the fiber saturation point, water exists as free water in the cell cavities and in the form of bound water in the cell walls. Under the fiber saturation point, water exists only as bound water in the cell walls of wood. The fiber saturation point of woody material is commonly considered between $0.28 - 0.3$.

4. Saturation: Volume fraction of the void space of a porous medium filled by free water is defined as the saturation. The saturation is calculated by dividing the moisture content of free water to the maximum value of the free water moisture content that the porous medium can possess. Some physical properties of wood are presented as a function of the saturation (Section 2.3).

$$S = \frac{liquid\ volume}{void\ volume} = \frac{M_{\text{fw}}}{M_{\text{fw-max}}} \tag{2.1}$$

$$M_{\text{fw-max}} = M_{\text{max}} - M_{\text{fsp}} \tag{2.2}$$

$$M_{\text{max}} = \langle \rho_l \rangle^l (\frac{1}{\langle \rho_{SD} \rangle} - \frac{1}{\langle \rho_s \rangle^s}) \tag{2.3}$$

5. Gas pressure: In the drying models, gas phase is commonly considered as a mixture of air and water vapor that it is assumed to obey ideal gas laws. The total gas pressure is the sum of partial pressure of air and water vapor. The gas pressure in some materials like wood that has rather low gas permeability can significantly affect the drying process. Convective transport of the gas phase in the cell cavities is done via pressure gradients.

6. Liquid pressure: Using the concept of capillary pressure, the liquid pressure in the cell cavities of a porous medium is related to the gas pressure. The capillary pressure depends on the shape of the gas-liquid menisci within the pores and it is expressed in the terms of surface tension, the size of the pore and the shape of the gas-liquid menisci. In order to predict the pressure driven transport of free water in the pores, it is important to measure the capillary pressure under different moisture contents and temperatures.

$$P_c = \langle P_g \rangle^g - \langle P_w \rangle^w \tag{2.4}$$

7. Relative humidity: The maximum value of the partial pressure of water vapor in a vapor-gas mixture that can be reached at a certain temperature is called saturated vapor pressure. The relative humidity is a measure of a vapor−gas mixture's fractional saturation with moisture. This parameter is defined as the ratio of the partial vapor pressure to the saturated vapor pressure at the same temperature.

8. Sorption isotherm: When a hygroscopic material is placed in an environment with constant humidity and temperature, due to the hygroscopicity, it takes up/release the moisture from/to the environment until it reaches to its equilibrium moisture content (EMC). The equilibrium moisture content is the value of moisture content at which a material gains moisture as much as it loses and the net moisture exchange is zero. The equilibrium moisture contents of a material for adsorption and desorption cases are not the same. The sorption isotherms are curves showing the relationship between equilibrium moisture content of a material and the relative humidity of the environment surrounded it at a constant temperature.

2.2.1.2 Transport phenomena

In well-accepted and more comprehensive drying models for porous medium such as Whitaker's model, temperature-, pressure- and moisture/concentration gradient are considered as driving forces for heat and mass transfer in the porous medium. The external heat and mass transfer are dominant during the period constant drying rate while internal heat and mass transfer mainly control the drying process during the period falling drying rate of a porous wet particle. Mass transport of free water, bound water and gas mixture and their resulting heat transport inside a wet wood particle can significantly affect the drying process of that particle. Tab. 2.1 and Tab. 2.2 present different mechanisms of internal heat and mass transport inside a

Table 2.1: *Transport mechanisms inside particle at period of constant drying rate*

Involved phase	Mass transfer	Heat transfer
free water	convection	conduction and convection
water vapor	convection/diffusion	conduction and convection/diffusion
solid	-	conduction

Table 2.2: *Transport mechanisms inside particle at period of falling drying rate*

Zone	Involved phase	Mass transfer	Heat transfer
I	water vapor	convection/diffusion	conduction and convection/diffusion
	solid	-	conduction
II	water vapor	convection/diffusion	conduction and convection/diffusion
	bound water	diffusion	conduction and diffusion
	solid	-	conduction
III	water vapor	convection/diffusion	conduction and convection/diffusion
	free water	convection/diffusion	conduction and convection/diffusion
	solid	-	conduction

hygroscopic particle with a moisture content higher than the fiber saturation point, during the drying process (Fig. 2.1).

2.2.1.3 Phase change

The phase change includes evaporation and re-condensation during the drying process. Three methods are commonly used for calculating the evaporation rate during high-temperature drying; equilibrium method, heat sink method and reaction method. The equilibrium method can describe both evaporation and re-condensation phenomena but the heat sink and reaction method are only able to describe the evaporation.

1. Equilibrium method: The phase change including evaporation and re-condensation can be formulated based on the hypothesis that in the pore space of the particle, water vapor is in phase equilibrium with free and bound water [18–23]. The partial pressure of water vapor in the equilibrium state is proportional to the saturated vapor pressure:

$$\begin{aligned} \langle P_v^{\mathrm{eq}} \rangle^g &= P_v^{sat}(T) && (M > M_{\mathrm{fsp}}) \\ \langle P_v^{\mathrm{eq}} \rangle^g &= P_v^{sat}(T) h(M_{bw}, T) && (M \leq M_{\mathrm{fsp}}) \end{aligned} \tag{2.5}$$

Where the saturated vapor pressure, P_v^{sat}, is obtained via an empirical equation and the relative humidity, $h(M_{bw}, T)$, is given by the sorption isotherm of wood. The phase change rate can be calculated by two methods based on the equilibrium assumption. In one method it is assumed that the water vapor density in each point in the particle is equal to equilibrium water vapor density of that point which can be calculated using the state equation and Eq. (2.5). Knowing the water vapor density, the phase change rate is calculated using mass conservation equation of water vapor (Eq. (2.16)). In the second method the phase change rate is given by a mass transfer expression with the difference between the equilibrium vapor density and the local vapor density.

$$\langle \dot{\omega}_v \rangle = K_o \epsilon_g (\langle \rho_v^{eq} \rangle^g - \langle \rho_v \rangle^g) \tag{2.6}$$

Here K_o is the reciprocal of the equilibration time. Considering the diameter of wood pores, the equilibration time is very small so K_o must be chosen big enough ($> 10^4[s^{-1}]$) to satisfy the equilibrium condition. In this thesis the latter method is used to determinate the phase change rate as a source term in the balance equations with an explicit expression.

2. Heat sink method: In the literature,the heat sink method has been implemented in three ways [22–34]. The evaporation rate can be modeled as a shrinking core with a moving boundary which separates the numerical domain into wet and dry zones. The second way is based on a conditional test on the local temperature. If the temperature is equal or higher than the evaporation temperature, its time derivative in the energy conservation equation is set to zero and the divergence of the heat flux is used to calculate the evaporation rate until the water is completely released. In the third way there is an energy balance in conjunction with an assigned evaporation (mostly boiling) temperature. If the temperature is higher than the evaporation temperature, the total energy needed to heat the local element beyond the evaporation temperature consumes for evaporation and the evaporation rate is obtained by dividing this heat flux to the heat of vaporization. by introducing the calculated evaporation rate to the energy equation, the temperature is corrected to the evaporation temperature. In present study the third way is used to implement the heat sink method.

$$\langle \dot{\omega}_v \rangle = \begin{cases} \frac{(T - T_{\text{evap}})\rho C_p}{\triangle h_v \triangle t} & \text{if} \quad T \geq T_{\text{evap}} \\ 0 & \text{if} \quad T < T_{\text{evap}} \end{cases} \tag{2.7}$$

3. Reaction method: In the heterogeneous reaction method, the evaporation rate is modeled as an Arrhenius-type kinetic equation [22, 23, 35–39].

$$\langle \dot{\omega}_v \rangle = A\ exp(-\frac{E}{RT})\langle \rho_{SD} \rangle M \tag{2.8}$$

Where the kinetic parameters of activation energy, E, and pre-exponential factor, A, can be obtained using experimental data. They also can be calculated to result in the maximum drying rate around the evaporation (boiling) temperature.

2.2.2 Governing equations

During the drying process of a porous wood particle, heat and mass transfer as well as phase change (evaporation and re-condensation) may occur simultaneously. This complex interplay of different phenomena has been modeled using a continuum approach based on Whitaker's theory [40] by several authors (for instance: [9, 16, 41–45]). Nowadays Whitaker's model is a well known model to describe drying processes in porous media. Since this model is the most rigorously formulated and comprehensive model in this field [46], it is selected to use in this thesis. Therefore, in this study a one-dimensional drying process inside a single wood particle is modeled based on the multiphase transport theory of Whitaker. The model considers water in three forms: free and bound water as well as water vapor. Different mechanisms of heat and mass transfer including free water flow due to capillary forces, diffusion of bound water, water vapor and air flow due to convection and diffusion and heat transfer by convection, diffusion and conduction are incorporated in the model. A full set of governing equations in drying of wood material is presented, based on Whitaker's model, which was further developed by Perre and his coworkers [9, 47].The macroscopic differential equations are achieved by averaging the conservation laws through a volume-averaging method. Resulting equations are in terms of average field quantities. The main simplifying assumptions of used mathematical model are:

1. Porous medium is considered to be one-dimensional, homogeneous and rigid.
2. Local thermal equilibrium exists between all the phases (all the phases are at a same temperature at each location).
3. Convection of free water and water vapor follows Darcy's law.
4. Bound water phase moves through the solid phase by molecular diffusion.

5. All gas species including water vapor and air obey the ideal gas law.
6. There is binary diffusion in the mixture of water vapor and air.
7. The enthalpy for all phases is a linear function of temperature.
8. No degradation of the solid phase occurs, i.e., the solid density is constant.

The governing equation of drying process in a wood particle are given, based on [9,45,47,48], as following. The sum of volume fractions for all the phases is equal to one:

$$\epsilon_g + \epsilon_s + \epsilon_{\text{fw}} + \epsilon_{\text{bw}} = 1 \tag{2.9}$$

where the volume fraction of each phase is obtained by $\epsilon_\gamma = \frac{\langle \rho_\gamma \rangle}{\langle \rho_\gamma \rangle^\gamma}$ and the averaged quantities are given by

$$\langle \phi \rangle = \frac{1}{\Omega} \int_{\Omega_\gamma} \phi d\Omega \qquad \langle \phi \rangle^\gamma = \frac{1}{\Omega_\gamma} \int_{\Omega_\gamma} \phi d\Omega \tag{2.10}$$

The moisture content (dry basis) M, by neglecting the mass of water vapor, is given by:

$$M = M_{\text{fw}} + M_{\text{bw}} = \frac{\langle \rho_{bw} \rangle + \langle \rho_{fw} \rangle}{\langle \rho_{SD} \rangle} \tag{2.11}$$

Mass conservation of the mixture of water vapor and air is given as :

$$\frac{\partial (\epsilon_g \langle \rho_g \rangle^g)}{\partial t} + \nabla . (\langle \rho_g \rangle^g \langle V_g \rangle) = \langle \dot{\omega}_v \rangle \tag{2.12}$$

where the density of the mixture is equal to the sum of densities of air and water vapor.

$$\langle \rho_g \rangle^g = \sum_{i=v,a} \langle \rho_i \rangle^g \tag{2.13}$$

The total gas pressure, using the equation of state, is written as:

$$\langle P_g \rangle^g = \frac{\langle \rho_g \rangle^g R_o \langle T \rangle}{M_g} \tag{2.14}$$

The molecular weight of the gas mixture, M_g, is given by:

$$M_g = (\sum_{i=v,a} \frac{\langle \rho_i \rangle^g}{\langle \rho_g \rangle^g M_i})^{-1} \tag{2.15}$$

Mass conservation of water vapor:

$$\frac{\partial (\epsilon_g \langle \rho_v \rangle^g)}{\partial t} + \nabla . \langle \rho_v V_v \rangle = \langle \dot{\omega}_v \rangle \tag{2.16}$$

where

$$\langle \rho_v V_v \rangle = \langle \rho_v \rangle^g \langle V_g \rangle - \langle \rho_g \rangle^g D_v^{\text{eff}} \nabla \left(\frac{\langle \rho_v \rangle^g}{\langle \rho_g \rangle^g} \right) \tag{2.17}$$

The mass conservation equation of free and bound water is written as:

$$\frac{\partial (\langle \rho_{\text{fw}} \rangle + \langle \rho_{\text{bw}} \rangle)}{\partial t} + \nabla . (\langle \rho_{\text{fw}} V_{\text{fw}} \rangle + \langle \rho_{\text{bw}} V_{\text{bw}} \rangle) = - \langle \dot{\omega}_v \rangle \tag{2.18}$$

where

$$\langle \rho_{\text{fw}} V_{\text{fw}} \rangle = \rho_w \langle V_{\text{fw}} \rangle \tag{2.19}$$

$$\langle \rho_{\text{bw}} V_{\text{bw}} \rangle = - \langle \rho_{SD} \rangle D_{\text{bw}} \nabla \left(\frac{\langle \rho_{\text{bw}} \rangle}{\langle \rho_{SD} \rangle} \right) \tag{2.20}$$

The superficial gas phase velocity and the superficial free water velocity are calculated using Darcy's law.

$$\langle V_g \rangle = - \frac{\mathbf{K}_g \mathbf{K}_{rg}}{\mu_g} \nabla \langle P_g \rangle^g \tag{2.21}$$

$$\langle V_{\text{fw}} \rangle = - \frac{\mathbf{K}_l \mathbf{K}_{rl}}{\mu_w} \nabla \langle P_w \rangle^w \tag{2.22}$$

where

$$\mu_g = \frac{\sum_{i=v,a} (\mu_i \langle \rho_i \rangle^g)}{\langle \rho_g \rangle^g} \tag{2.23}$$

The energy equation in porous media with the local thermal equilibrium assumption is written as:

$$\begin{aligned} &(C_{ps} \langle \rho_{SD} \rangle + C_{pw} \langle \rho_{\text{fw}} \rangle + C_{pw} \langle \rho_{bw} \rangle + C_{pg} \epsilon_g \langle \rho_g \rangle^g) \frac{\partial \langle T \rangle}{\partial t} \\ &+ (C_{pw} \langle \rho_{\text{fw}} V_{fw} \rangle + C_{pw} \langle \rho_{\text{bw}} V_{\text{bw}} \rangle + C_{pg} \langle \rho_g V_g \rangle + \sum_{i=v,a} C_{pi} \langle \rho_i U_i \rangle) . \nabla \langle T \rangle \\ &= \nabla . (k_{\text{eff}} \nabla \langle T \rangle) - \langle \dot{\omega}_v \rangle \triangle h_v + \langle \rho_{\text{bw}} V_{\text{bw}} \rangle . \nabla (\triangle h_{\text{sorp}}) \end{aligned} \tag{2.24}$$

where

$$\begin{aligned} \triangle h_v &= \triangle h_w + \triangle h_{\text{sorp}} && (M < M_{\text{fsp}}) \\ \triangle h_v &= \triangle h_w && (M \geq M_{\text{fsp}}) \end{aligned} \tag{2.25}$$

and the diffusion flux in the gas phase is given by:

$$\langle \rho_i U_i \rangle = - \langle \rho_g \rangle^g D_i^{\text{eff}} \nabla \left(\frac{\langle \rho_i \rangle^g}{\langle \rho_g \rangle^g} \right) \tag{2.26}$$

The specific heat capacity for the gaseous mixture, C_{pg}, is defined by:

$$C_{pg} = \sum_{i=v,a} C_{pi} \frac{\langle \rho_i \rangle^g}{\langle \rho_g \rangle^g} \tag{2.27}$$

2.2.3 Initial conditions

Initially, the biomass particle is at ambient- pressure and temperature conditions and the initial moisture content is introduced in the model. Since the free and bound water are assumed to be in equilibrium with water vapor inside the particle, the pore spaces are initially assumed to be filled by humid air. The distribution of initial moisture content as well as initial temperature is assumed to be uniform inside the particle.

2.2.4 Boundary conditions

Symmetry is assumed for the boundary condition at the center of particle, that is, the velocities and the gradients of the independent variables are equal to zero at this point. Pressure at the boundary subjected to the outside environment that is convective drying flow in this study, is assumed to remain the ambient pressure during the drying process:

$$\langle P_g \rangle^g_{\text{surf}} = \langle P_g \rangle^g_{\infty} = P_{atm} \tag{2.28}$$

Heat and mass transfer from/to the surface of the particle are modeled in two types, in this thesis.

2.2.4.1 Boundary conditions - type 1

If there is an insignificant pressure gradient at the boundary then by assuming no blowing phenomenon at the surface, the velocity of water vapor is considered to be negligible there. Therefore all vapor fluxes, those of vapor transport from inside the particle as well as those resulting from evaporation at the surface, are supposed to leave the particle surface only by surface convection. It is assumed that free and bound water are evaporated at the drying front on the surface of the particle during first stage of drying, before leaving the particle. Heat and mass balances at the boundary of the particle model is given by:

$$(\langle \rho_{\text{fw}} V_{\text{fw}} \rangle + \langle \rho_{\text{bw}} V_{\text{bw}} \rangle + \langle \rho_v V_v \rangle).n|_{\text{surf}} = (\epsilon_g + \epsilon_{\text{fw}} + \epsilon_{\text{bw}}) \beta (\langle \rho_v \rangle^g_{\text{surf}} - \langle \rho_v \rangle^g_{\infty}) \tag{2.29}$$

$$(k_{\text{eff}} \nabla \langle T \rangle + \langle \rho_{\text{fw}} V_{\text{fw}} \rangle \triangle h_v + \langle \rho_{\text{bw}} V_{\text{bw}} \rangle \triangle h_{\text{sorp}}).n|_{\text{surf}} = -\alpha (\langle T_{\text{surf}} \rangle - \langle T_{\infty} \rangle) \tag{2.30}$$

2.2.4.2 Boundary conditions - type 2

In the second type of boundary condition of heat and mass transfer, both phenomena of blowing and convection are considered to be contributed to the water vapor transport at the surface of the particle. But it is still assumed that free and bound water don't cross the boundary and they are evaporated at the surface:

$$\begin{aligned}(\langle\rho_{\mathrm{fw}}V_{\mathrm{fw}}\rangle + \langle\rho_{\mathrm{bw}}V_{\mathrm{bw}}\rangle + \langle\rho_v V_v\rangle).n|_{\mathrm{surf}} = \\ (-\langle\rho_v\rangle^g \frac{\mathbf{K}_g\mathbf{K}_{rg}}{\mu_g}\nabla\langle P_g\rangle^g)|_{\mathrm{surf}} + (\epsilon_g + \epsilon_{\mathrm{fw}} + \epsilon_{\mathrm{bw}})\beta(\langle\rho_v\rangle^g_{\mathrm{surf}} - \langle\rho_v\rangle^g_\infty)\end{aligned} \tag{2.31}$$

$$(k_{\mathrm{eff}}\nabla\langle T\rangle + \langle\rho_{\mathrm{fw}}V_{\mathrm{fw}}\rangle \triangle h_v + \langle\rho_{\mathrm{bw}}V_{\mathrm{bw}}\rangle \triangle h_{\mathrm{sorp}}).n|_{\mathrm{surf}} = -\alpha(\langle T_{\mathrm{surf}}\rangle - \langle T_\infty\rangle) \tag{2.32}$$

Assuming the effect of the blowing for the liquid phases, different types of boundary condition for heat and mass transfer can be considered for drying process of a particle but in this thesis these two above mentioned types are used for modeling. The total vapor flux in the boundary condition has contributions from evaporation of free water, bound water and water vapor existing at the surface. By multiplying the volume fraction of free water, bound water and water vapor to the vapor flux at the particle surface, the total vapor flux at the boundary is determined [49]. α and β are heat and mass transfer coefficients at the surface respectively and the effect of Stefan flow is neglected in the particle model of this study [50].

2.3 Coefficients of the model equations

Despite the comprehensive descriptions of transport phenomena in drying of wood material by the model based on Whitaker's theory, determination of heat and mass transfer coefficients of this model is very difficult. But for the applicability of the model predictions in practical cases, reliable information regarding material properties and transport coefficients of governing equations is required. These coefficients depend on grain orientation and physico-chemical properties of the wood species. Furthermore, these coefficients depend on the moisture content and temperature of the particle, which are varying during the drying process and may affect these coefficients significantly. Therefore the determination of these coefficients for different species of wood over different conditions is very time consuming. The information on the transport coefficients of this model is scarce and limited to few species of wood over a rather limited range of conditions. This fact increases the uncertainty degree of these coefficients in modeling. On the other hand the accuracy of the predictions of a mathematical model depends on the accuracy of these coefficients.

Available values and empirical correlations of the transport coefficients in previous works which can be used for modeling of drying process in pine wood are collected in the next subsections. It is obvious that their variation is remarkable although these correlations have been developed only for a single species of wood: pine wood. Among different correlations and values reported in the literature with respect to different grain directions, the physical properties of a wet pine particle in transverse direction are listed. The values of the model parameters in transverse direction are considered to be the arithmetic mean of the values in radial and tangential directions. The correlations and values of nine model parameters in transverse direction are brought in Tab. 2.3, Tab. 2.4 and also Tab. A.1 to Tab. A.7 (in the appendix). Variation of these model parameters over different moisture contents from 0.1 $kg/kg(d.b)$ to 0.8 $kg/kg(d.b)$ as well as over a range of temperature from 30° C to 150° C are shown in Fig. 2.2 to Fig. 2.8.

2.3.1 Effective thermal conductivity and specific heat capacity

The effective thermal conductivity and the specific heat capacity are two model parameters that appear only in the enegry equation. Different correlations and values for the effective thermal conductivity with respect to different grain directions have been reported for dry as well as for wet pine wood in the literature. Also for the specific heat capacity of dry and wet pine wood particles several correlations and values are available. For a case that only thermal conductivity of dry wood is available, the effective thermal conductivity of wet wood is obtained by adding the contribution to thermal conductivity of the moisture content. The contribution to thermal conductivity of the moisture content is calculated by multiplying the volume fraction of the moisture with the thermal conductivity of water, according to [12]. In a same way, by adding the specific heat capacity of water, the specific heat capacity of wet wood is calculated. The contribution of the gas phase is neglected in the calculation of specific heat capacity of wet wood. Fig. 2.2 shows the minimum and maximum effective thermal conductivity of a wet pine particle differ by a factor of approximately three, over the studied ranges of moisture content and temperature. Fig. 2.3 shows that the correlations for the specific heat capacity of a wet wood particle differ by a factor of approximately two, for the extreme cases.

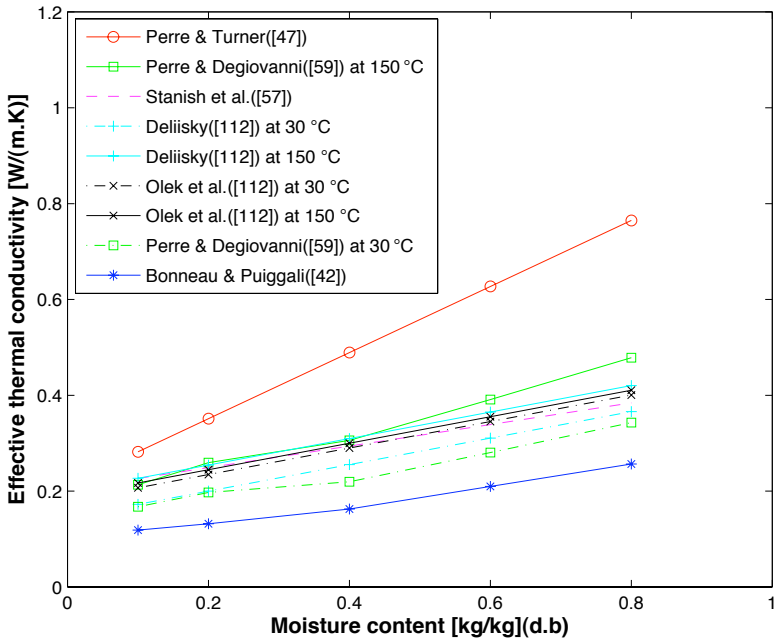

Figure 2.2: *Effective thermal conductivity versus moisture content*

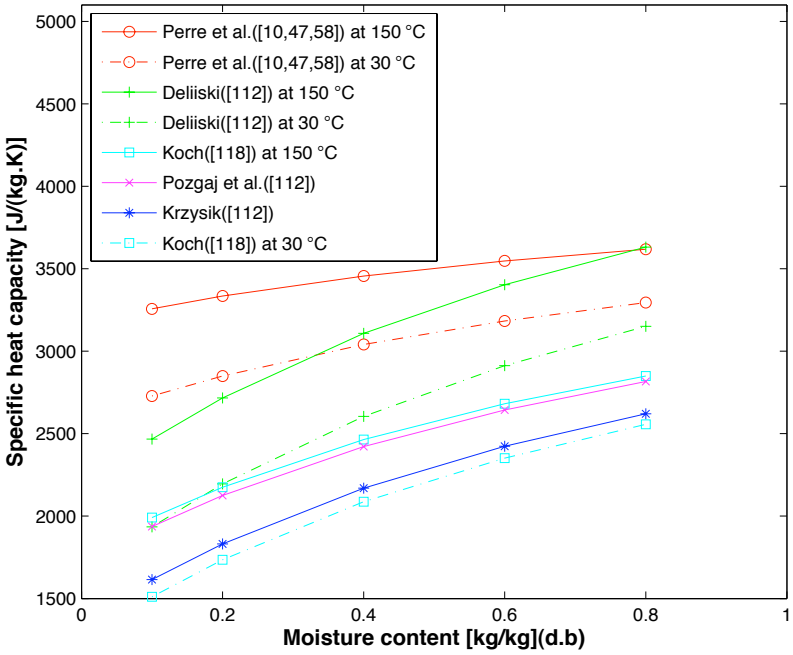

Figure 2.3: *Specific heat capacity versus moisture content*

2.3.2 Diffusive transport coefficients

The bound water diffusivity and the effective diffusivity of water vapor are two model parameters that characterize diffusive flow inside the particle. In the literature there are few studies dealing with the determination of mass transport coefficients in wood (for instance: [51–54]). The separation of the effects of the different modes of mass transfer during drying process is experimentally extremely challenging. In light of these experimental difficulties, it is not surprising that there is a very broad range of values and correlations for these diffusion coefficients reported by different authors, even for a certain type of wood. The variation between maximum and minimum values of the diffusion coefficient of bound water reaches up to three orders of magnitudes for some temperatures and moisture contents, as shown in Fig. 2.4. Since several parameters affect the effective diffusivity of water vapor in porous media (molecular diffusivity, porosity, tortuosity) this coefficient is very variable from one kind of material to another. Recently, Kang and Chung [55] pointed out that the effective diffusivity of water vapor in wood is actually still unknown. Fig. 2.5 shows that different values with a difference of two orders of magnitude have been used for the effective diffusivity of water vapor in wood, in the literature.

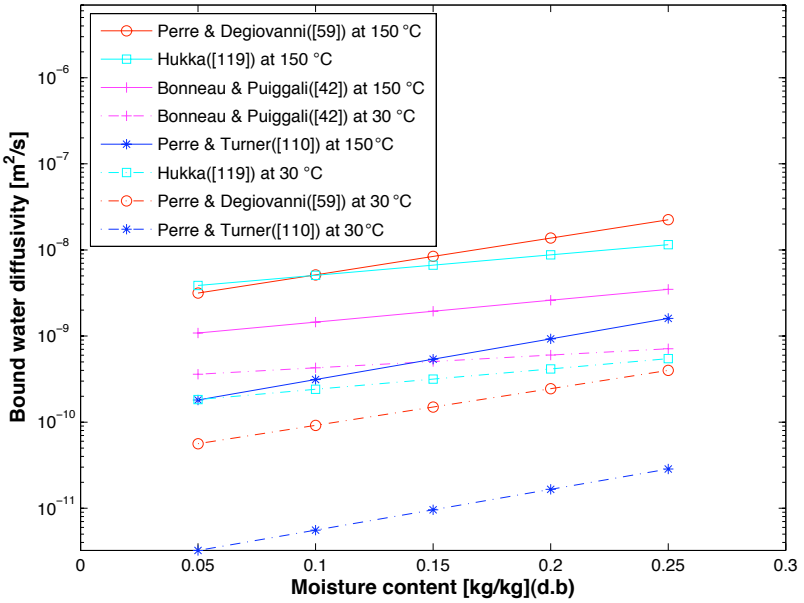

Figure 2.4: *Bound water diffusivity versus moisture content*

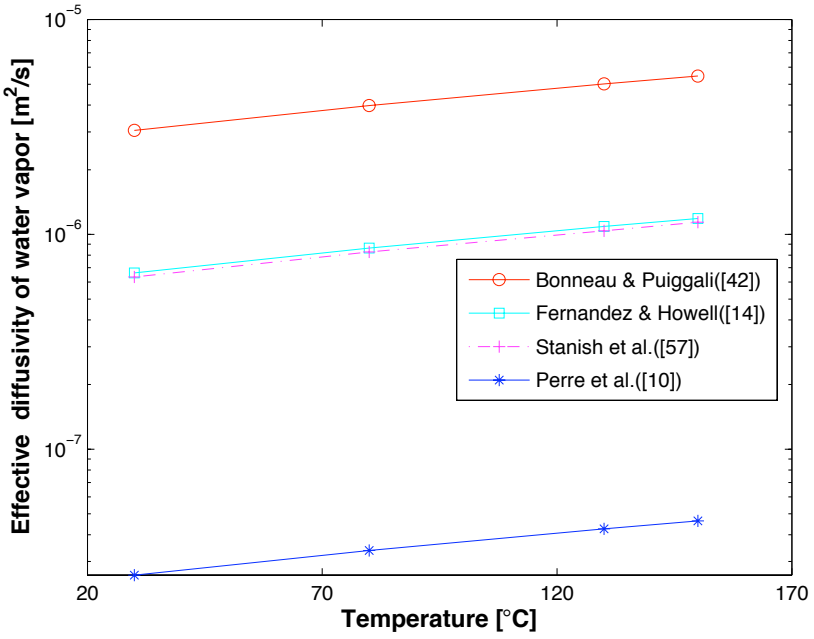

Figure 2.5: *Effective diffusivity of water vapor versus temperature*

Table 2.3: *Gas intrinsic permeability in pine wood in transverse direction*

Value	Species	Reference
$\mathbf{K}_g = 5 \cdot 10^{-15}$	Southern pine	Stanish et al. [57]
$\mathbf{K}_g = 4 \cdot 10^{-15}$	Softwood	Perre & Turner [58]
$\mathbf{K}_g = 1.096 \cdot 10^{-15}$	Maritime pine	Perre & Agoua [52]
$\mathbf{K}_g = 4 \cdot 10^{-16}$	Pine (Sapwood)	Couture et al. [43]
$\mathbf{K}_g = 1 \cdot 10^{-16}$	Pine	Bonneau & Puiggali [42]
$\mathbf{K}_g = 5 \cdot 10^{-18}$	Softwood	Perre & Degiovanni [59]

2.3.3 Convective transport coefficients

The convective flow of gas - including water vapor and air - is dependent on the intrinsic and the relative permeability of the gas. Capillary pressure, intrinsic and relative permeability of liquid are the model parameters influencing the convection of free water in the pores of a particle.

2.3.3.1 Convective transport coefficients of gas mixture

The intrinsic permeability refers to the permeability in a single-phase saturated medium. The reported values for gas intrinsic permeability in wood differ by three to four orders of magnitude, even for one type of wood [56]. Tab. 2.3 presents different values of the gas intrinsic permeability of pine wood used by researchers in the literature.The relative permeability is defined as the permeability of a fluid phase in an unsaturated medium. The value of gas relative permeability varies from 0 to 1 over different saturation so that at fully saturated case the value of gas relative permeability reaches to zero. Fig. 2.6 shows the variation of different correlations of the gas relative permeability over different saturation values.

2.3.3.2 Convective transport coefficients of free water

Presented values of minimum and maximum capillary pressure in the pores of wood, under studied conditions, range from 10^3 to 10^6 (Pa) over different saturation, as shown in Fig. 2.7. Perre and Karimi [51] reported that entrapped air and particulate matter may appear in the pathway of the liquid water flow during the measurement of the intrinsic permeability of liquid water in wood. They stated that for these reasons the measured value of the gas intrinsic permeability is much more accurate than the liquid intrinsic permeability. By considering the phenomena of pit aspiration during the drying process, Perre et al. [10] assumed the liquid intrinsic permeability

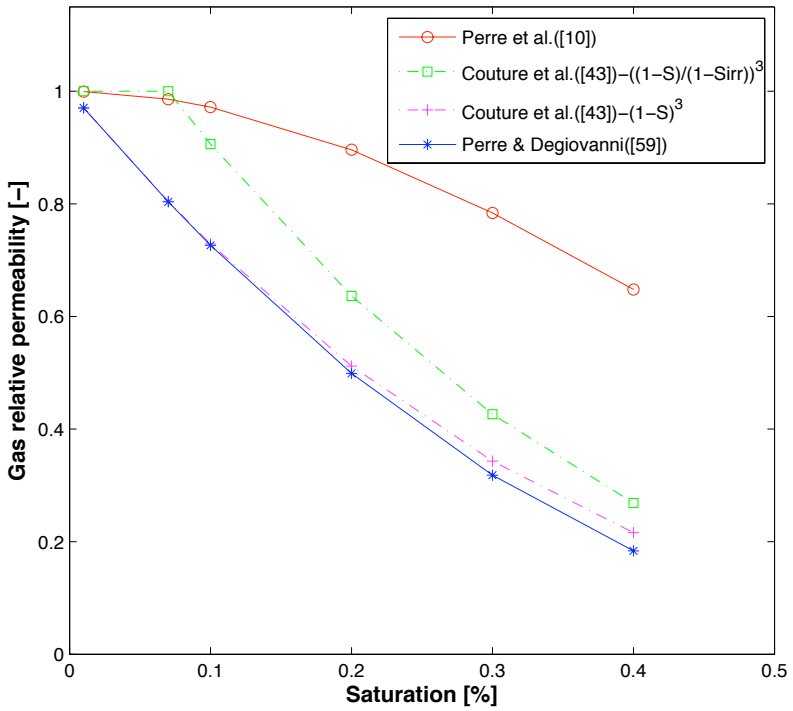

Figure 2.6: *Gas relative permeability versus saturation*

Table 2.4: *Liquid intrinsic permeability in pine wood in transverse direction*

Empirical correlation	Species	Reference
$\mathbf{K}_l = 10\,\mathbf{K}_g$	Southern pine	Stanish et al. [57]
$\mathbf{K}_l = 5\,\mathbf{K}_g$	Softwood	Perre & Turner [58]
$\mathbf{K}_l = \mathbf{K}_g$	Pine	Couture et al. [43]
$\mathbf{K}_l = 0.1\,\mathbf{K}_g$	Softwood	Perre & Degiovanni [59]

being 5 times greater than the gas intrinsic permeability . Stanish et al. [57] have taken into account the value of the liquid intrinsic permeability being one order smaller than the gas intrinsic permeability. Tab. 2.4 presents different values of the liquid intrinsic permeability of a woody biomass particle. Over the studied range of saturation, there are three to six orders of magnitude differences between maximum and minimum value of the relative permeability of liquid water, as shown in Fig. 2.8.

2.4 Concluding remarks

The drying characteristics of a hygroscopic porous particle, particularly a wood particle, has been outlined. Whitaker's model, as a well-accepted model for drying of

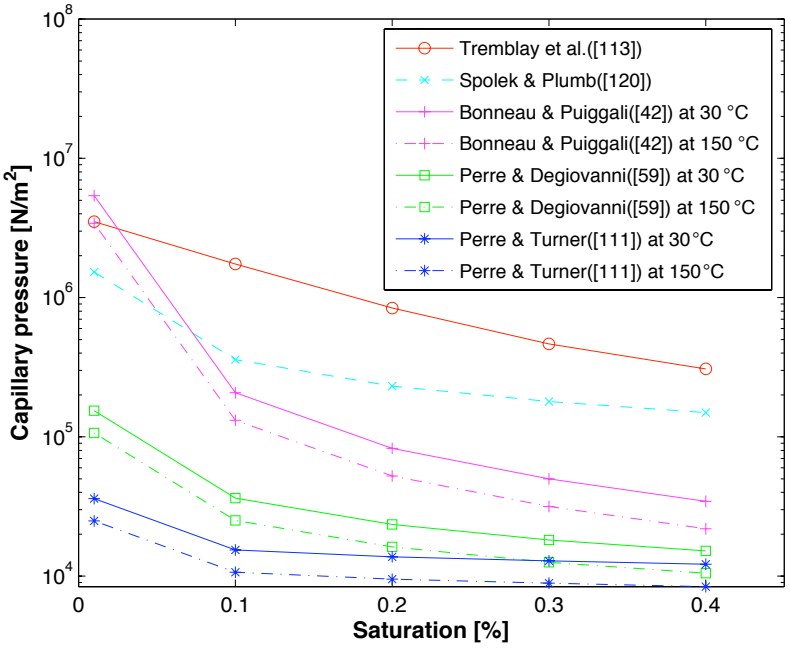

Figure 2.7: *Capillary pressure versus saturation*

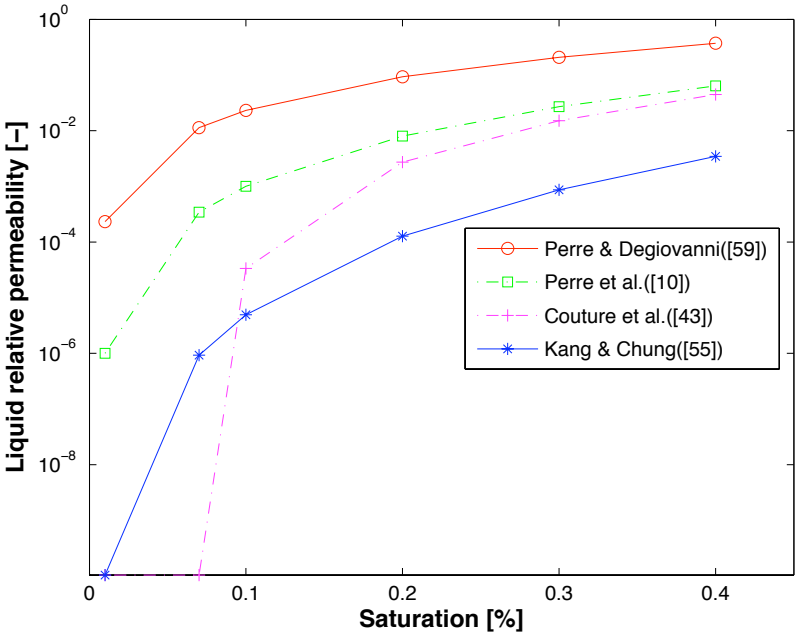

Figure 2.8: *Liquid relative permeability versus saturation*

porous media, has been presented. Nine physical properties of wood as well as transport coefficients of the model have been examined. Different values and correlations of these parameters which could be used for modeling the drying of pine wood have been collected from the literature. By plotting the variation of these parameters over a typical conditions of wood drying (drying temperature varying from 30° C to 150° C and the moisture contents from 0.1 $kg/kg(d.b)$ to 0.8 $kg/kg(d.b)$) lower and upper bounds of the values of these parameters have been determined. The range of values of the model parameters that are reported in the literature for a certain species of wood (pine) is considerably broad. For some properties or transport coefficients, three to four orders of magnitude differences in the values have been reported. This shows the variety of properties in wood, even in the same species. These broad range of the values reported for each model parameter increase the uncertainty of the model output significantly. The sensitivity analysis is needed to evaluate the most effective models parameters on the variation of the model output. Taking an arbitrary value of a model parameter from the broad range of reported values, without enough justifications, may lead to remarkable inaccuracy.

Chapter 3

Drying model at fixed-bed reactor scale

At the reactor scale, there are different mechanisms and conditions in comparison to the particle scale. At first, the physics governing on fixed-bed drying of solid porous particles is presented in Section 3.1. Different types of models to describe the processes in packed bed reactors are discussed in Section 3.2. Among others, a continuum model (heterogeneous quasi-continuous model) and a multi-scale model (Representative Particle Model) are outlined in this chapter.

3.1 Phenomena involved in fixed-bed drying

Different mechanisms of heat and mass transfer are involved in a process like drying in a fixed-bed reactor with fluid flow, at particle- and reactor scale. Different mechanisms of heat and mass transfer during drying process at particle scale have been introduced in previous chapter, Tab. 2.1 and Tab. 2.2. Following the transport mechanisms which must be taken into account for analysis of a process such as drying in a fixed-bed reactor are given [60–63]:

1. Conduction through solid-solid contact points.
2. Radiation between surfaces of particles.
3. Conduction and diffusion through fluid film near solid-solid contact points.
4. Heat and mass transfer (convective transport) between particle domain and gas phase.
5. Conduction and diffusion within fluid (interstitial gas phase).
6. Convection and dispersion within fluid (interstitial gas phase).

7. Convective transport between reactor wall and gas phase.
8. Conduction through contact points of particle domain and reactor wall.
9. Radiation between particle domain and reactor wall.
10. Conduction through reactor wall.

Furthermore, during fixed-bed drying of woody biomass particles, phase change including evaporation and re-condensation are accompanied with transport phenomena within the interstitial gas phase as well as inside the particles. For a complete description of the complex physical-chemical phenomena taking place in the fixed-bed reactors, the velocity, temperature and concentration fields in three dimensions must be known. A mathematical model being capable to perfectly predict these fields, has to consider the full local resolution at different scales; from molecular to reactor scale. Such a detailed model may lead to a very complex model that is not affordable for practical cases. Measurement of the exact value of the parameters involved in every phenomenon in fixed-bed reactors is really challenging and this makes difficult the solving of a detailed mathematical model with several parameters. On the other hand, depending on the properties of the particular system under study, the share of the phenomena in controlling the process can be different so that some of them can be neglected in description of the behavior of the system. These properties of the system can include the properties of used materials and the type of the processes taking place in the system under different conditions. There are several classes of models with different levels of accuracy and computational effort for modeling the behavior of phenomena taking place in fixed-bed reactors. The best model is selected to be fit to the system under consideration on the basis of the required accuracy and the computational cost that can be spent.

3.2 Mathematical modeling of fixed-bed drying

Mathematical models used in the literature for modeling of the process like drying in fixed-bed reactors can be categorized as shown in Fig. 3.1. In homogeneous quasi-continuous model, the model variables such as temperature and concentration are considered as the local averages between the phases and the system is modeled as one phase. Thanks to the low computational effort, this model that is also known as continuum model is the most commonly used model (For instance: [64–69]). Homogeneous quasi-continuous model can provide acceptable accuracy for a system with specific properties under certain conditions. However in the cases

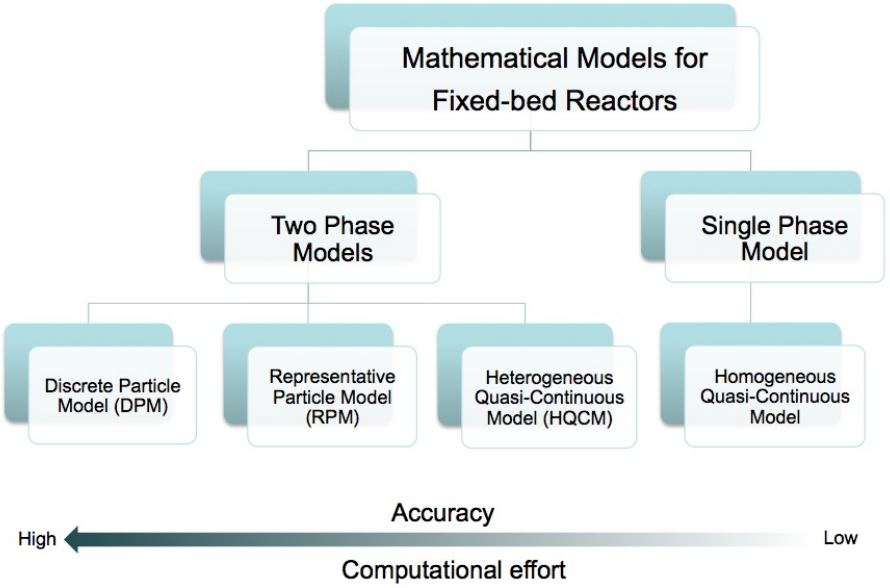

Figure 3.1: *Mathematical models for modeling of fixed-bed reactors.*

that there are significant discrepancies between the phases with steep gradients in the particle domain, averaging the system by this model may lead to remarkable errors. For description of a fixed-bed reactor with significant discrepancies between the phases, Discrete Particle Model (DPM) [70–74] as a multi-scale model provides higher accuracy and detailed information of velocity, temperature and concentration fields at different scales. Nowadays with the help of commercially available codes, fully resolved 3D computations of the DPM - also referred to as Discrete Element Method or Euler-Lagrange model - is possible. But at industrial scale where the number of the particles reaches more than 10^6 in the bed, the computational cost will dramatically increase. One of the important application of such a mathematical model can be real-time monitoring of the process taking place in the reactor in order to control it, while for the DPM in industrial application the computational time is much bigger than the running time of the process. Against these two above-mentioned limiting models, there are two other models which have higher accuracy than homogeneous quasi-continuous model and less computational effort than the DPM. In this thesis, two models of heterogeneous quasi-continuous model (HQCM) and Representative Particle Model (RPM) are studied for modeling of fixed-bed drying of hygroscopic porous solid particles. Both models are formulated based on the following simplifying assumptions:

1. The bed of particles is cylindrical and isotropic and the variables are considered one dimensional in space, varying along the axial direction, and transient in time

2. Void fraction of the bed is constant in time (there is no shrinkage in particle domain)
3. Low Mach number
4. All gas species including water vapor and air obey the ideal gas law
5. No phase change reactions in the interstitial gas phase including evaporation and re-condensation
6. The net momentum of the gases leaving the particles vanishes due to the 1D-spherically symmetric nature of the particles
7. Transport of energy due to species diffusion can be neglected as compared to convective energy transport in the interstitial gas phase
8. Radiation is neglected because of considered range of temperature
9. Adiabatic reactor walls
10. External forces such as gravity are negligible

Regarding the assumption of adiabatic reactor walls, some transport mechanisms associated to the reactor wall, listed in Section 3.1, are not taken into account in these models.

3.2.1 Heterogeneous Quasi-Continuous Model (HQCM)

Fig. 3.2 shows how a fixed-bed reactor can be modeled via the heterogeneous quasi-continuous model (HQCM). Since the interstitial gas phase as well as particle domain are considered as quasi-homogeneous phase therefore this model is also classified as continuum model. In the homogeneous quasi-continuous model no fluid-to-particle heat and mass transfer resistances are taken into account. While in the heterogeneous quasi-continuous model, interface resistances between interstitial gas phase and the particle domain are considered (For instance: [66, 75–78]). Intra-particle heat and mass transfer resistance are considered in some sorts of the heterogeneous quasi-continuous model. In a case that the difference between the fluid phase and particle domain is negligible homogeneous quasi-continuous model can provide acceptable prediction of the process behavior. But if the differences between fluid and solid temperatures and concentrations are more pronounced then the heterogeneous quasi-continuous model can provide better accuracy.

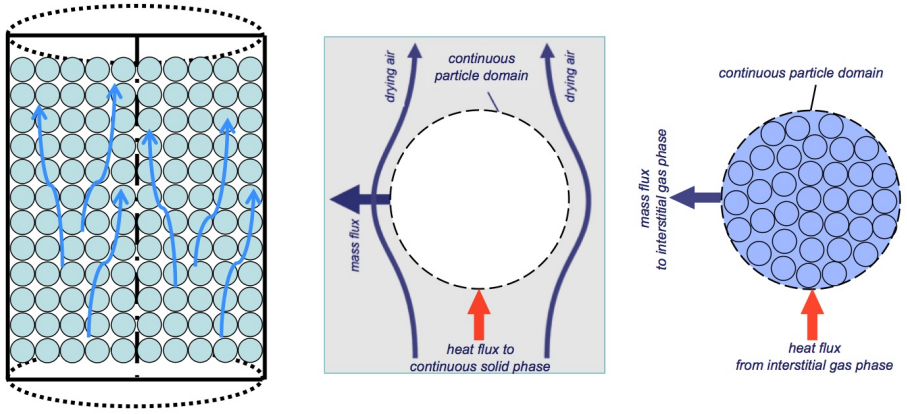

Figure 3.2: *Modeling of a fixed-bed reactor by the heterogeneous quasi-continuous model.*

3.2.1.1 Fluid phase: interstitial gas phase

Since Darcy law is not accurate enough for all types of situation of modeling flow in porous media therefore for some conditions, an extended form of Darcy law is used. Here, the Brinkman-Forchheimer equation [79] that is a more general form of the momentum balance for porous media, is employed. Flow domain is divided to several finite volumes in the shape of cylinders with the same length and with the radius equals to the radius of the bed. Balances equations are applied to the gas phase in each finite volume. It should be noted that the volume of particle domain is not contained in these balance volumes. Based on the assumptions discussed in Section 3.2, the following partial differential equations of balances are resulting for the interstitial gas phase in the reactor. The primed quantities refer to the values at the external surface of the particle domain. The governing equations of employed two-phase system are similar to [80–83].

Mass balance of the gas phase:

$$\frac{\partial \rho_g}{\partial t} = -\frac{\partial (w_z \rho_g)}{\partial z} + \sum_{i=v,a} \left(s \frac{(1-\epsilon_b)}{\epsilon_b} \left\{ \beta_i' [(\rho_g Y_i)' - (\rho_g Y_i)] \right\} \right) \tag{3.1}$$

Mass balance of gas species i:

$$\frac{\partial (\rho_g Y_i)}{\partial t} = -\frac{\partial (\rho_g Y_i w_z)}{\partial z} + \frac{\partial}{\partial z} \left(\rho_g D_{z,i} \frac{\partial Y_i}{\partial z} \right) + s \frac{(1-\epsilon_b)}{\epsilon_b} \left\{ \beta_i' [(\rho_g Y_i)' - (\rho_g Y_i)] \right\} \tag{3.2}$$

Momentum balance:

$$\frac{\partial (\rho_g w_z)}{\partial t} = -\frac{\partial (\rho_g w_z w_z)}{\partial z} - \frac{\partial p}{\partial z} - f_1 w_z - \epsilon_b f_2 w_z |\vec{w}| + 2 \frac{\partial}{\partial z} \left(\mu_{eff} \frac{\partial w_z}{\partial z} \right) \tag{3.3}$$

Energy balance:

$$\rho_g c_{p,g} \frac{\partial T_g}{\partial t} = -\rho_g c_{p,g} w_z \frac{\partial T_g}{\partial z} + \frac{\partial}{\partial z}\left(\Lambda_z \frac{\partial T_g}{\partial z}\right) - s\frac{(1-\epsilon_b)}{\epsilon_b}[\alpha'(T_g - T'_p)] \tag{3.4}$$

Heat and mass transfer between the interstitial gas phase and continuous particle domain, shown in Fig. 3.2, appear in balance equations as source terms. There is no source term from phase change in these equations because it is assumed that no phase change occurs in the interstitial gas phase. The specific surface s of the particles exposing the interstitial gas phase, for the spherical particles, is as follow:

$$s = \frac{6}{d_p} \tag{3.5}$$

The coefficients f_1 and f_2 in the Brinkman-Forchheimer momentum equation are adapted from [69, 84], as follows:

$$f_1 = 150\frac{(1-\epsilon_b)^2 \mu_{eff}}{\epsilon_b^3 d_p^2} \tag{3.6}$$

$$f_2 = 1.75\frac{(1-\epsilon_b)\rho_g}{\epsilon_b^3 d_p} \tag{3.7}$$

where

$$\mu_{eff} = 2\mu_g exp(0.002 Re_p) \tag{3.8}$$

Temperature, density and pressure are coupled through the equation of state:

$$\rho_g = \frac{pM_m}{\bar{R}T_g} \tag{3.9}$$

3.2.1.2 Particle domain: continuous particle domain

In the heterogeneous quasi-continuous model (HQCM), the particle domain is modeled as a continuum media so that all particles in the bed are assumed to be connected together as a continuum media. The particles are considered as zero dimensional particles. By modification and combination of different mechanisms involved

in fixed-bed drying at particle as well as reactor scales, discussed in Section 3.1, different forms of the heterogeneous quasi-continuous model can be made. Although intra-particle transport resistance can be taken into account in the heterogeneous quasi-continuous model ([85]) however in this study only the inter-particle heat transfer by conduction is considered in the continuous particle domain. Since the particles are assumed to be zero dimensional therefore no resistance of mass and heat transfer in the particle is individually considered and all particles are treated as a continuous media. The main assumptions of the continuous particle domain are:

1. The particle is porous and spherical, it is assumed to be zero dimensional.
2. there is no resistance of heat and mass transfer inside the particle.
3. There is local thermal equilibrium between the solid, the liquid and the gas phase inside the particle.
4. Conduction is taken into account for heat transfer between neighbor particles
5. Phase change including evaporation and re-condensation occurs inside the particle
6. External forces are negligible
7. No shrinkage and degradation of the particle

Based on these assumptions the following partial differential equations of balances are resulting for the continuous particle domain in the reactor.

Mass balance of the gas phase in the continuous particle domain:

$$\frac{\partial(\epsilon_g \rho_g)_s}{\partial t} = \sum_{i=v,a} (-s(1-\epsilon_b)\Big(\beta_i'[(\rho_g Y_i)_s - (\rho_g Y_i)]\Big)) + \dot{\omega}_v \tag{3.10}$$

Mass balance of gas species i in the continuous particle domain:

$$\frac{\partial(\epsilon_g \rho_g Y_i)_s}{\partial t} = -s(1-\epsilon_b)\Big(\beta_i'[(\rho_g Y_i)_s - (\rho_g Y_i)]\Big) + \dot{\omega}_v \tag{3.11}$$

Mass balance of the liquid phase in the continuous particle domain:

$$\frac{\partial(\epsilon_l \rho_l)}{\partial t} = -\dot{\omega}_v \tag{3.12}$$

Energy balance in the continuous particle domain:

$$(\epsilon_s \rho_s c_{p,s} + \epsilon_l \rho_l c_{p,l} + \epsilon_g \rho_g c_{p,g}) \frac{\partial T_s}{\partial t} = \frac{\partial}{\partial z}\left(K_{eff,s} \frac{\partial T_s}{\partial z} \right) + s(1-\epsilon_b)[\alpha'(T_g - T_s)] - \dot{\omega}_v \triangle h_v \tag{3.13}$$

where

$$\epsilon_s + \epsilon_l + \epsilon_g + \epsilon_b = 1 \tag{3.14}$$

and the effective thermal conductivity of the bed, $K_{eff,s}$, is adopted from Zehner and Schlünder equation [69] by not considering the thermal conductivity of the fluid phase.

3.2.2 Representative Particle Model (RPM)

In the Representative Particle Model (RPM), all particles in a finite volume segment of solution domain of the reactor are characterized based on the intra-particle solution resulting from one of them. It is assumed that every particle in the finite volume behaves like other particles in that finite volume therefore the intra-particle solution of one of them represents other particles' characterization. This particle is called the representative particle of that finite volume. Fig. 3.3 illustrates the concept of this model in a 1D fixed-bed drying process. Dieterich [86] and Chejne et al. [87] used this concept to simulate thermo-chemical processes in packed bed reactors. This model was applied to thermo-chemical conversion of biomass in fixed-beds by Wurzenberger [88] and Wurzenberger et al. [21]. Zobel [89] has presented very detailed information on deriving the governing equations of the RPM. Porteiro et al. [90] employed this model in simulation of fixed-bed combustion of biomass boilers. Anca-Couce [91] developed this model for pyrolysis of biomass particles in fixed-bed reactor by improving its solution method. In this study the RPM is developed for fixed-bed drying of hygroscopic porous particles such as woody fuel particles. 1D+1D model is considered so that the reactor is descritized in the axial direction and the wet solid particles are descritized in the radial direction. In comparison with other studies of the RPM including fixed-bed drying of biomass (such as Wurzenberger [88], [21] and Zobel [89]), in this work, more comprehensive equations at reactor scale as well as particle scale are used. Moreover the numerical solution method is improved based on [92]. Fig. 3.4 shows how a fixed-bed drying process can be modeled via coupling the solutions of two scales by the RPM. The equations governing on the interstitial gas phase and at particle scale are presented in following. For a detailed derivation of these balance equations the reader is referred to [89].

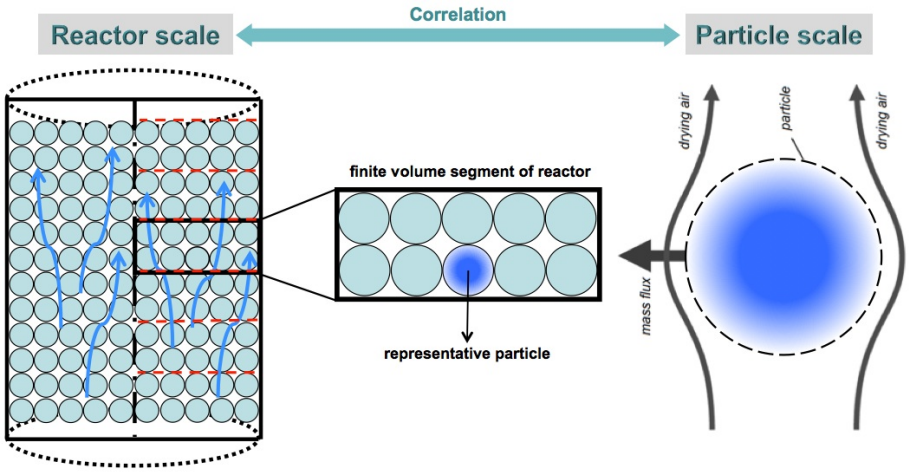

Figure 3.3: *Schematic of the RPM concept*

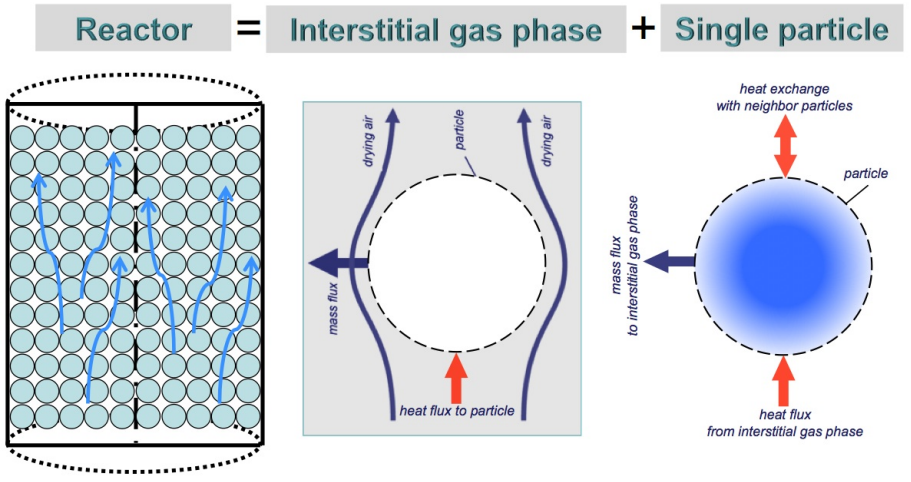

Figure 3.4: *Modeling of a fixed-bed reactor by the RPM.*

3.2.2.1 Fluid phase: interstitial gas phase

In the RPM, the interstitial gas phase is described as a quasi-homogeneous phase as discussed in section 3.2.1.1. The transient balance equations are summarized below:

Mass balance of the gas phase:

$$\frac{\partial \rho_g}{\partial t} = -\frac{\partial (w_z \rho_g)}{\partial z} + s\frac{(1-\epsilon_b)}{\epsilon_b}(\rho_g v)' + \sum_{i=v,a} s\frac{(1-\epsilon_b)}{\epsilon_b}\left\{\beta_i'[(\rho_g Y_i)' - (\rho_g Y_i)]\right\} \quad (3.15)$$

Mass balance of gas species i:

$$\frac{\partial (\rho_g Y_i)}{\partial t} = -\frac{\partial (\rho_g Y_i w_z)}{\partial z} + \frac{\partial}{\partial z}\left(\rho_g D_{z,i}\frac{\partial Y_i}{\partial z}\right) + s\frac{(1-\epsilon_b)}{\epsilon_b}\left\{(\rho_g Y_i v)' + \beta_i'[(\rho_g Y_i)' - (\rho_g Y_i)]\right\} \quad (3.16)$$

Momentum balance:

$$\frac{\partial (\rho_g w_z)}{\partial t} = -\frac{\partial (\rho_g w_z w_z)}{\partial z} - \frac{\partial p}{\partial z} - f_1 w_z - \epsilon_b f_2 w_z |\vec{w}| + 2\frac{\partial}{\partial z}\left(\mu_{eff}\frac{\partial w_z}{\partial z}\right) \quad (3.17)$$

Energy balance:

$$\rho_g c_{p,g}\frac{\partial T_g}{\partial t} = -\rho_g c_{p,g} w_z \frac{\partial T_g}{\partial z} + \frac{\partial}{\partial z}\left(\Lambda_z \frac{\partial T_g}{\partial z}\right) - s\frac{(1-\epsilon_b)}{\epsilon_b}\left[\left((\rho_g c_{p,g} v)' + \alpha'\right)(T_g - T_p')\right] \quad (3.18)$$

Temperature, density and pressure are coupled through the equation of state.

In contrary to the HQCM, intra-particle transport phenomena are taken into account in the RPM therefore the net mass flux leaving the particles (with velocity v') appears in the mass balances. This mass flux is resulting from water evaporation inside the solid particles. However in case of the momentum balance, due to assumed 1D-spherically symmetric nature of the particles, the convective source term can be neglected. The major differences between the RPM and the HQCM in modeling of the interstitial gas phase are the convective heat and mass tarnsfer from the particle domain that appeared in mass and energy balances.

3.2.2.2 Particle domain: single particle

The comprehensive single particle drying model presented in Section 2.2 is used for modeling of the particle scale in the RPM. Some extra simplifications are applied in the particle model coupled to the reactor model that will be discussed in Chapter 5.

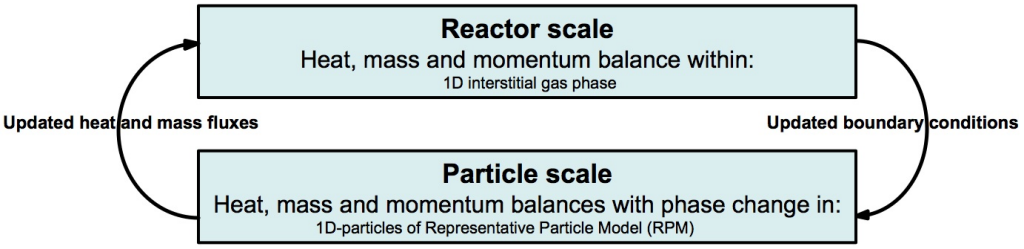

Figure 3.5: *Two-way coupling between particle and reactor scales in the RPM.*

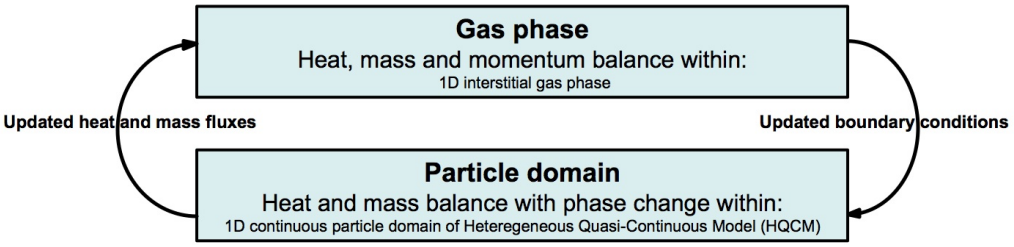

Figure 3.6: *Two-way coupling between gas phase and particle domain in the HQCM.*

3.2.3 Boundary conditions

At the reactor scale, as boundary conditions ($t > 0$), uniform plug flow is assumed at the inlet and atmospheric pressure at the reactor outlet. For other scalar variables, Dirichlet boundary conditions are used at the inlet, whereas Neumann conditions are used at the outlet. The reactor wall is assumed to be isolated. Both models chosen here for description of the drying process inside the reactor are classified in two-phase category of the mathematical models. The governing equations of each phase are coupled and solved simultaneously. Fig. 3.2 and Fig. 3.4 show the interaction between phases including heat and mass transfer in both considered models. Since two solution domains, one for the interstitial gas phase and another for the particle domain, are considered for simulation of fixed-bed drying by two-phase models therefore the boundary conditions at the interface between the phases must be defined in addition to the boundary conditions at reactor scale. Fig. 3.5 and Fig. 3.6 show two-way coupling between the solutions resulting from each scale (phase) in the RPM and the HQCM, respectively. The governing equations of the interstitial gas phase from the reactor scale and the equations of the particle domain from the particle scale are properly coupled via the boundary conditions at the interface. The interaction between phases along with the inter-particle transport phenomena must be taken into account to define the boundary conditions at the interface of the phases.

As above mentioned, in the heterogeneous quasi-continuous model the particles are considered zero dimensional and whole particle domain is assumed as a continuum medium so that inter-particle heat transport is modeled by a Fourier-type term in the energy balance of particle domain. But in the RPM, It is tried to capture more phenomena occurring in the fixed-bed reactor, discussed in Section 3.1. For calculation of inter-particle heat transport between the surfaces of two contacting particles Slavin et al. [93] considered four distinct modes of heat transfer: gaseous conduction in an inner and an outer region, and solid conduction through the contact. Expressing the inter-particle heat transfer between contacting hemispheres in terms of conductance (G) as in [93], the energy balance of the particle surface is given as Eq. (3.19). If the representative particle is located at the axial position k in a one-dimensional reactor being in contact with neighbor particles in upstream and downstream directions then $T'_{p,k+1}$ ($T'_{p,k-1}$) is the surface temperature of the next representative particle in upstream (downstream) direction. $T'_{p,up}$ ($T'_{p,down}$) is the surface temperature of a neighbor particle in upstream (downstream) direction which can be determined by interpolation between two representative particles (i.e. between $T'_{p,k}$ and $T'_{p,k+1}$ ($T'_{p,k-1}$)). For determination of the different conductances the reader is referred to [93].

$$\lambda'_p\Big(\frac{\partial T_p}{\partial r}\Big)' A_p = \alpha'(T'_p - T_{g,k})A_p + G_{up}(T'_p - T'_{p,up}) + G_{down}(T'_p - T'_{p,down}) \qquad (3.19)$$

Inter-particle mass transfer is not considered in the RPM of this study. Gas mass fractions Y'_i at the external particle surface is calculated from the gas species mass balance at this point by:

$$\rho'_g D'_i\Big(\frac{\partial Y_i}{\partial r}\Big)' A_p = \beta'_i[(\rho_g Y_i)' - (\rho_g Y_i)_k]A_p \qquad (3.20)$$

It is worth pointing out that the boundary conditions considered for the particle scale in the RPM of this work, is type 2 discussed in Section 2.2.4.

Chapter 4

Numerical solution methods

Two mathematical models for fixed-bed drying of the hygroscopic porous particles have been discussed in chapter 3; the heterogeneous quasi-continuous model (HQCM) and the representative particle model (RPM). Each of these models includes a system of partial differential equations (PDEs), ordinary differential equations (ODEs) and algebraic equations (AEs). A similar system of equations is governed for single particle drying presented in chapter 2. In this chapter, different numerical solution methods used for solving these systems of equations at single particle scale as well as reactor scale are presented.

4.1 Numerical procedure for particle model

In the model equations of single particle drying presented in chapter 2, Darcy's law is a spatial ODE, equation of state is an AE and mass and energy balance equations are PDEs. By substitution of AEs and ODEs in the PDEs a system consisting of PDEs is resulted. The method of line is used to convert this PDEs system to a system of ODEs. By this technique all terms of the equations in the PDEs system are discretized but time derivatives that are kept unchanged. The discretization is done by a finite volume scheme. The convective terms are discretized with the upwind differencing scheme (UDS) whereas the diffusive and conductive terms are discretized with the second order central differencing scheme in this thesis. Since the model is going to be solved for spherical as well as slab shape of the particle therefore the adequate shape factors should be considered for different geometries in the discretization. A staggered grid is used for the description of the one-dimensional solution domain for the spherical and slab shape particles. The velocity is calculated at cell edges, while the scalar variables including pressure, densities, mass fractions

and temperature are calculated at the cell centers. For the coefficients of the convective terms, upstream weighting is used because the calculation face lies at the cell edges while for the coefficients of other terms, the average of two neighbor nodal points is used because the calculation face lies at the middle of the cell.

The resulting system of ODEs can be integrated by different numerical solution methods. Anca-Couce and Zobel [94] studied different numerical solution methods for such a system of ODEs used for description of pyrolysis of single biomass particle. Among four numerical methods studied by them [94], two methods that showed better efficiency under the conditions of coupling of a particle model to a reactor model are studied for solving a particle drying model, in this thesis.

4.1.1 One-step ODEs solver: LIMEX

It was concluded by Anca-Couce and Zobel [94] once a single particle model with constant boundary conditions is not coupled to a reactor model and has no limitation to the maximal time step then the multi-step ODEs solver is the fastest solver. When the particle model is coupled to a reactor model then its boundary conditions would be variable and also its maximal time step would be limited to the time step of the reactor model. In this case in each time step, the solver of particle model must give a solution to the reactor model. Typical time steps used by reactor solvers for fixed-bed thermo-chemical processes of biomass particles are in the order of milliseconds [89, 95]. Anca-Couce and Zobel [94] showed that at this order of time steps, one-step solver such as LIMEX is faster than multi-step solver because the initialization step is done easier by a one-step solver. LIMEX [96] is a one-step solver that is able to handle the stiff system of equations. This solver has been used for solving the model of thermo-chemical processes, including drying, of single biomass particle [97, 98]. Wurzengerger et al. [21] used this method for thermal conversion of biomass for particle as well as reactor models. Despite the fact that in comparison to the multi-step solver, the initialization step is done faster by LIMEX but still the need to the initialization and calculation of a new Jacobian at each time step is the most time-consuming task of this solver.

4.1.2 Iterative solution method

For a case that the particle model is coupled to a reactor model and its boundary conditions must be updated in each time step, an iterative solution method was proposed by Anca-Couce and Zobel [94]. This method was developed similar to

the iterative solution method used by Mermoud et al. [99] and Di Blasi [100] for simulation of thermo-chemical conversion of biomass particle. Di Blasi [100] used similar iterative solution method for simulation of high-temperature drying of wood particle. In this thesis the iterative solution method developed by Anca-Couce and Zobel [94] is employed for solving the model equations of drying of woody biomass particle, discussed in chapter 2. The system of ODEs are solved with the operator splitting technique. The characteristic time of each phenomenon involved in the model equations is evaluated and then the most appropriate solution method is employed for each equation based on its characteristic time. Moghtaderi [101] calculated the characteristic times of different phenomena involved in pyrolysis of a biomass particle at two different temperatures. Anca-Couce and Zobel [94] calculated the characteristic times of different phenomena during pyrolysis of a wood particle under fixed-bed as well as fluidized-bed conditions. Tab. 4.1 shows the characteristic times of different phenomena involved in drying of a woody biomass particle. These values are calculated with the length of the control volume (H) of 10^{-4} m. As already mentioned in chapter 2, a broad range of values was reported for each property of wood in the literature. The characteristic times of Tab. 4.1 are calculated based on the values of parameters involved in wood drying, presented in Tab. 4.2. These characteristic times are considered as the criteria for making the decision of the most suited method (explicit or implicit) to solve each phenomenon in simulation of wood drying, in this study.

In this iterative method, the transport phenomena that have rather low characterstic time such as convection and diffusion of water vapor as well as conduction term are solved by semi-implicit method so that some part of the equation is solved implicitly and some others explicitly. The driving force of each phenomenon including temperature-, concentration- and pressure gradient are solved implicitly. In the convection term of water vapor, the part including the pressure wave that is called Darcy convection in Tab. 4.1 is solved implicitly while the other part of this term that is called Courant convection, has big enough characteristic time to be solved with an explicit method. The convection term of free water and the diffusion of bound water are solved explicitly. Reaction characteristic time of the evaporation under the pure drying conditions is of the order of second, therefore the evaporation term can be solved explicitly. By taking advantage the Tri-Diagonal-Matrix Algorithm (TDMA) in solving the equations by semi-implicit method, the required computational time of using a semi-implicit solution method is not too higher than the solution time of an explicit method. Fig. 4.1 shows the flow chart of employed iterative method . In each time step n, after updating the properties, the pressure equation (Eq. 4.1), resulting from combining the equation of state, Darcy's Law and

Table 4.1: *Characteristic times*

Phenomenon	Characteristic time (s)	Solution method
Evaporation ($\rho_v/\dot{\omega}_v$)	2.7	Explicit
Darcy convection of gas ($\mu_g H^2/(\mathbf{K}_g \mathbf{K}_{rg} p_0)$)	$3.0{\cdot}10^{-4}$	Implicit
Courant convection of gas (H/V_g^{max})	$2.0{\cdot}10^{-1}$	Explicit
Convection of free water (H/V_{fw}^{max})	250	Explicit
Conduction ($\overline{\rho c_p} H^2/k_{\mathrm{eff}}$)	$5.0{\cdot}10^{-2}$	Semi-implicit
Diffusion of water vapor (H^2/D_v^{eff})	$1.0{\cdot}10^{-2}$	Semi-implicit
Diffusion of bound water (H^2/D_{bw})	1000	Explicit

continuity for the gas phase, is solved to advance the gas pressure. This gas pressure can be calculated with the TDMA solving Eq. (4.2). The pressure of liquid phase is updated by new gas pressure. Using Darcy's law, the velocity of gas phase as well as the velocity of free water in the next time step are calculated via these predicted pressures. Gas species balance, moisture mass balance and energy balance equations are solved with above mentioned operator splitting technique. Finally, the equation of state is applied to obtain the gas pressure of the new time step n+1. The difference between the predicted gas pressure at intermediate step, calculated with Eq. (4.2), and the gas pressure of the new time step n+1 calculated with the equation of state, is considered as the convergence criterion. If the sum of the absolute values of these differences for all control volumes is lower than 0.01 Pa then the convergence criterion is satisfied otherwise the iteration continues with updated approximations of $(\epsilon_g M_g/(R_o T))^{n+1}$ resulting from the current iteration.

$$\frac{\partial}{\partial t}\Big(\epsilon_g \frac{P_g M_g}{R_o T}\Big) + \frac{\partial}{\partial r}\Big(-\frac{P_g M_g}{R_o T}\frac{\mathbf{K}_g \mathbf{K}_{rg}}{\mu_g}\frac{\partial P_g}{\partial r}\Big) = \dot{\omega}_v \tag{4.1}$$

$$\Big[\Big(\frac{\epsilon_g M_g P_g}{R_o T}\Big)^{n+1} - \Big(\frac{\epsilon_g M_g P_g}{R_o T}\Big)^{n}\Big]/\Delta t + \frac{\partial}{\partial r}\Big(-\rho_g^n \frac{\mathbf{K}_g^n \mathbf{K}_{rg}^n}{\mu_g^n}\frac{\partial P_g^{n+1}}{\partial r}\Big) = \dot{\omega}_v^n \tag{4.2}$$

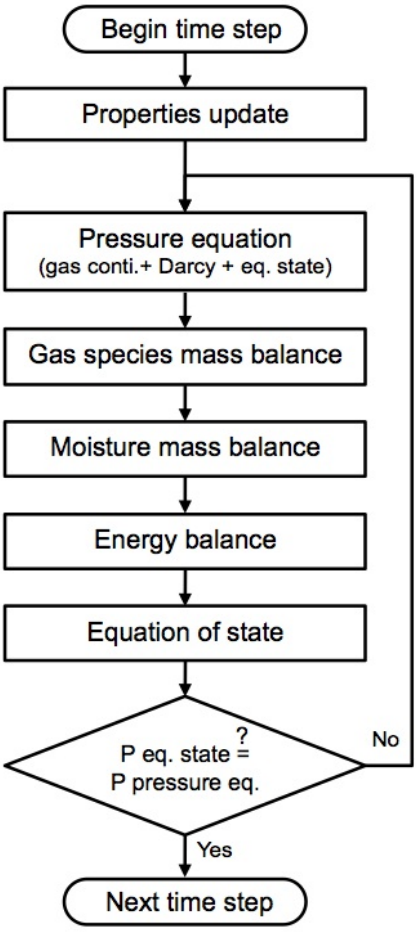

Figure 4.1: *Flow chart of the iterative solution method.*

Table 4.2: *Typical properties of wood used in calculation of characteristic time*

Parameter	Value	Unit	reference
μ_g	10^{-6}	$[kgm^{-1}s^{-1}]$	[101]
$\mathbf{K}_g$	$5.0{\cdot}10^{-15}$	$[m^2]$	[57]
$\mathbf{K}_{rg}$	$6.48{\cdot}10^{-1}$	[-]	[10]
p_0	101325	$[Nm^{-2}]$	standard
V_g^{max}	$5.0{\cdot}10^{-4}$	$[ms^{-1}]$	[44] and [102]
V_{fw}^{max}	$4.0{\cdot}10^{-7}$	$[ms^{-1}]$	[44] and [102]
$\overline{\rho c_p}$	10^6	$[Jm^{-3}K^{-1}]$	[45]
k_{eff}	$2.0{\cdot}10^{-1}$	$[Wm^{-1}K^{-1}]$	[59]
D_v^{eff}	10^{-6}	$[m^2s^{-1}]$	[101]
D_{bw}	10^{-11}	$[m^2s^{-1}]$	[59]

4.2 Numerical procedure for reactor model

Jakobsen et al. [95, 103] used a numerical method for the simulation of dynamic reactive flows in chemical reactors. The model equations of reactive flows in a fixed-bed chemical reactor were solved by a modular method enabling a split between the flow- and chemistry model parts. Then a fractional-step algorithm was employed with an an-elastic filter for solving the flow part of the model. The model equations of the chemistry part were solved by using the operator splitting integration steps. Zobel [89] and Anca-Couce et al. [91] have extended this integration algorithm with the inclusion of the particle solution for multi-scale simulation of fixed-bed thermo-chemical conversion of biomass particles. In this section, this extended numerical method is used for solving two mathematical models for fixed-bed drying of wet solid particles discussed in chapter 3, the HQCM and the RPM.

The governing equations of the reactor scale are discretized by a finite volume scheme, as it was done for the single particle scale. A staggered grid is used for the description of the cylindrical domain of the reactor. For more details about the discretization and numerical solution methods used at reactor scale, the reader is referred to [91, 95, 103]. The solution algorithm is sketched in four steps as shown in Fig. 4.2 that its steps are described as following:

1) The velocity and pressure fields of the next time step are calculated by solving the momentum equation and a temporary time-independent version of the continuity equation. By a fractional-step method, a form of the momentum equation (Eq. (4.3)) including the pressure gradient (free of sound wave) is used for advancing the velocity field ($\mathbf{v}^*$). The sound wave part of momentum equation is considered in a separate equation (Eq. (4.4)). By combining Eq. (4.5), resulting from taking the divergence of Eq. (4.4), and an equation (Eq. (4.6)) resulting from applying an an-elastic filter to the continuity equation, pressure Poisson equation (Eq. (4.7)) is obtained. The pressure field in the next time step (P^{n+1}) is calculated via pressure Poisson equation and then the corrected velocity in the next time step ($\mathbf{v}^{n+1}$) is calculated via Eq. (4.4).

$$\frac{\rho_g^n \mathbf{v}^* - \rho_g^n \mathbf{v}^n}{\Delta t} = H^n - F^n - \nabla p^n \tag{4.3}$$

$$\frac{\rho_g^n \mathbf{v}^{n+1} - \rho_g^n \mathbf{v}^*}{\Delta t} = -\nabla(p^{n+1} - p^n) \tag{4.4}$$

$$\frac{\nabla \cdot (\rho_g^n \mathbf{v}^{n+1}) - \nabla \cdot (\rho_g^n \mathbf{v}^*)}{\Delta t} = -\nabla^2(p^{n+1} - p^n) \tag{4.5}$$

$$\frac{\partial \rho}{\partial t} = 0 = R_c^n - \nabla \cdot (\rho_g^n \mathbf{v}^{n+1}) \tag{4.6}$$

$$-\nabla^2(p^{n+1} - p^n) = \frac{R_c^n - \nabla \cdot (\rho_g^n \mathbf{v}^*)}{\Delta t} \tag{4.7}$$

Where H represents the convective and viscous terms and F the friction. R_c represents the source term of the continuity equation including mass flow coming from the particle domain. The particle domain is treated as a continuous phase in the HQCM while in the RPM the solution of particle model is coupled to the interstitial gas phase. The source term of gas continuity equation, R_c^n, for these two reactor models are given by:

$$R_c^n \mid_{HQCM} = \sum_{i=v,a} (-s(1-\epsilon_b)\left(\beta_i'[(\rho_g Y_i)'^n - (\rho_g Y_i)^n]\right)) \tag{4.8}$$

$$R_c^n \mid_{RPM} = \sum_{i=v,a} (-s(1-\epsilon_b)\left(\beta_i'[(\rho_g Y_i)'^n - (\rho_g Y_i)^n]\right)) + s\frac{(1-\epsilon_b)}{\epsilon_b}(\rho_g v)'^n \tag{4.9}$$

2) The distribution of temperature as well as component densities of the gas phase in the next time step along the height of the reactor are calculated by the integration of the transport equations in the interstitial gas phase using operator splitting. The transport equations are splitted to some operators determining different parts of these equations including conduction, convection, diffusion and source terms. These predefined operators are successively applied to the transport equations by intermediate time integrations so that the intermediate solution of the first operator is used in the second operator, and so on. The source terms, R_{gs} and R_T, in the transport equations are calculated by simultaneously solving of the equations of the particle domain part, the same as calculation of the source term, R_c, in the continuity equation in the step 1.

$$\frac{\rho_{g,i}^* - \rho_{g,i}^n}{\Delta t} = -\frac{\partial[(\rho_g Y_i)^n w_z^{n+1}]}{\partial z} \tag{4.10}$$

$$\frac{\rho_{g,i}^{**} - \rho_{g,i}^*}{\Delta t} = \frac{\partial}{\partial z}\left((\rho_g D_z)^n \frac{\partial Y_i^{**}}{\partial z}\right) \tag{4.11}$$

$$\frac{\rho_{g,i}^{n+1} - \rho_{g,i}^{**}}{\Delta t} = R_{gs}^{n+1} \tag{4.12}$$

$$\frac{\rho_{g,i}^{n+1}-\rho_{g,i}^{n}}{\Delta t}=-\frac{\partial[(\rho_g Y_i)^n w_z^{n+1}]}{\partial z}+\frac{\partial}{\partial z}\left((\rho_g D_z)^n\frac{\partial Y_i^{**}}{\partial z}\right)+R_{gs}^{n+1} \tag{4.13}$$

$$\frac{T_g^{*}-T_g^{n}}{\Delta t}=-\frac{1}{(\rho_g c_{p,g})^n}(\rho_g c_{p,g})^n w_z^{n+1}\frac{\partial T_g^{n}}{\partial z} \tag{4.14}$$

$$\frac{T_g^{**}-T_g^{*}}{\Delta t}=\frac{1}{(\rho_g c_{p,g})^n}\frac{\partial}{\partial z}\left(\Lambda_z^n\frac{\partial T_g^{**}}{\partial z}\right) \tag{4.15}$$

$$\frac{T_g^{n+1}-T_g^{**}}{\Delta t}=R_T^{n+1} \tag{4.16}$$

$$\frac{T_g^{n+1}-T_g^{n}}{\Delta t}=-\frac{1}{(\rho_g c_{p,g})^n}(\rho_g c_{p,g})^n w_z^{n+1}\frac{\partial T_g^{n}}{\partial z}+\frac{1}{(\rho_g c_{p,g})^n}\frac{\partial}{\partial z}\left(\Lambda_z^n\frac{\partial T_g^{**}}{\partial z}\right)+R_T^{n+1} \tag{4.17}$$

LIMEX solver is used for solving the equations governing on the particle domain part of the HQCM. For the RPM, a comprehensive particle model of drying of a solid particle is coupled to the reactor model. The main disadvantage of coupling such a comprehensive particle model to the reactor model is the high computational time. To decrease the computational time of the simulation of fixed-bed drying process by the RPM, the iterative solution method discussed in section 4.1.2 is used for solving a particle model describing drying of a solid particle. This method was successfully employed for the solution of the particle model coupled to the reactor model in fixed-bed pyrolysis of biomass particles ([91]).

The source term of the species mass balance of the gas phase, R_{gs}^{n+1}, for two reactor models are given by:

$$R_{gs}^{n+1}\mid_{HQCM}= s\frac{(1-\epsilon_b)}{\epsilon_b}\left\{\beta_i'[(\rho_g Y_i)'^{n+1}-(\rho_g Y_i)^{n+1}]\right\} \tag{4.18}$$

$$R_{gs}^{n+1}\mid_{RPM}= s\frac{(1-\epsilon_b)}{\epsilon_b}\left\{(\rho_g Y_i v)'^{n+1}+\beta_i'[(\rho_g Y_i)'^{n+1}-(\rho_g Y_i)^{n+1}]\right\} \tag{4.19}$$

The source term of the energy balance of the gas phase, R_T^{n+1}, for two reactor models are given by:

$$R_T^{n+1}\mid_{HQCM}= \frac{1}{(\rho_g c_{p,g})^n}s\frac{(1-\epsilon_b)}{\epsilon_b}\left[\alpha'(T_g^{n+1}-T_p'^{n+1})\right] \tag{4.20}$$

$$R_T^{n+1} \mid_{RPM} = \frac{1}{(\rho_g c_{p,g})^n} s \frac{(1-\epsilon_b)}{\epsilon_b} \Big[(\rho_g c_{p,g} v T_p)'^{n+1} + \alpha'(T_g^{n+1} - T_p'^{n+1}) \Big] \tag{4.21}$$

3) The mixture gas density is updated by new temperature and gas component densities calculated in previous step, through the equation of state (Eq. (4.22)):

$$\rho_g^* = \frac{p^{n+1} M_m^{n+1}}{\bar{R} T^{n+1}} \tag{4.22}$$

4) By an elastic step, the time-dependent density of mixture gas at next time step is determined from the gas continuity equation:

$$\frac{\rho_g^{n+1} - \rho_g^*}{\Delta t} = -\nabla \cdot (\rho_g^* \mathbf{v}^{n+1}) + R_c^{n+1} \tag{4.23}$$

Where the source term of gas continuity equation at time step n+1, R_c^{n+1}, for two reactor models are given by:

$$R_c^{n+1} \mid_{HQCM} = \sum_{i=v,a} (-s(1-\epsilon_b) \Big(\beta_i' [(\rho_g Y_i)'^{n+1} - (\rho_g Y_i)^{n+1}] \Big)) \tag{4.24}$$

$$R_c^{n+1} \mid_{RPM} = \sum_{i=v,a} (-s(1-\epsilon_b) \Big(\beta_i' [(\rho_g Y_i)'^{n+1} - (\rho_g Y_i)^{n+1}] \Big)) + s \frac{(1-\epsilon_b)}{\epsilon_b} (\rho_g v)'^{n+1} \tag{4.25}$$

The solutions resulting from this four-step scheme for fixed-bed drying under studied conditions in this thesis are stable, similar to the solutions for fixed-bed pyrolysis of wood particles ([91]) and the conversion process of natural gas into synthesis gas ([95, 103]). If this scheme is not stable then a corrector step can be considered following these predictor steps, as presented in [95]. In order to lower the computation costs for simulation of the processes at reactor scale, Jakobsen's group developed a code based on parallelizing the program. They used a continuum model for simulation of the dynamic reactive flows in chemical reactors. Zobel [89] developed a multi-scale model (RPM) by adding the particle model to the continuum model of Jakobsen's group. Anca-Couce [92] optimized the latter by introducing an efficient iterative method for the solution of particle model and applied it on fixed-bed pyrolysis of wood particles. In this thesis, the parallelized code of Jakobsen's group, after optimizing by introducing a new momentum equation, is used

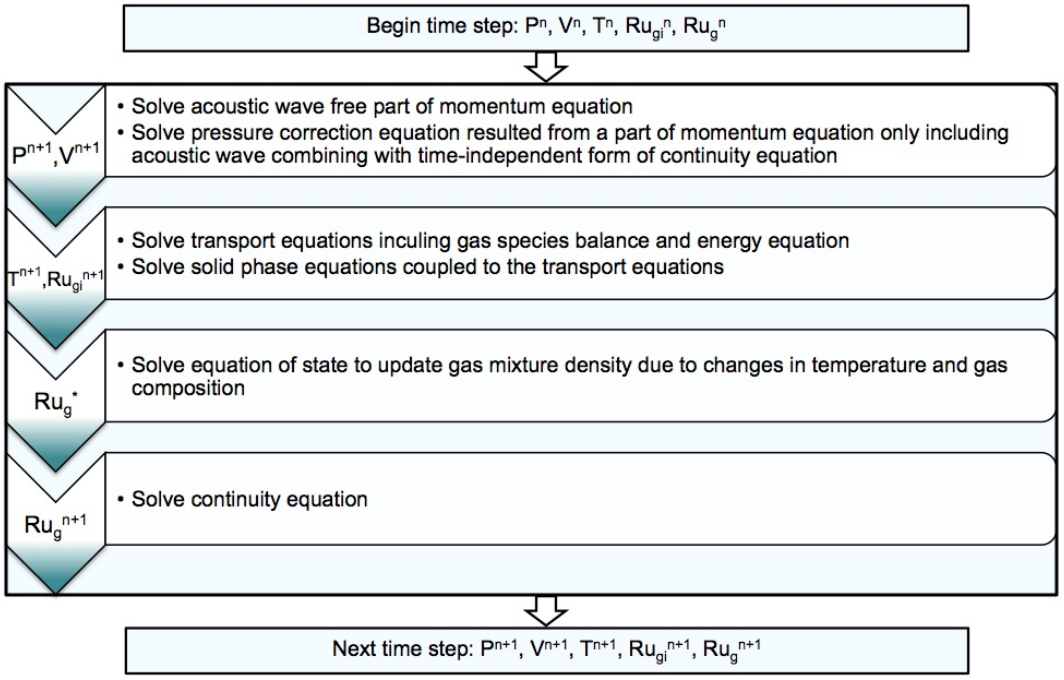

Figure 4.2: *Fractional-step algorithm for reactor model.*

for solving the interstitial gas phase at the reactor scale for both the HQCM and the RPM. The drying particle model solved by an iterative method is coupled to the reactor scale through the RPM. In the HQCM, the continuous particle domain solved by LIMEX solver is coupled to the interstitial gas phase at the reactor scale. The model equations of the interstitial gas phase are solved with message passing programing (MPI; message passing interface) in a computer cluster at the EVUR with 8 processors.

4.3 Concluding remarks

Two mathematical models considered for modeling fixed-bed drying in chapter 3 are categorized as two-phase models. Numerical solutions of these models are done by coupling the equations of each phase; the interstitial gas phase and the particle domain. The equations governing on the interstitial gas phase are solved by a fractional-step algorithm so that a split is made between flow- and chemistry model parts. The flow part includes the momentum and continuity equations and the chemistry part includes the energy and gas species mass balance equations. Since these two parts reflect different physics therefore in this way more optimal solution methods can be adopted for each operator involved in the equations of these parts. It has been assumed in this study that there is no reaction in the interstitial gas

phase; no heterogeneous reaction nor homogeneous. The particle domain solutions for the HQCM and the RPM are coupled to the solution of transport phenomena of the interstitial gas phase.

For solving equations of the particle domain, two numerical solution methods have been presented; LIMEX solver for the HQCM and iterative method for the particle model of the RPM. The iterative solution method is based on the operator splitting technique so that each phenomenon in the equations is solved by a suitable solution method according to its characteristic time. The characteristic time of each phenomenon involved in the particle model has been calculated based on the typical values of wood drying under the conditions studied in this thesis. It is obvious that for other conditions or different materials, new characteristic times must be calculated to find a suitable solution method for each operator.

Chapter 5

Simulation results

The drying models presented in this study are able to simulate drying of hygroscopic porous materials at particle scale as well as reactor scale. The main focus of this thesis is study of drying process of woody fuel particles, however the applicability of these models are examined for drying of lignite particles too. Wood and lignite particles are widely used as fuel particles although the high initial moisture content of these feedstocks unfavorably impact the energy efficiency of their conversion processes. That's why the pre-drying is usually an unavoidable stage in processing of such fuel particles. As before mentioned, an accurate description of the drying characterstic is required for optimal design of dryers and reactors for thermo-chemical conversion of these fuel particles. Simulation results of drying of wood and lignite particles resulted from some mathematical models using different numerical procedures at particle as well as reactor scale are presented in this chapter, as listed in Tab. 5.1. All codes are written in Fortran.

5.1 Single particle drying

At single particle scale firstly the computational performance of a drying model formulated based on Whitaker's model, discussed in chapter 2, is verified. Afterwards,

Table 5.1: *Simulations results of drying of solid fuel particles*

Scale	Model	Numerical method	Feedstock	Case study
Particle	Whitaker	LIMEX	Wood & Lignite	[14], [45], [57] & [102]
		Iterative		
Reactor	HQCM	Fractional-step + LIMEX	Wood & Lignite	[34], [32] & [104]
	RPM	Fractional-step + Iterative		

The effect of different values of model parameters on the presented drying model is studied and the most significant parameters affecting the model output are determined. The capability of presented particle drying model is examined for predicting single particle drying based on experimental data ans simulation results of wood and lignite drying from the literature.

5.1.1 Verification of model's computational performance

A comparison to the numerical simulation results of Gronli [45] is made to verify if (1) the model equations are implemented correctly and (2) the numerical solution procedure used in this study is appropriate. Gronli's numerical results are chosen as a benchmark because he used a complete set of Whitaker's formulation including almost all phenomena taking place during drying of a wood particle, as in this thesis. He presented the model predictions for a one-dimensional simulation of pyrolysis of a wet wood pellet with an initial moisture content of 0.3 $kg/kg(d.b)$ and a length of 0.06 m, which was exposed to a heat flux of 130 kW/m^2 for 10 minutes. In this study, 152 grid points is considered for the simulation along the half length of the particle (0.03 m), as Gronli did. All model parameters and formulations are the same as reported in Gronli's thesis (page 209) with one exception regarding the calculation of the evaporation rate. While in Gronli's model the evaporation rate equation was formulated implicitly by setting the partial water vapor pressure equal to saturated vapor pressure, in this thesis a mass transfer expression gives the phase change rate of moisture explicitly. Fig. 5.1 shows the comparison between the results obtained in this study and the results of Gronli for the spatial profiles of moisture content, temperature and evaporation rate inside the wet wood particle during pyrolysis and drying processes,under intensive heating conditions after 600 s. The results are in very good agreement. These results show that the presented model is able to perfectly predict the gradients of different variables inside the particles. Although, it will be shown in next sections that the reliability of the model predictions are dependent on the correct values of model coefficients and relevant physical properties of the material under study. It's worth mentioning that the equations of pyrolysis process were added to the model equations of drying based on the equations presented in [45]. The simulation results related to pyrolysis process are not shown here.

5.1.2 Importance of model parameters

The importance of model parameters for drying of a long cylindrical pine wood particle is studied in the section. The particle is considered to be one-dimensional

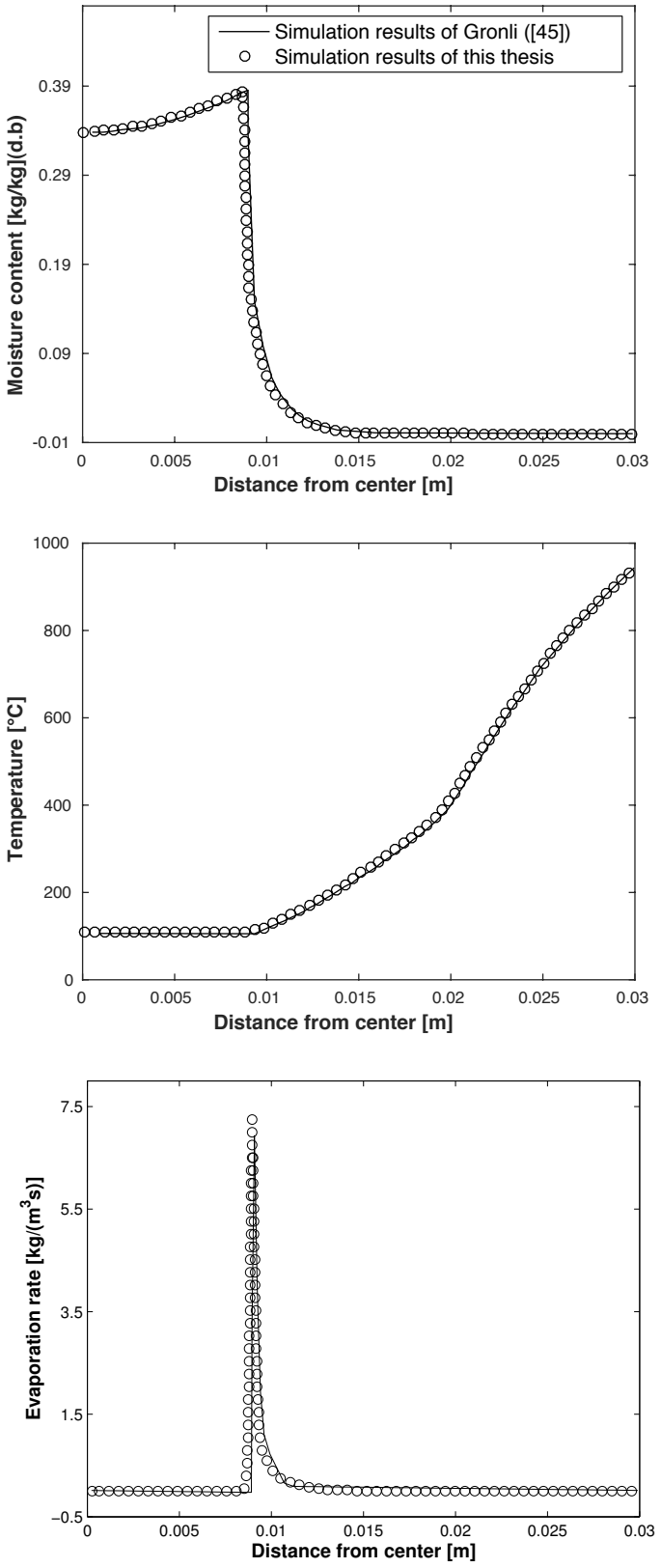

Figure 5.1: *Spatial profiles of moisture content, temperature and evaporation rate inside the particle after 600s*

Table 5.2: *Model inputs for simulation of drying of wood specimen*

Parameter	Correlation/Value	Unit	Reference
$\langle \rho_{SD} \rangle$	450	(kgm^{-3})	[105]
T_{bc}	423	(K)	-
ϵ	0.7	(-)	[105]
P_{atm}, P_{bc}	101325	(Nm^{-2})	-
M_{init}	0.8	$(kgkg^{-1})$	[105]
α	$5.69 + 0.0098\,T_{bc}$	$(Wm^{-2}K^{-1})$	[25]
β	$\frac{\alpha}{950}$	(ms^{-1})	[13]
r_p	0.0125	(m)	-
M_{fsp}	0.598-0.001 T	$(kgkg^{-1})$	[106]
$h(M_{\text{bw}}, T)$	$1 - (1 - \frac{M_{\text{bw}}}{M_{\text{fsp}}})^{6.453 \cdot 10^{-3}\,T}$	(-)	[45]
$P_v^{sat}(T)$	$\exp(24.1201 - 4671.3545\,T^{-1})$	(Nm^{-2})	[107]
$\triangle\, h_w$	$3.1749 \cdot 10^6 - 2460\,T$	(Jkg^{-1})	[107]
$\triangle\, h_{\text{sorp}}$	$400 \triangle\, h_w (1 - \frac{M_{\text{bw}}}{M_{\text{fw}}})^2$	(Jkg^{-1})	[57]

in radial direction. Physical properties of the wood particle as well as initial and boundary values are chosen so that they are representing typical values of pine wood and typical conditions of drying of wood chips in industrial dryers, listed in Tab. 5.2. For the nine model parameters, different correlations and values from the literature collected in chapter 2 and the appendix are used. All other coefficients and properties are taken from [45]. At first, the effect of these nine model parameters on the model output are evaluated under two extreme scenarios. Then by sensitivity analysis, the impact of variation of each parameter on the model output is studied.

5.1.2.1 Extreme scenarios

Since the drying time is one of the most important output parameter in the drying process, this quantity is considered as the model output. The drying time is calculated according to the approximation that the particle is supposed to be dried when its average moisture content reaches 0.001. This value (0.001) is selected, as in [12], to avoid wasting computational time and numerical problems around zero moisture content. By plotting different empirical expressions and comparing different values over the conditions of this study, maximum and minimum values of each transport coefficient were determined in chapter 2. Thanks to sensitivity analysis conducted previously [9, 11, 12] the qualitative effect of variations of effective thermal conduc-

tivity, capillary pressure, bound water diffusivity, effective diffusivity of water vapor and permeability on the drying time are known. Based on this information and reasoning, two extreme scenarios according to two sets of nine empirical correlations and values for model parameters are defined. In one scenario, Tab. 5.3, the maximum drying time is obtained and in the other one, Tab. 5.4, the minimum drying time is resulted.

The grid-independence study is done by increasing the number of grid points from 30 to 60, 120 and 240. By choosing 120 grid points the numerical solution is almost independent of the mesh. Order of reduction of the error is calculated based on Richardson extrapolation method [108] for two extreme scenarios as well as the reference case (later defined). For the cases of maximum drying time, reference and minimum drying time based on 120 grid points, order of reduction of the errors are 0.955, 0.914 and 0.973, respectively, and the total discretization errors are 1.35%, 1.62% and 1.95%, respectively. The errors obtained with 120 grid points are small enough in comparison to the differences obtained in total drying time with the different inputs employed in this work. The results are presented based on 120 grid points. The temporal resolution is determined by the LIMEX solver, as explained in [109].

In Fig. 5.2 numerical simulation results of moisture loss dynamics during drying of a pine wood particle are shown. They are resulting from two extreme scenarios. The maximum drying time is 16.45 times bigger than the minimum drying time. As it can be seen, using the model parameters arbitrarily from the literature can lead to a significant inaccuracy of the predicted drying time. This big difference between maximum and minimum drying time is the response of the studied model against these two extreme scenarios. This shows that two researchers can obtain two numerical simulation results with up to 16 times difference, although both of them can correctly argue that they have used properties of pine wood that are reported in the literature. It should be emphasized that all model parameters considered in this study have been established for only one type of wood: pine. It can be expected that the range of predicted drying times is even bigger if parameters of different types of wood are used.

Despite this significant uncertainty inherent in wood drying models, it was shown in previous studies that modeling results and experimental results agree very well, even if the parameters that have been used were determined for different types of wood. This may in some cases be attributed to the fact that the errors due to simplifications of the physical model on one hand and the errors related to model parameters on the other hand can cancel each other. Considering the findings of this

Table 5.3: *Model parameters for scenario 1 (max. drying time) of modeling*

Model parameter	Correlation/Value	Reference
$k_{\text{eff}}(Wm^{-1}K^{-1})$	$6 \cdot 10^4 \langle \rho_{SD} \rangle \frac{1+M}{1+0.15} - 0.166$ If$(M > M_{\text{fsp}})$ $6 \cdot 10^4 \langle \rho_{SD} \rangle \frac{1+M}{1+0.44\,M} - 0.166$ If$(M \leq M_{\text{fsp}})$	[42]
$C_p(Jkg^{-1}K^{-1})$	$\frac{1113+4.85T+4185\,M}{1+M}$	[10, 47, 58]
$D_{bw}(m^2s^{-1})$	$\exp(-12.8183933 + 10.8951601\,M_{\text{bw}} - \frac{4300}{T})$	[110]
$D_v^{\text{eff}}(m^2s^{-1})$	$10^{-3}[1.192 \cdot 10^{-4}(\frac{T^{1.75}}{P})]$	[10]
$P_c(Nm^{-2})$	$(77.5 - 0.185(T - 273)) \cdot 10^{-3} \cdot [\frac{3150}{S+10^{-4}} -$ $\frac{1047+3.368\langle \rho_{SD} \rangle}{1.02-S} + 149.8\langle \rho_{SD} \rangle (1 - S)$ $+52350 + 168.4\langle \rho_{SD} \rangle - \frac{3150}{1+10^{-4}}]$	[111]
$\mathbf{K}_g(m^2)$	$5 \cdot 10^{-18}$	[59]
$\mathbf{K}_l(m^2)$	$0.1\,\mathbf{K}_g$	[57]
$\mathbf{K}_{rg}(-)$	$0.95(1 - \frac{M_{\text{fw}}}{M_{cr}})^2 + 0.05$ If $(0 < M_{fw} < M_{cr})$ $0.05\frac{M_{sat}-M_{\text{fw}}}{M_{sat}-M_{cr}}$ If $(M_{cr} < M_{\text{fw}} < M_{sat})$	[59]
$\mathbf{K}_{rl}(-)$	$S^{0.5}[1 - (1 - S^{\frac{1}{m}})^m]^2$, $m = (1 - \frac{1}{1.921})$	[55]
	$M_{sat} = 1.33, M_{cr} = 0.8$	

Table 5.4: *Model parameters for scenario 2 (min. drying time) of modeling*

Model parameter	Correlation/Value	Reference
$k_{\text{eff}}(Wm^{-1}K^{-1})$	$1.5\,(0.142 + 0.46\,M)$	[47]
$C_p(Jkg^{-1}K^{-1})$	$\frac{C_{pw}\,M+1357}{1+M}$	[112]
$D_{bw}(m^2s^{-1})$	$\exp(-9.9 + 9.8\,M_{bw} - \frac{4300}{T})$	[59]
$D_v^{\text{eff}}(m^2s^{-1})$	$\epsilon^6[1.192 \cdot 10^{-4}(\frac{T^{1.75}}{P})]$	[42]
$P_c(Nm^{-2})$	$\exp(16.38 - 0.3909\,M - 17.761\,M^2 + 21.228\,M^3 - 7.0784\,M^4)$	[55, 113]
$\mathbf{K}_g(m^2)$	$5 \cdot 10^{-15}$	[57]
$\mathbf{K}_l(m^2)$	$10\,\mathbf{K}_g$	[59]
$\mathbf{K}_{rg}(-)$	$1 + (2S - 3)S^2$	[10]
$\mathbf{K}_{rl}(-)$	$0.95(\frac{M_{\text{fw}}}{M_{cr}})^2$, $M_{cr} = 0.8$	[59]
	$M_{cr} = 0.8$	

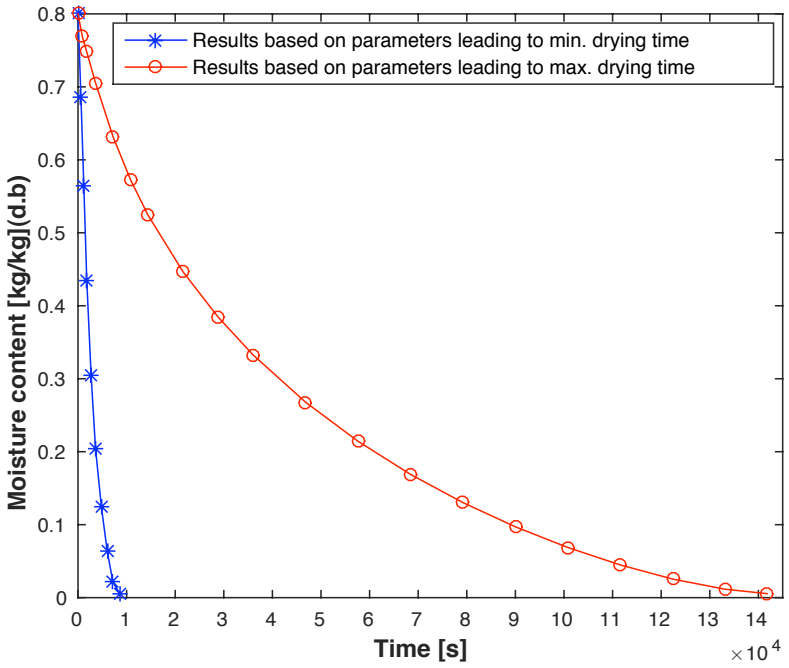

Figure 5.2: *Evolution of average moisture content based on two extreme scenarios of modeling*

section, it may be supposed that the predictions of these models for other conditions than the ones for which they have been evaluated can be rather inaccurate.

5.1.2.2 Global sensitivity analysis

A method for quantifying the impact of model parameters on the model predictions is the sensitivity analysis. The methods of sensitivity analysis can be categorized into local and global. Local sensitivity analysis, based on model derivatives with respect to the parameters, is commonly employed to study the role of model parameters in the model. But when the model parameters are very uncertain and cover a large range, the techniques of local sensitivity analysis are not very useful and global sensitivity analysis is used instead. In the global sensitivity analysis the output variability is evaluated when the model parameters can vary in their whole uncertainty ranges [114]. Sensitivity analysis was applied to wood drying models in several previous works: Plumb et al. [115] showed that their model for low-temperature drying of wood (i.e. the drying takes place below the normal boiling point of water) is very sensitive with respect to the intrinsic gas permeability. Perre et al. [10] showed that the latter is also true for high-temperature drying of wood (which occurs at temperatures above the normal boiling point of water). Di Blasi [12] and Fyhr & Rasmuson [11] have analyzed the sensitivity of their models for high-temperature drying of woody biomass particles for a limited number of physical properties. A

comprehensive sensitivity analysis has been conducted by Nassrallah & Perre [9] on low-temperature drying of wood material.

Most of these sensitivity analyses of wood drying models have been conducted by arbitrarily changing a model parameter irrespective of the relevant uncertainty of this parameter. Fyhr & Rasmuson [11] reported that they considered the relevant uncertainties for the input parameters, but they didn't state how they determined those relevant uncertainties. Gronli [45] although presented an excellent review of empirical correlations and values for physical properties of wood, but he conducted the sensitivity analysis regarding the pyrolysis model, not the drying model. Couture et al. [43] investigated the impact of different correlations for the relative permeabilities of gas and liquid on their model for low-temperature drying of wood material. So far no comprehensive global sensitivity analysis has been conducted which takes into account the whole range of uncertainty reported in the literature for the parameters of a wood drying model.

In this section a global sensitivity analysis is done on the drying model in which the model parameters are changed not by an arbitrary value, but by values according to the range of established correlations for the respective parameter in the literature. The contribution of nine above mentioned model parameters are evaluated to the variation of the model output, i.e., the drying time. The one-at-a-time (OAT) approach is applied to perform the global sensitivity analysis [114, 116]. The effect of variation in each model parameter on the model output is evaluated while the other model parameters are held constant at their base values. Hence, a set of base or reference values of each model parameter is needed. To this end, an intermediate correlation or value of each model parameter is considered as the reference case and shown in Tab. 5.5. The global sensitivity analysis is performed by varying each model parameter (one-at-a-time) from its minimum value to its maximum value. Although some parameters such as relative permeability of gas and liquid may be related to each other, in this work all model parameters are considered to be independent from each other. Following the impact of variation of the model parameters on the model output are presented.

5.1.2.2.1 Effective thermal conductivity and specific heat capacity Fig. 5.3 shows the results of mass loss during drying of a single wood particle for minimum and maximum effective thermal conductivity of wet wood. Although the two correlations differ by a factor of approximately three, the drying time varies only by 14%. This finding is in agreement with the results obtained by Ben Nassrallah & Perre [9], who also concluded that their drying model is not very sensitive to the changes in the effective thermal conductivity parameter. It was shown in Fig. 2.3, the

Table 5.5: *Reference case of model parameters for drying of pine wood on transverse direction*

Model parameter	Unit	Species	Reference
$k_{\text{eff}} = 0.17681 + 0.83535 \cdot 10^{-4} \cdot (T - 273) + 0.2765\, M$	$(Wm^{-1}K^{-1})$	Scotspine	[112]
$C_p = \frac{C_{pw}M+1710}{1+M}$	$(Jkg^{-1}K^{-1})$	Scotspine	[112]
$D_{\text{bw}} = \frac{1}{\langle \rho_{SD} \rangle} \exp[(\frac{-2590.1}{T} + 11.954)M - \frac{1046.63}{T} - 12.35]$	$(m^2 s^{-1})$	Pine	[42]
$D_v^{\text{eff}} = 0.05\epsilon^2[1.192 \cdot 10^{-4}(\frac{T^{1.75}}{P})]$	$(m^2 s^{-1})$	Southern pine	[57]
$P_c = 1.364 \cdot 10^5 \sigma(T)(M_{fw} + 1.2 \cdot 10^{-4})^{-0.63}$	(Nm^{-2})	Softwood	[59]
$\mathbf{K}_g = 4 \cdot 10^{-16}$	(m^2)	Pine (Sapwood)	[43]
$\mathbf{K}_l = \mathbf{K}_g$	(m^2)	Pine	[43]
$\mathbf{K}_{rg} = (\frac{1-S}{1-S_{irr}})^3$	(-)	Pine	[43]
$\mathbf{K}_{rl} = S^3$	(-)	Pine	[43]

$S_{irr} = 0.07$
$\sigma(T) = (1.28 \cdot 10^2 - 0.185T)10^{-3}$

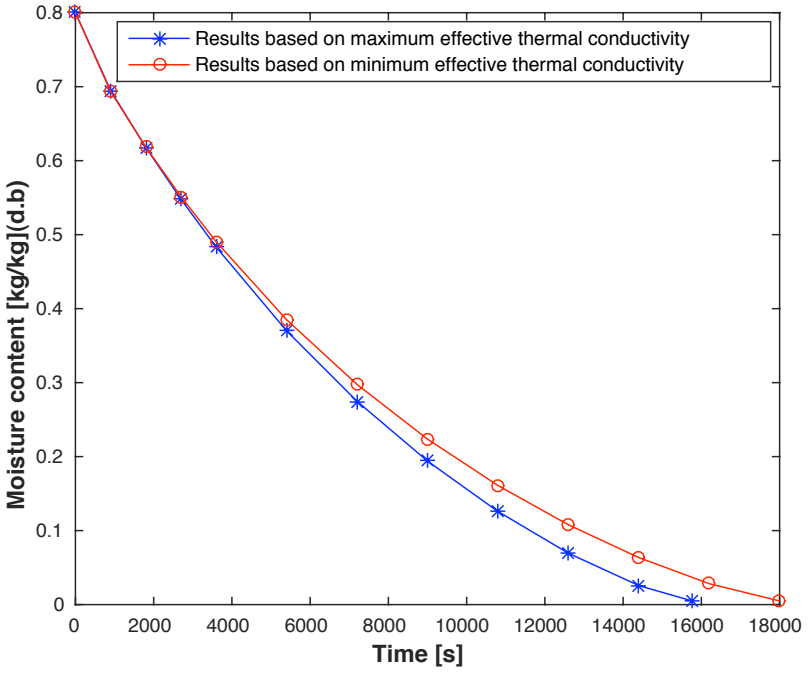

Figure 5.3: *Evolution of average moisture content based on minimum and maximum effective thermal conductivity*

correlations for the specific heat capacity of a wet wood particle differ by a factor of approximately 1.5, but nevertheless the difference in the results is negligible, as shown in Fig. 5.4. Therefore one can use all the expressions for specific heat capacity of wet wood listed in the appendix, for the simulation of the drying of a pine wood particle without a significant error in the model output.

5.1.2.2.2 Diffusive transport coefficients As shown in Fig. 5.5, the effect of the variation of bound water diffusivity on the drying time over the studied conditions is negligible. The ratio of maximum to minimum drying time resulting, respectively, from minimum and maximum value of the diffusion coefficient of bound water is 1.065. Despite of up to three orders of magnitudes difference between maximum and minimum values of the diffusion coefficient of bound water, for some temperatures and moisture contents as shown in Fig. 2.4, the maximum drying time is only 6.5% bigger than the minimum drying time. In contrary to the bound water diffusivity, the variation of effective diffusivity of water vapor causes a significant uncertainty on the predicted drying time, of a factor of approximately two, as shown in Fig. 5.6. This 97% increase of the drying time is actually not in agreement with the results reported by Bonneau & Puiggali [42], who stated that the vapor diffusion has a minor effect on the moisture transport during wood drying. However, Ben Nassarrah & Perre [9] reported that in the case of wood drying, the resistance of

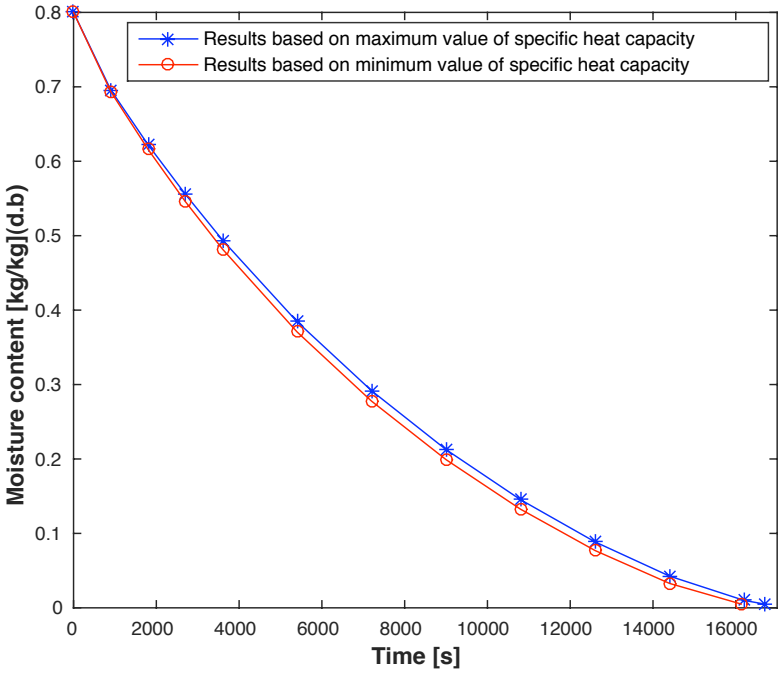

Figure 5.4: *Evolution of average moisture content based on minimum and maximum specific heat capacity*

the porous medium to gaseous migration is very important and showed that their model is sensitive to the changes in effective diffusivity of water vapor. The latter statement is approved with the results obtained in this study.

5.1.2.2.3 Convective transport coefficients

5.1.2.2.3.1 Convective transport coefficients of gas mixture

Fig. 5.7 shows that the ratio of maximum to minimum drying time, associated to the minimum and maximum values of gas intrinsic permeability, respectively, is 2.93. The impact of this parameter on the model output is very remarkable. On the other hand, it was mentioned that this property differs by three to four orders of magnitude, even for one type of wood [56]. Therefore, for reasonable accurate predictions of the drying time, it is recommended that at least the order of magnitude of gas intrinsic permeability is experimentally determined for the wood under examination. Fig. 5.8 shows that three times difference between maximum and minimum value of relative permeability of gas , as shown in Fig. 2.6, is not enough to make a considerable change in the results of the model. Under these conditions the model is not sensitive to the different expressions of the relative permeability of gas listed in the appendix and one can use each of these expressions freely.

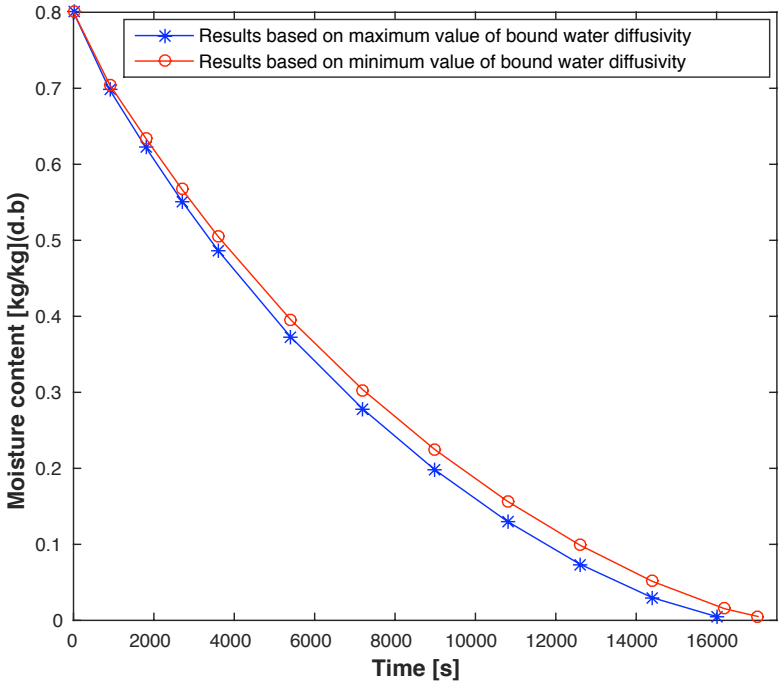

Figure 5.5: *Evolution of average moisture content based on minimum and maximum bound water diffusivity*

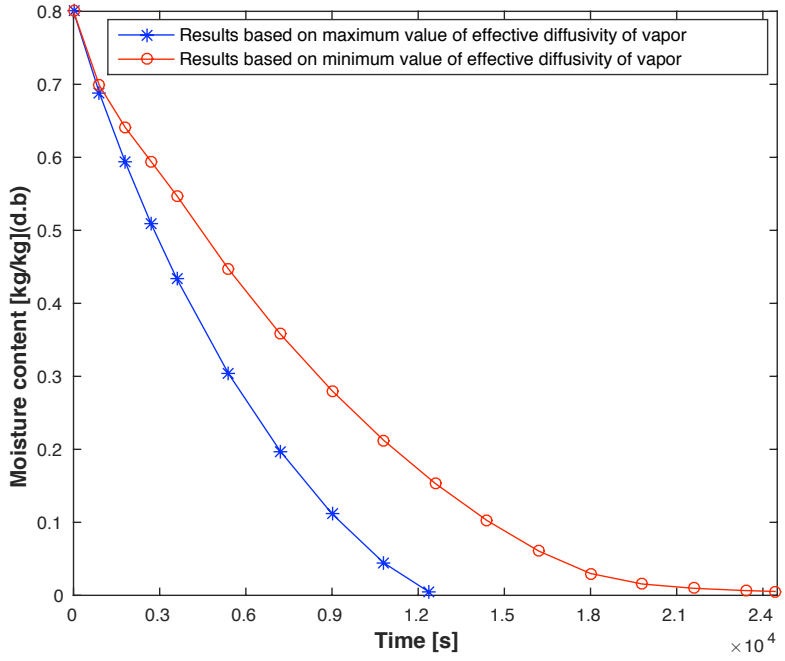

Figure 5.6: *Evolution of average moisture content based on minimum and maximum effective diffusivity of water vapor*

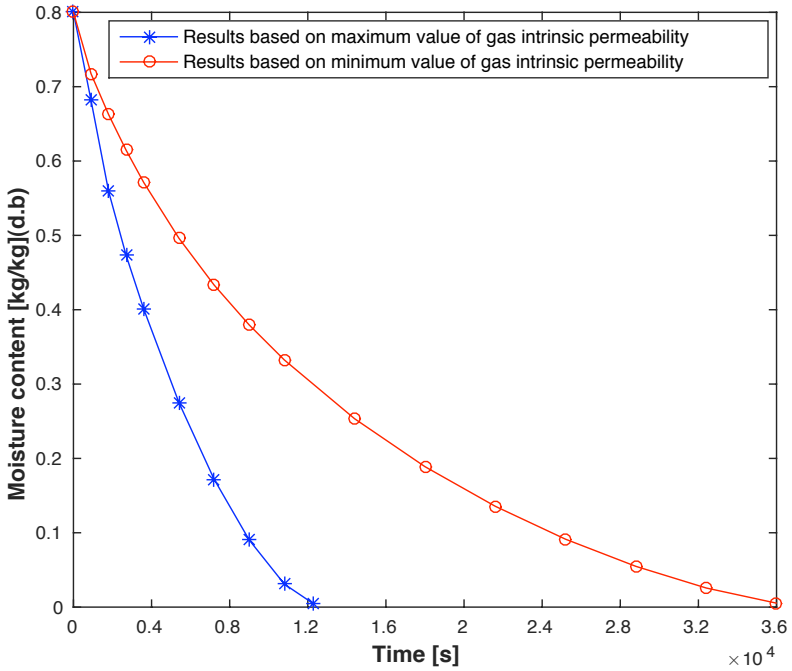

Figure 5.7: *Evolution of average moisture content based on minimum and maximum gas intrinsic permeability*

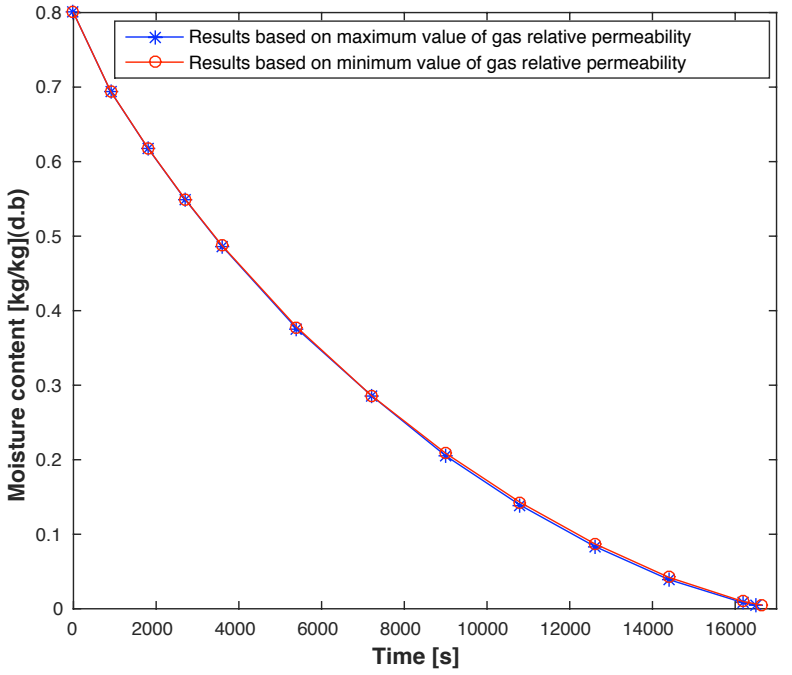

Figure 5.8: *Evolution of average moisture content based on minimum and maximum gas relative permeability*

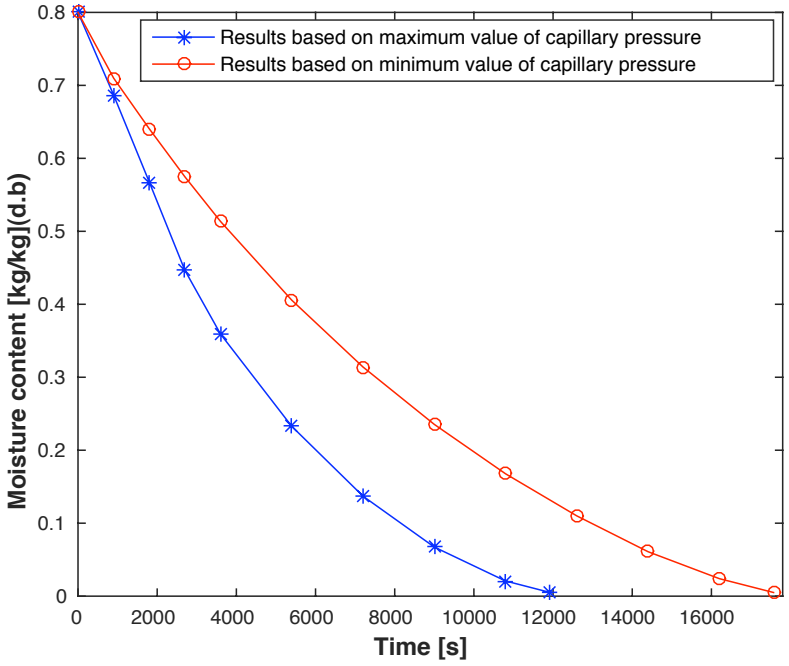

Figure 5.9: *Evolution of average moisture content based on minimum and maximum capillary pressure*

5.1.2.2.3.2 Convective transport coefficients of free water It has been shown in Fig. 2.7 that minimum and maximum capillary pressures in the pores of wood, under studied conditions, range from 10^3 to 10^6 (Pa). This three orders of magnitude difference between capillary pressures affects the drying time considerably. The drying time associated to the maximum value of capillary pressure is 47% bigger than the minimum drying time, as shown in Fig. 5.9. Fyhr & Rasmuson [11] have reported a similar remarkable effect of changes in capillary pressure on their model. The effect of maximum and minimum values of the liquid intrinsic permeability is significant on the model results as shown in Fig. 5.10 and the maximum drying time is 25% bigger than minimum drying time. This considerable sensitivity to not big changes in the value of the parameter can be related to the prominent contribution of the convective liquid-phase flow in drying process under the studied conditions. There are three to six orders of magnitude differences between maximum and minimum value of the relative permeability of liquid water over the studied range of saturation, as shown in Fig. 2.8. The effect of this wide range of changes in the value of the liquid relative permeability on the model results is shown in Fig. 5.11., the maximum drying time is 35% bigger than the minimum drying time. It is obvious that these latter convective coefficients appear in the model only when the fuel particle has a moisture content higher than fiber satuarion point.

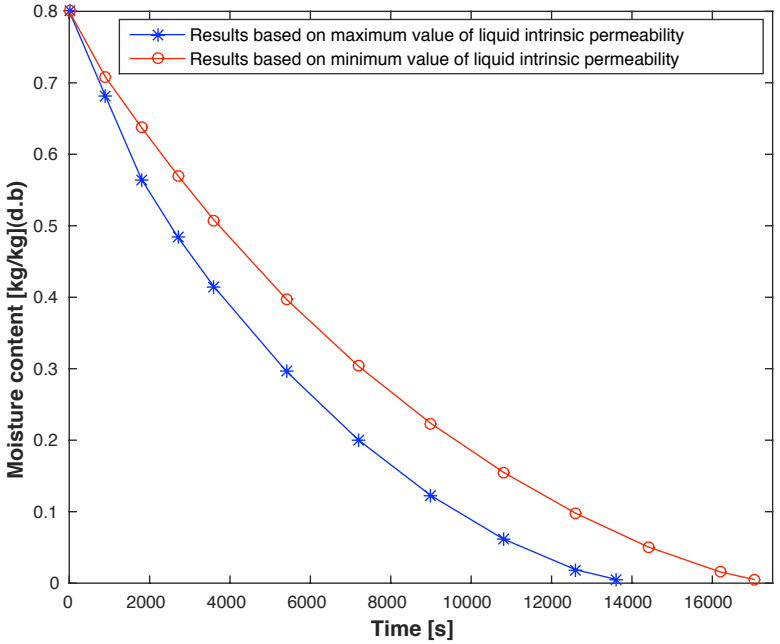

Figure 5.10: *Evolution of average moisture content based on minimum and maximum liquid intrinsic permeability*

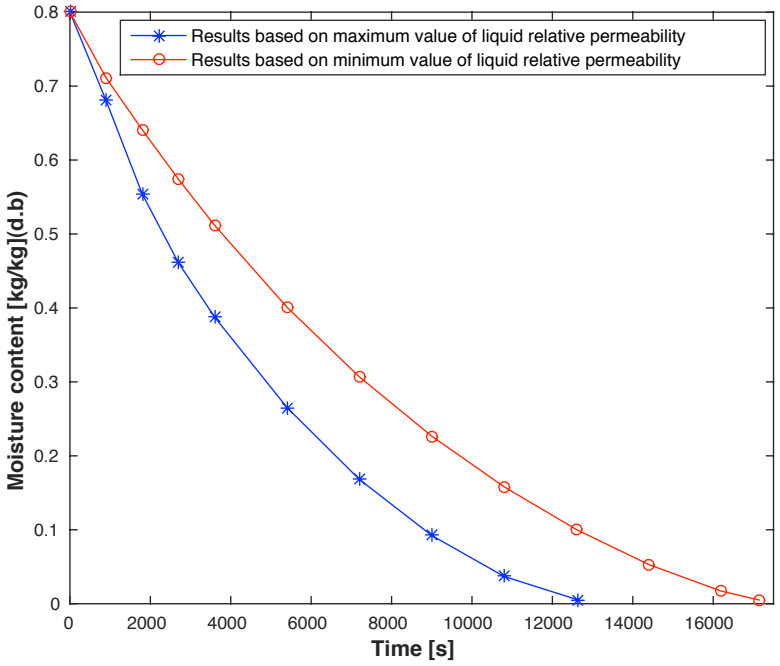

Figure 5.11: *Evolution of average moisture content based on minimum and maximum liquid relative permeability*

5.1.3 Predictions of particle model

Drying experiments of two hygroscopic fuel particles, wood and lignite, are considered as case studies to show the prediction capability of the presented particle model. Simulation results obtained from both numerical solution methods, LIMEX solver and iterative solution method, are presented. It should be pointed out that although both particle models with different solution methods have the same formulation based on Whitaker model however there are some differences between. The drying model solved by LIMEX solver includes almost all important phenomena of drying process and it is a rather comprehensive model. But for the model with iterative solution method, some simplifications are performed in the model because this particle model is going to be coupled to a multi-scale model of drying. In order to reduce the computational cost in solving of the particle model with iterative method, it is assumed that the bound water does not move inside the fuel particle. So the diffusion of bound water is neglected in mass balance as well as energy balance equations. In addition, the diffusion of water vapor is neglected in the energy balance. Since in the model with iterative solution method every phenomenon is solved separately therefore the boundary condition type 2 is more suitable to be employed in this model while in the model solved by LIMEX solver, the boundary condition type 1 is used. Slight differences between the simulation results obtained by these two numerical solution methods are related to the mentioned simplifications.

5.1.3.1 Drying of a wood particle

Stanish el al. [57] conducted some experiments of wood drying under different conditions and tested their developed mathematical model by these experimental data. In this section, two different sets of data of southern pine lumber drying are selected to examine the prediction capability of the particle model of this thesis. Southern pine lumber specimens were prepared with the length of 40 cm and the sections 5×15 cm. The samples were located in a drying chamber under convective drying air flow. In order to have a one-dimensional moisture transport, four side faces of the samples were coated with a moisture sealer so that the drying took place through only the upper and lower faces along the 5 cm thickness of the samples. The mathematical model developed by Stanish et al. is somewhat different from the Whitaker model used for the particle model of this thesis. Although the solution of conservation equations is used in both models but some parameters and expressions are different. For instance, the diffusion of bound water was modeled in the model of Stanish et al. by taking the chemical potential as a driving force while it is modeled in the present model based on the gradient of bound water (in the model solved by LIMEX solver). The used sorption isotherm expression is not the same in these models too. Input parameters of the model of this study for simulation of the drying of southern pine lumber specimens are listed in Tab. 5.6.

Fig. 5.12 and Fig. 5.13 show the history of changes in average moisture content as well as the center point temperature for convectively dried southern pine samples, respectively. The comparison between the results shows that the predictions of the present particle model solved by two solution methods are in very good agreement with the experimental data and the simulation results of Stanish el al.

Table 5.6: *Model inputs for simulation of drying of southern pine lumber specimens based on experiments of Stanish et al. ([57])*

Parameter	Correlation/Value	Unit	Reference
$\langle \rho_{SD} \rangle$	405	(kgm^{-3})	[57]
T_{bc}	398	(K)	[57]
ϵ	0.73	(-)	[57]
P_{atm}, P_{bc}	101325	(Nm^{-2})	-
M_{init}	1.25 (for experiment with $V_g = 7m/s$)	$(kgkg^{-1})$	[57]
M_{init}	0.525 (for experiment with $V_g = 13m/s$)	$(kgkg^{-1})$	[57]
α	58 (for experiment with $V_g = 7m/s$)	$(Wm^{-2}K^{-1})$	[57]
α	87 (for experiment with $V_g = 13m/s$)	$(Wm^{-2}K^{-1})$	[57]
β	$\frac{\alpha}{950}$	(ms^{-1})	[13]
C_{ps}	1360	$(Jkg^{-1}K^{-1})$	[57]
C_{pw}	4200	$(Jkg^{-1}K^{-1})$	[45]
C_{pv}	2000	$(Jkg^{-1}K^{-1})$	[102]
C_{pa}	1000	$(Jkg^{-1}K^{-1})$	[102]
D_v^{eff}	$0.05\epsilon^2[1.192 \cdot 10^{-4}(\frac{T^{1.75}}{P})]$	(m^2s^{-1})	[57]
k_{eff}	$\frac{\langle \rho_{SD} \rangle}{1000}(0.4 + 0.5\,M) + 0.024$	$(Wm^{-1}K^{-1})$	[57]
D_{bw}	$\exp(-9.9 + 9.8\,M_{bw} - \frac{4300}{T})$	(m^2s^-1)	[59]
$\mathbf{K}_g$	$5 \cdot 10^{-15}$	(m^2)	[57]
$\mathbf{K}_l$	$5 \cdot 10^{-16}$	(m^2)	[57]
P_c	$1.364 \cdot 10^5 \sigma(T)(M_{fw} + 1.2 \cdot 10^{-4})^{-0.63}$	(Nm^{-2})	[59]
$\mathbf{K}_{rg}$	$1 + (2S - 3)S^2$	(-)	[10]
$\mathbf{K}_{rl}$	$0.95(\frac{M_{\text{fw}}}{M_{cr}})^2$ If $(0 < M_{\text{fw}} < M_{cr})$ $0.05\frac{M_{\text{fw}} - M_{cr}}{M_{sat} - M_{cr}} +$ 0.95 If $(M_{cr} < M_{\text{fw}} < M_{sat})$	(-)	[59]
M_{fsp}	0.598-0.001 T	$(kgkg^{-1})$	[106]
$h(M_{bw}, T)$	$1 - (1 - \frac{M_{\text{bw}}}{M_{\text{fsp}}})^{6.453 \cdot 10^{-3}\,T}$	(-)	[45]
P_v^{sat}	$\exp(24.1201 - 4671.3545\,T^{-1})$	(Nm^{-2})	[107]
$\triangle\, h_w$	$3.1749 \cdot 10^6 - 2460\,T$	(Jkg^{-1})	[107]
$\triangle\, h_{\text{sorp}}$	$400 \triangle\, h_w(1 - \frac{M_{\text{bw}}}{M_{\text{fw}}})^2$	(Jkg^{-1})	[57]

$M_{cr} = 0.8$, $M_{sat} = 1.33$, $\sigma(T) = (1.28 \cdot 10^2 - 0.185T)10^{-3}$

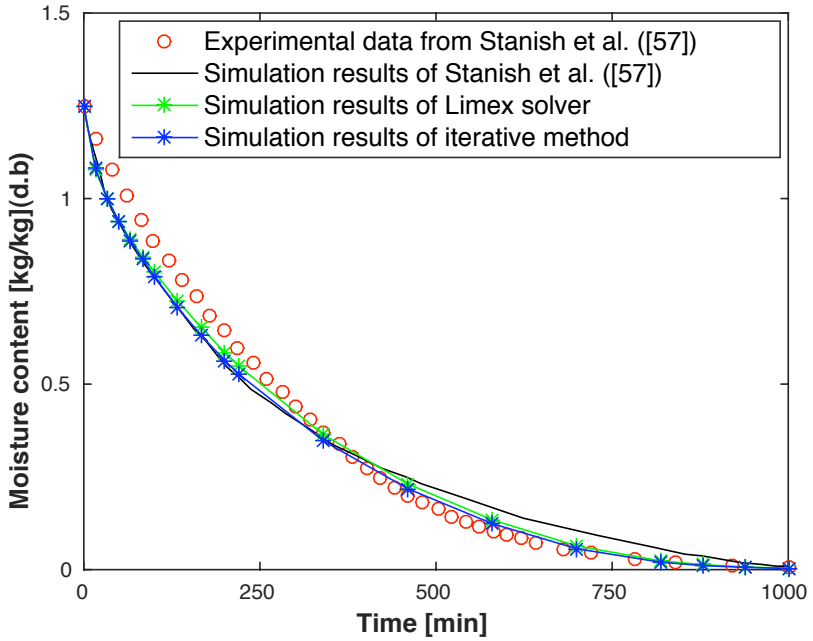

Figure 5.12: *Comparison of simulation results with experimental data for convective drying of a southern pine particle; evolution of average moisture content.* $T_g = 125°C$, $V_g = 7m/s$

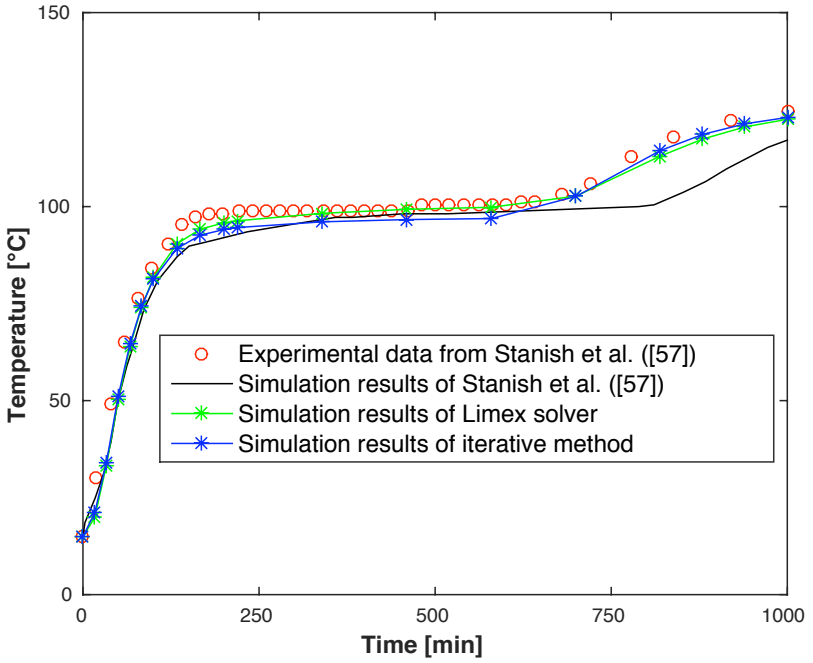

Figure 5.13: *Comparison of simulation results with experimental data for convective drying of a southern pine particle; evolution of temperature of center point.* $T_g = 125°C$, $V_g = 7m/s$

5.1.3.1.1 Intra-particle profile of moisture and temperature during single particle drying Fernandez and Howell [14] simulated the drying experiment of southern pine specimen with the initial moisture content of 0.525 kg/kg(d.b) subjected to the hot air with the velocity of $V_g = 13\ m/s$, conducted by Stanish et al. They developed a mathematical model similar to the model of Stanish et al. and presented their model predictions of the moisture loss history and temperature evolution and also the spatial profiles of moisture content and temperature inside the wood particle; Fig. 5.14 to Fig. 5.19. The simulation results of the particle model of this thesis with two solution methods are compared with the simulation results of Fernandez and Howell in these figures and it is seen that there are acceptable agreements between the results. Fig. 5.17 to Fig. 5.19 show that after 270 minutes since the start of drying there is still a remarkable gradient in the moisture content as well as temperature profile inside the particle. It is shown in Fig. 5.16 to Fig. 5.19 that even under such a moderate heating condition ($T_g = 125°C$), the gradients of moisture content and also temperature inside the particle from 38 minutes to 270 minutes is remained around 40% and $30°C$, respectively. The whole period of drying process is 1000 minutes that Fernandez and Howell [14] showed after around 500 minutes the moisture content inside at the center point of the particle started to decrease. With respect to such significant gradients within the moisture content and temperature profiles inside a thermally thick wood particle even under moderate heating conditions, neglecting these gradients and averaging the properties is not reasonable and may lead to remarkable errors. The simulation results of wood drying (Fig. 5.1) have shown that the gradient of the model parameters inside the particle for the case with intensive heating conditions are much bigger than the case with moderate heating conditions.

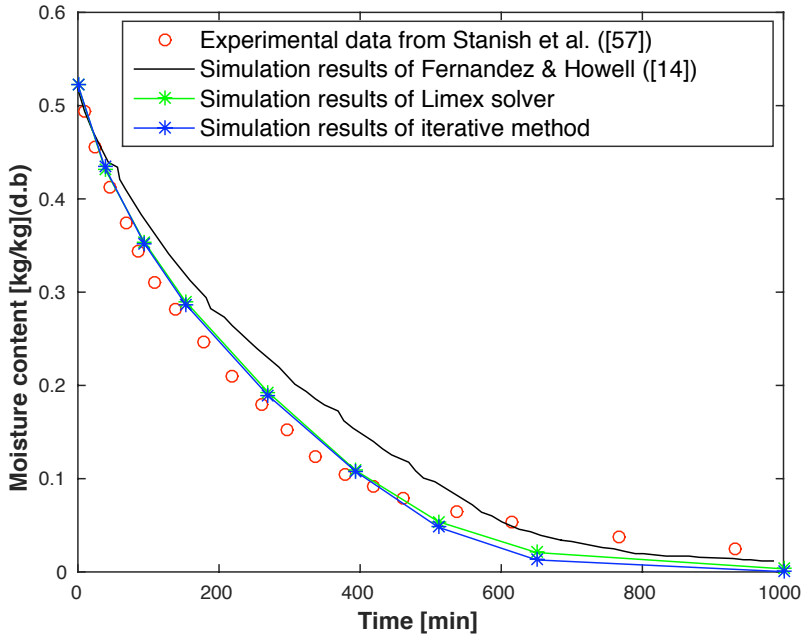

Figure 5.14: *Comparison of simulation results with experimental data for convective drying of a southern pine particle; evolution of average moisture content.* $T_g = 125°C$, $V_g = 13m/s$

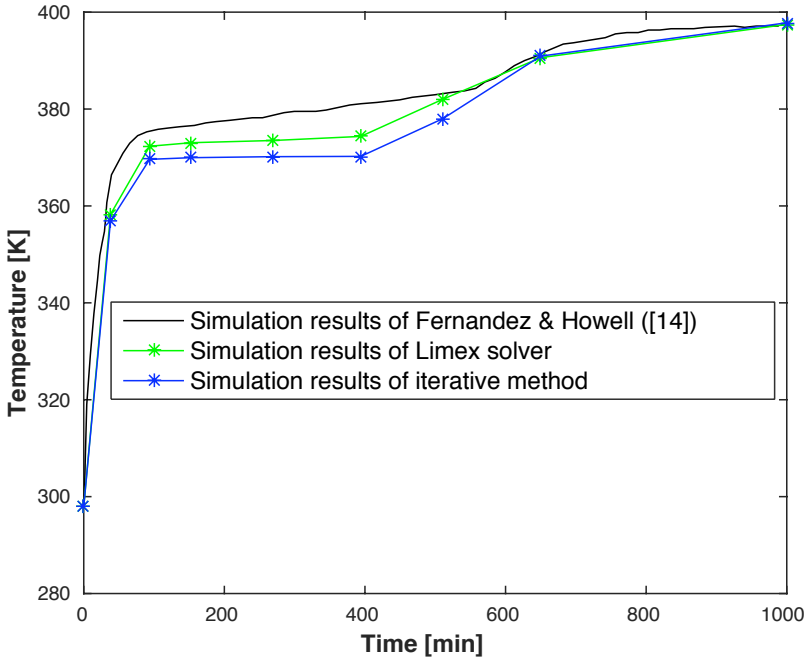

Figure 5.15: *Comparison of simulation results of different models for convective drying of a southern pine particle; evolution of temperature of center point.* $T_g = 125°C$, $V_g = 13m/s$

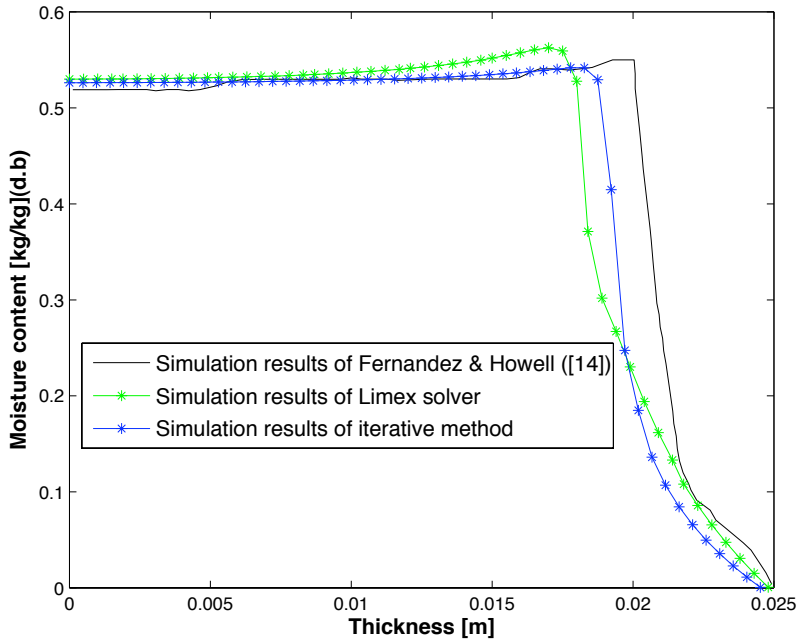

Figure 5.16: *Comparison of simulation results of different models for convective drying of a southern pine particle; spatial profiles of moisture content inside the particle after 38 min.* $T_g = 125°C$, $V_g = 13m/s$

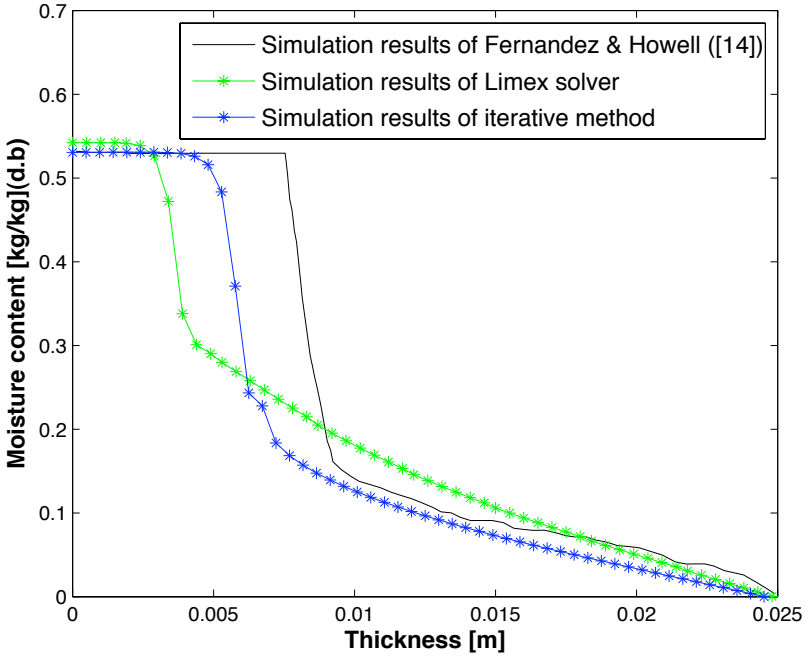

Figure 5.17: *Comparison of simulation results of different models for convective drying of a southern pine particle; spatial profiles of moisture content inside the particle after 270 min.* $T_g = 125°C$, $V_g = 13m/s$

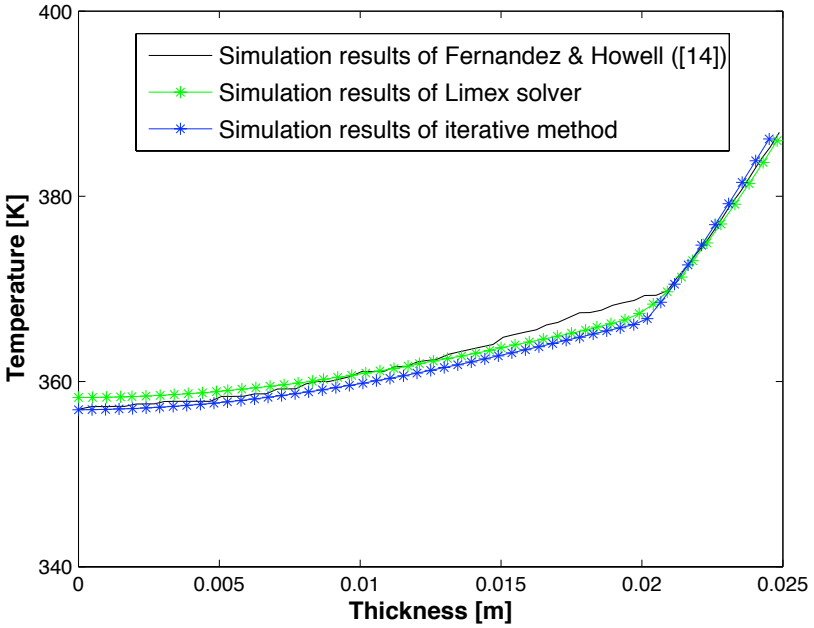

Figure 5.18: *Comparison of simulation results of different models for convective drying of a southern pine particle; spatial profiles of temperature inside the particle after 38 min.* $T_g = 125°C$, $V_g = 13m/s$

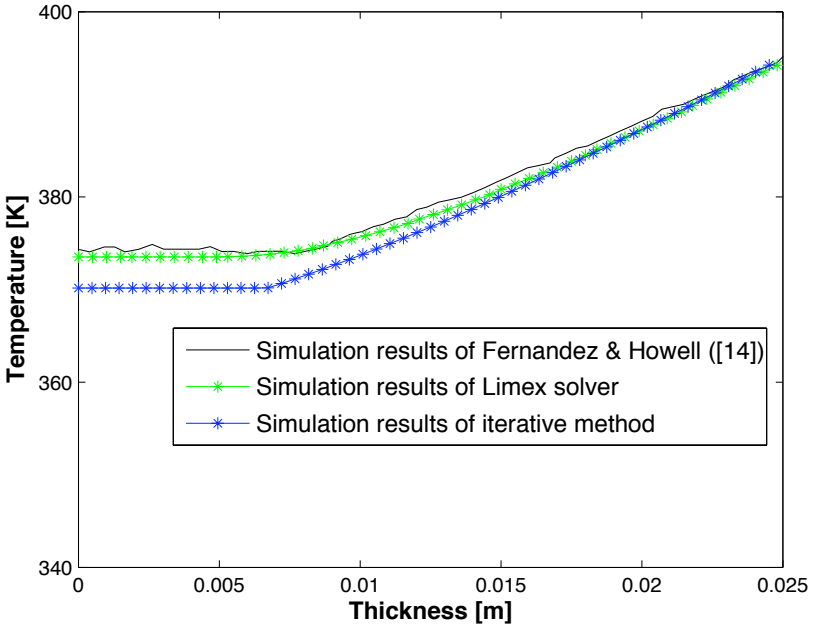

Figure 5.19: *Comparison of simulation results of different models for convective drying of a southern pine particle; spatial profiles of temperature inside the particle after 270 min.* $T_g = 125°C$, $V_g = 13m/s$

5.1.3.2 Drying of a lignite particle

Zhang and You [102] conducted the drying experiments of two kinds of Chinese lignite; Huolinhe lignite and Hailaer lignite. The samples were prepared into spherical shape of particles. These lignite particles with the radius of 30 mm were subjected to the hot air in a drying chamber. In addition to the mass-loss measurement of the lignite particles, the temperature at the center point and also at the half radius of the samples were measured during the drying. A comprehensive drying model based on Whitaker's model was presented by them too. Comparisons between the simulation results of the particle model of this thesis with the experimental as well as computational data of Zhang and You are presented in this part. The input parameters of the present particle model are mainly taken from [102], presented in Tab. 5.7 . Fig. 5.20 to Fig. 5.25 show the comparison between these results that are in good agreement.

Similar to the drying of woody biomass particles, a remarkable gradient is seen in the graphs of temperature profile of the lignite particles; Fig. 5.21 and Fig. 5.22 also Fig. 5.24 and Fig. 5.25. Simulation results of the spatial profile of moisture content inside the lignite particles (presented by Zhang and You, not shown here) showed also significant gradients inside the lignite particles.

Table 5.7: *Model inputs for simulation of drying of lignite particles based on experiments of Zhang & You ([102])*

Parameter	Correlation/Value	Unit	Reference
$\langle\rho_s\rangle^s_{huo}$	1435	(kgm^{-3})	[102]
ϵ_{huo}	0.42	(-)	[102]
$\langle\rho_s\rangle^s_{hai}$	1370	(kgm^{-3})	[102]
ϵ_{hai}	0.38	(-)	[102]
T_{bc}	413	(K)	[102]
P_{atm}, P_{bc}	101325	(Nm^{-2})	-
r_p	0.015	(m)	[102]
$M_{init(huo)}$	0.47	$(kgkg^{-1})$	[102]
$M_{init(hai)}$	0.41	$(kgkg^{-1})$	[102]
k_s	0.19	$(Wm^{-1}K^{-1})$	[102]
k_l	0.658	$(Wm^{-1}K^{-1})$	[102]
k_g	0.02577	$(Wm^{-1}K^{-1})$	[102]
C_{ps}	1000	$(Jkg^{-1}K^{-1})$	[102]
C_{pw}	4200	$(Jkg^{-1}K^{-1})$	[102]
C_{pv}	2000	$(Jkg^{-1}K^{-1})$	[102]
C_{pa}	1000	$(Jkg^{-1}K^{-1})$	[102]
D_v^{eff}	$0.05[1.192 \cdot 10^{-4}(\frac{T^{1.75}}{P})]$	(m^2s^{-1})	[102]
D_{bw}	$\exp(-12.81 + 10.89M_{\text{bw}} - \frac{4300}{T})$	(m^2s^-1)	[110]
$\mathbf{K}_g$	10^{-14}	(m^2)	[44]
$\mathbf{K}_l$	10^{-16}	(m^2)	[44]
P_c	$1.364 \cdot 10^5\sigma(T)(M_{fw} + 1.2 \cdot 10^{-4})^{-0.63}$	(Nm^{-2})	[59]
$\mathbf{K}_{rg}$	$(1-S)^2$	(-)	[102]
$\mathbf{K}_{rl}$	S^2	(-)	[102]
M_{fsp}	0.3	$(kgkg^{-1})$	[102]
h	$1 - \exp[-2.53(T-273)^{0.47} \cdot M^{1.58}]$	(-)	[102]
P_v^{sat}	$\exp[17.58 - (5769\,T^{-1}) - 0.005686\,T]$	(Nm^{-2})	[102]
$\triangle\ h$	$3.1749 \cdot 10^6 - 2460\,T$	(Jkg^{-1})	[102]
	$\sigma(T) = (1.28 \cdot 10^2 - 0.185T)10^{-3}$		

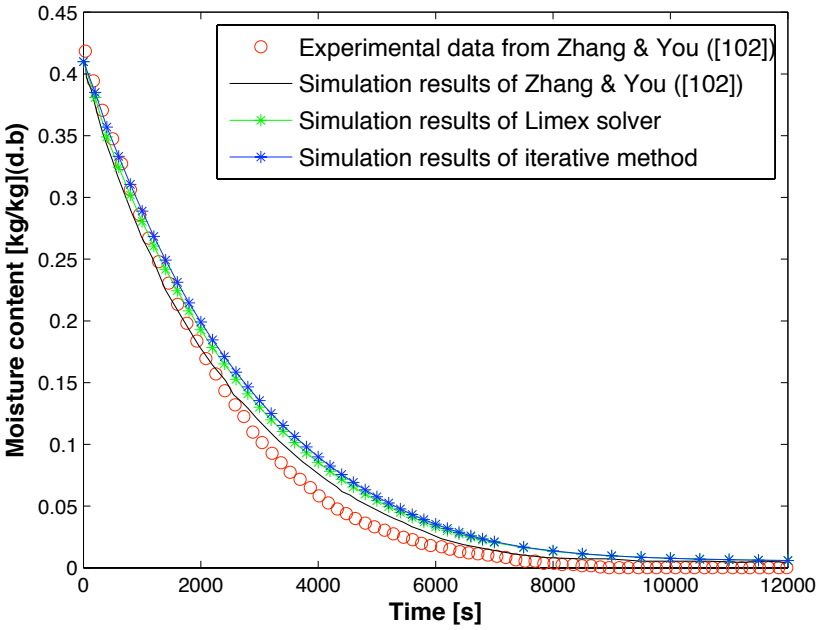

Figure 5.20: *Comparison of simulation results with experimental data for convective drying of a Hailaer lignite particle; evolution of average moisture content.* $T_g = 140°C$, $V_g = 1.5m/s$

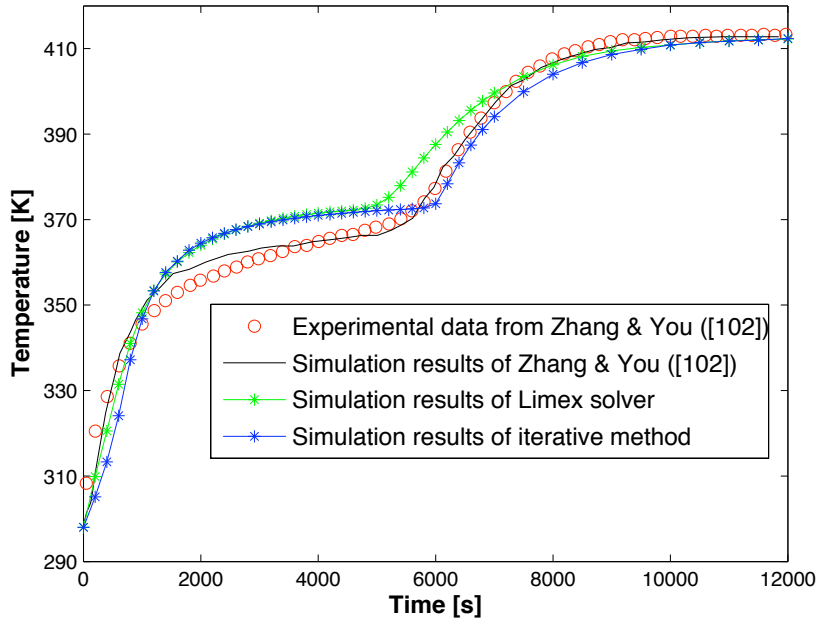

Figure 5.21: *Comparison of simulation results with experimental data for convective drying of a Hailaer lignite particle; evolution of temperature of center point.* $T_g = 140°C$, $V_g = 1.5m/s$

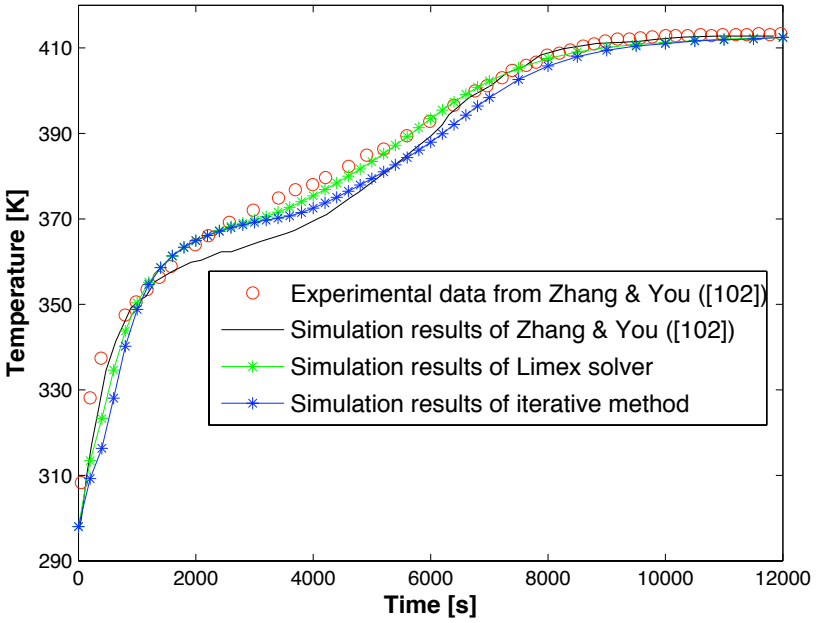

Figure 5.22: *Comparison of simulation results with experimental data for convective drying of a Hailaer lignite particle; evolution of temperature at half radius.* $T_g = 140°C$, $V_g = 1.5m/s$

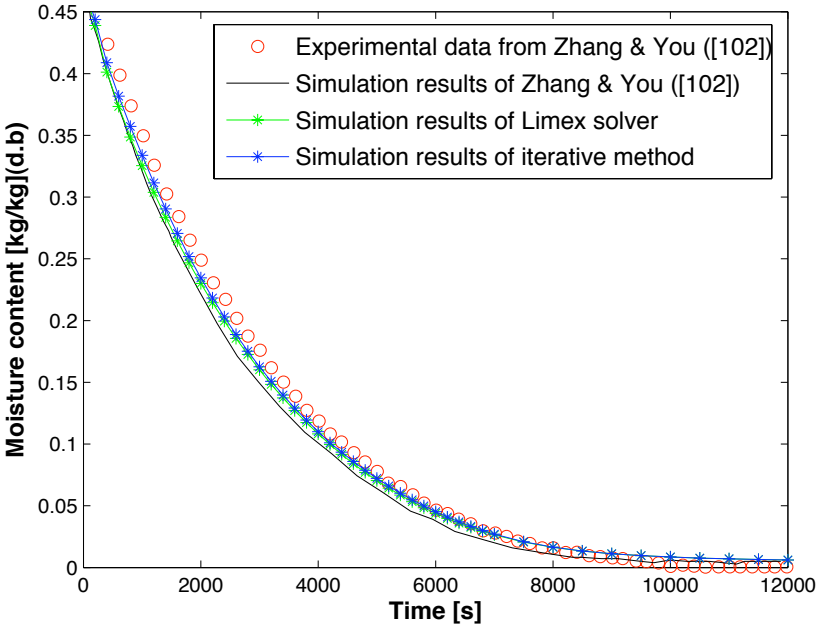

Figure 5.23: *Comparison of simulation results with experimental data for convective drying of a Huolinhe lignite particle; evolution of average moisture content.* $T_g = 140°C$, $V_g = 1.5m/s$

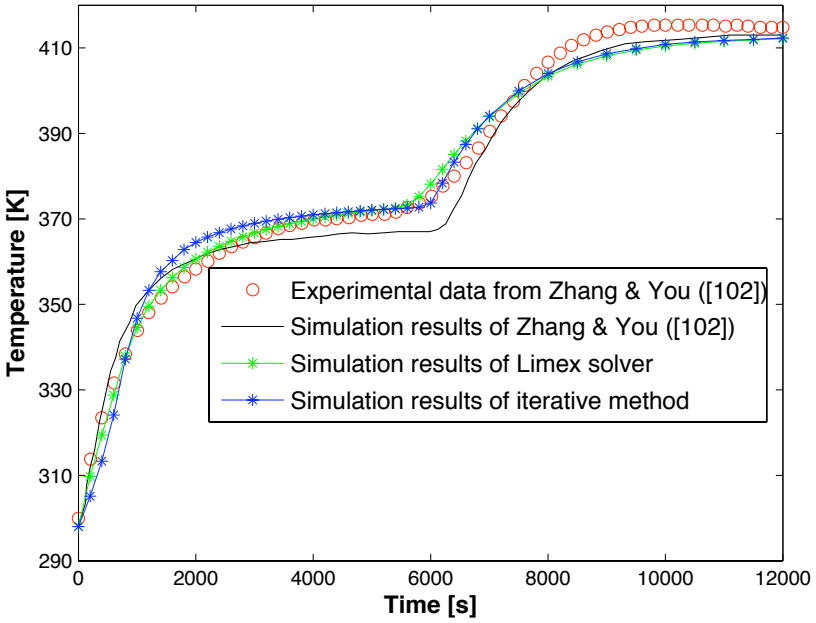

Figure 5.24: *Comparison of simulation results with experimental data for convective drying of a Huolinhe lignite particle; evolution of temperature of center point.* $T_g = 140°C$, $V_g = 1.5m/s$

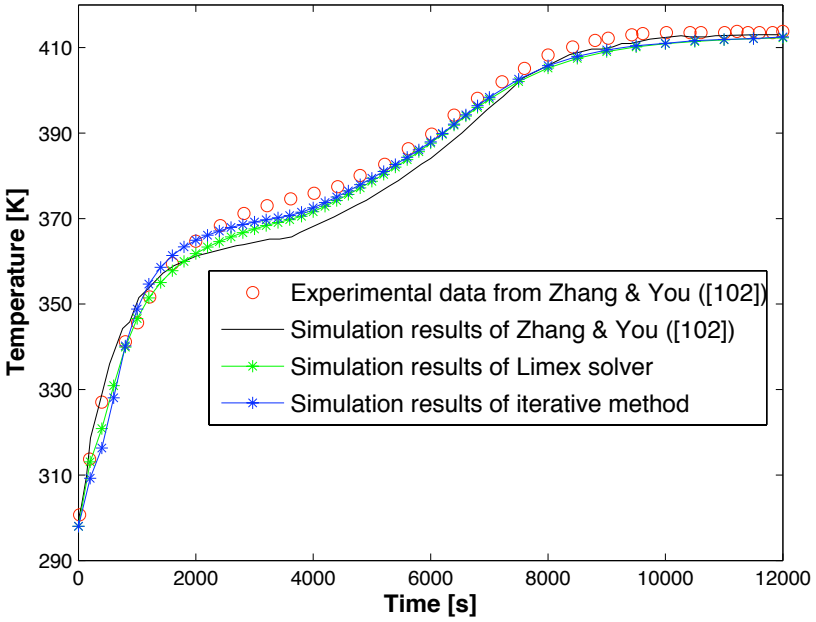

Figure 5.25: *Comparison of simulation results with experimental data for convective drying of a Huolinhe lignite particle; evolution of temperature at half radius.* $T_g = 140°C$, $V_g = 1.5m/s$

5.1.4 Concluding remarks

Single particle drying has been simulated by a one-dimensional particle model based on Whitaker model. The computational performance of this model has been verified under high-temperature drying. For highlighting the importance of the model coefficients, the drying of an infinite cylindrical pine wood particle has been studied numerically. By applying the lower and upper bounds of nine model parameters to the model a bounded model output has been calculated. It shows a sixteen times difference between the predicted maximum and minimum drying times. It means that the arbitrary adoption of the model parameters from the literature without enough justifications based on considered case study can lead to totally wrong predictions of the model output.

By applying the variation of each model parameter, from its minimum to maximum value, to the model the sensitivity analysis has been done. The following points are concluded from the sensitivity analysis: (i) The global sensitivity analysis shows that the impact of the variation of effective thermal conductivity and specific heat capacity on the model output is almost negligible. So each correlation listed in the the appendix for the above mentioned parameters can be adopted for modeling drying of pine wood under the studied conditions. (ii) The model output changed slightly with the different correlations of bound water diffusivity. But the effect of the variation of effective diffusivity of water vapor on the model output was significant. Therefore the adoption of a correlation for bound water diffusivity is not critical for drying modeling, but a wrong selection of the value of effective diffusivity of water vapor may lead to 100% error in the predictions of drying time. (iii) The variation of all investigated convective transport coefficients, except gas relative permeability, have shown a remarkable impact on the predicted drying time. Among all model parameters, the gas intrinsic permeability is the most significant parameter affecting the model output. Wrong adoption of the value of gas intrinsic permeability may lead to predictions of the model that are three times higher (or lower) than the accurate results.

To obtain reliable predictions of a model of drying of a single wood particle the gas intrinsic permeability, effective diffusivity of water vapor and capillary pressure, in order of their importance, must be experimentally determined for the studied conditions. Besides, this study shows that the drying of a coarse wood particle under studied conditions is mainly controlled by transport phenomena inside the particle, particularly mass transport phenomena. Therefore neglecting each phenomenon inside the particle needs to be reasonably justified.

The drying of wood as well as lignite particle has been simulated by two different solution methods; LIMEX solver and iterative solution method. The simulation results have shown very good agreements with the experimental data and the simulation results of others from the literature. In spite of the simplifications applied to the particle model with iterative solution method, the predictions of this model is quite close to the prediction of the model with comprehensive model equations; the particle model with LIMEX solver. Even over moderate drying conditions studied in this thesis, the remarkable gradients of moisture content and temperature can be seen inside the wood as well as lignite particles. These remarkable gradients of the properties inside the particle imply that averaging these properties is not acceptable and can lead to significant error in prediction of the drying characteristics of the particle.

5.2 Fixed-bed drying

Simulation results of fixed-bed drying of wood and lignite particles obtained by the HQCM and the RPM are presented in this section. The simulation results are compared with the experimental data and the simulation results of the DPM from the literature. Prediction capability of two fixed-bed drying models, the HQCM and the RPM, are examined under different conditions of fixed-bed drying. Different values of the temperature and velocity of the inlet gas, height and porosity of the bed, initial moisture content and also different types of the materials are simulated during fixed-bed drying. In this section, at the first, the fixed-bed drying of wood particles with two different temperatures of the inlet gas are simulated. Following, the fixed-bed drying of two kinds of lignite particles are presented. Simulation results of the fixed-bed drying of Hailaer and Huolinhe lignite particles are shown for the cases of weight loss rate, the evolution of gas temperature in the bed and also the intra-particle temperature and moisture in the particles located at different heights of the bed. The share of parallel computing on the reduction of computational times is presented before the concluding remarks.

5.2.1 Fixed-bed drying of wood particles

Peters et al. [32] conducted the experiments of fixed-bed drying with different inlet gas temperatures. The experiments were carried out with beech wood particles with initial moisture content of 10% (dry basis). 2 kg of cube beech particles with $10 \times 10 \times 10\ mm^3$ in size were located in a drying chamber with inner diameter of 250 mm where the height of bed reached to 100 mm. The bed was preheated to $T = 90°C$ and then a flux of heated nitrogen ($\dot{m} = 16\ kgh^{-1}$) streamed through the bed to dry it. Recently, Mahmoudi et al. [34] have simulated two sets of these fixed-bed drying with the drying temperature of $135°C$ and $150°C$, by the DPM. They coupled the particle solution to a CFD tool solving the equations of interstitial gas phase. Instead of cube particles, they simulated one dimensional drying of spherical particles with the same volume. Considering the thermal capacity of the test facility, they presented an exponential form relation for the temperature of inlet gas. The evolution of inlet gas temperatures which reach to steady state values of $135°C$ and $150°C$, are given by equations of Eq. (5.1) and Eq. (5.2), respectively [34].

$$T_{in} = 135 + 115 \exp^{-0.001t} \tag{5.1}$$

$$T_{in} = 150 + 126 \exp^{-0.001t} \tag{5.2}$$

Fig. 5.26 and Fig. 5.27 show the comparison between the simulation results of the HQCM and the RPM with two sets of the experimental data from [32] as well as the simulation results of the DPM from [34]. The properties of beech wood and other input parameters for the simulation are given in Tab. 5.8. It should be noted that the parameters shown in this table are related to the involved phenomena under the experiment conditions so that the free water does not appear in the model equations, because of low moisture content of the considered particles. The heat sink method is used for the calculation of the evaporation rate of wood particles, as Mahmoudi et al. [34] did. For the simulation by the RPM, 10 representative particles along the height of the bed are solved so that 15 grid points are considered in the radial direction of each particle. As already mentioned, for the RPM the bound water diffusion is neglected in the particles and the effect of gas diffusion on the heat transport is not taken into account. Mahmoudi et al. also neglected the heat transported through bulk motion and diffusion of gas phase in their simulation by the DPM, because of the negligible thermal mass of the gas phase compared to the solid and liquid phase. They did not consider the bound water diffusion in their model too.

For the simulation by the HQCM, after the grid-independence study, 24 grid points are considered along the height of the bed. The simulation results of the RPM show very good agreement with the simulation results of the DPM as well as the experimental data. Although there are deviations between the simulation results of the HQCM and the other data however it is seen that the HQCM can acceptably predict the mass loss during wood fixed-bed drying under the conditions of these experiments. This is related to the low moisture content of the particles (10 % d.b), rather small size of the particles ($r_p = 0.0062m$) and also the low height of the bed ($H_{bed} = 0.1m$). The HQCM presents acceptable predictions under the conditions close to the assumptions of this model; no gradient for the properties inside the particle domain. In both models, the evaporation occurs inside the particle domain but the drying rate is limited to the heat and mass exchanges between the interstitial gas phase and the particle domain. In the HQCM, no internal heat and mass transfer resistances are considered while in the RPM these resistances inside the particles are taken into account. In the experiments of wood drying with rather low moisture contents, the heat and mass exchanges from the particle domain to the interstitial gas phase for both models are similar because the mass exchange by convection flux in the RPM (which is extra term rather the mass exchange in the HQCM) is negligible. Vapor diffusion plays a key role as an interal mass transfer resistance which is captured by the RPM. Therefore the HQCM predicts the drying

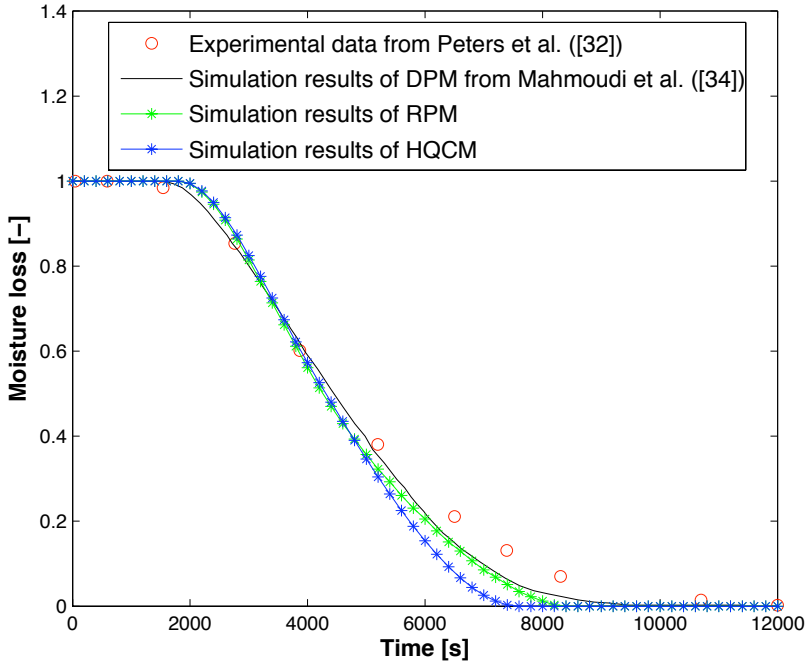

Figure 5.26: *Comparison of simulation results with experimental data for fixed-bed drying of wood particles; evolution of moisture loss.* $T_{drying} = 135°C$

rate higher (the drying time shorter) while the RPM predicts the drying rate lower that is more close to the simulation results of the DPM and the experimental data.

5.2.1.1 Intra-particle profiles of moisture and temperature during fixed-bed drying of wood particles

Fig. 5.28 and Fig. 5.31 show the simulation results of the RPM for the intra-particle profiles of moisture and temperature inside the wood particles located at the inlet and middle layers of the bed based on the drying experiment with $T_{drying} = 150°C$. It can be seen that there are negligible gradients in the temperature profiles of the wood particles at both layers in the bed. Althought the gradients in the moisture profiles seem to be remarkable however, because of low moisture content, averaging the moisture content by the HQCM does not affect the results dramatically. The intra-particle profiles show that the evaporation is started later in the middle layer and it takes longer, in comparison to the particles in the inlet layer. This is because of the fact that a part of the heat of drying gas is consumed for drying of the particles in the layers before the middle layer. Moreover, the water vapor released from the layer before the middle layer are transported by the drying gas to this layer and the concentration of water vapor in the interstitial gas increases in this layer . The higher concentration of water vapor at middle layer causes lower mass transfer from

Table 5.8: *Model inputs for simulation of fixed-bed drying of wood particles based on experiments of Peters et al. ([32])*

Parameter	Correlation/Value	Unit	Reference
	Particle scale		
$\langle \rho_{SD} \rangle$	750	(kgm^{-3})	[34]
ϵ	0.64	(-)	[34]
P_{atm}, P_{bc}	101325	(Nm^{-2})	-
r_p	0.0062	(m)	[34]
M_{init}	0.1	$(kgkg^{-1})$	[34]
k_s	0.47	$(Wm^{-1}K^{-1})$	[34]
k_l	0.685	$(Wm^{-1}K^{-1})$	[45]
k_g	0.02577	$(Wm^{-1}K^{-1})$	[102]
C_{ps}	2551.3	$(Jkg^{-1}K^{-1})$	[34]
C_{pw}	4200	$(Jkg^{-1}K^{-1})$	[102]
C_{pv}	2000	$(Jkg^{-1}K^{-1})$	[102]
D_v^{eff}	$0.001[1.192 \cdot 10^{-4}(\frac{T^{1.75}}{P})]$	(m^2s^{-1})	[10]
$\mathbf{K}_g$	$4 \cdot 10^{-16}$	(m^2)	[43]
M_{fsp}	0.598-0.001 T	$(kgkg^{-1})$	[106]
$\triangle\, h$	$3.1749 \cdot 10^6 - 2460\,T$	(Jkg^{-1})	[102]
	Reactor scale		
ϵ_{bed}	0.46	(-)	[34]
H_{bed}	0.1	(m)	[34]
$D_{z,v}$	1.165×10^{-5}	(m^2s^{-1})	[104]
Λ_z	0.0279	$(Wm^{-1}K^{-1})$	[104]
	Interface		
α	$\frac{Nu\lambda_g}{d_p}$*	$(Wm^{-2}K^{-1})$	
β	$\frac{(2+1.1Re^{0.6}Sc^{1/3})D_g}{d_p}$	(ms^{-1})	[117]

*$Nu = 3$ based on Reynolds number of $Re \leq 40$, Adopted from [32]

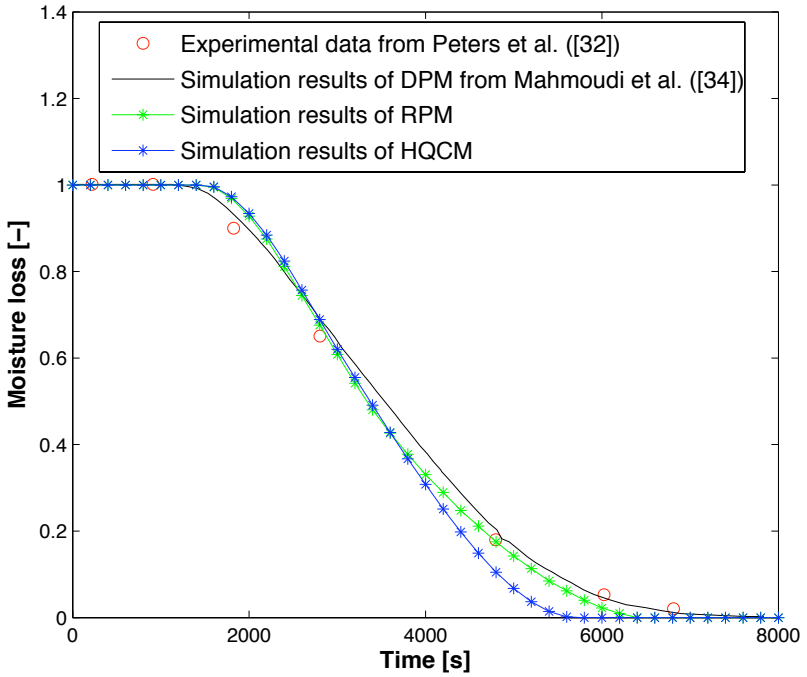

Figure 5.27: *Comparison of simulation results with experimental data for fixed-bed drying of wood particles; evolution of moisture loss.* $T_{drying} = 150°C$

the particle domain to the interstitial gas phase therefore the drying rate decreases in this layer.

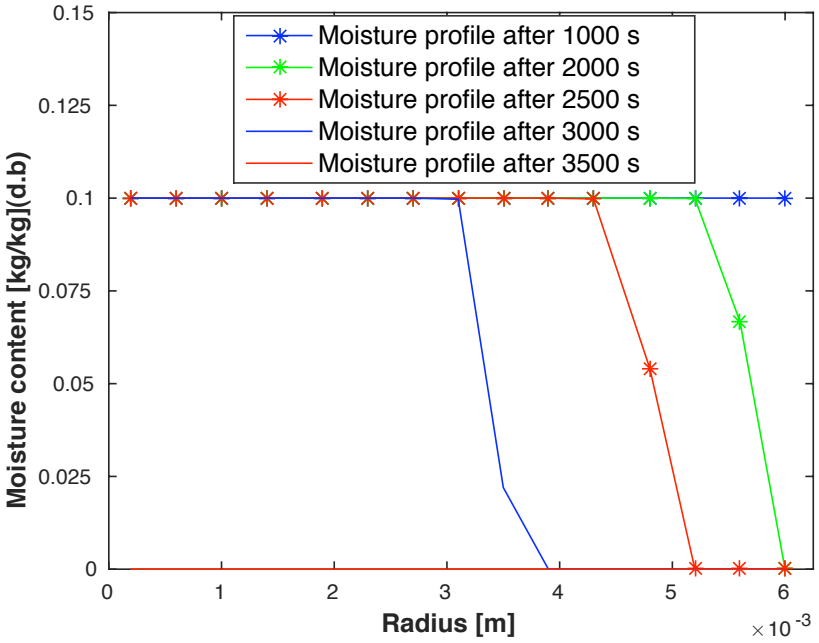

Figure 5.28: *Simulation results of the RPM for spatial profiles of moisture inside a particle from inlet layer of the bed during fixed-bed drying of wood particles.* $T_{drying} = 150°C$

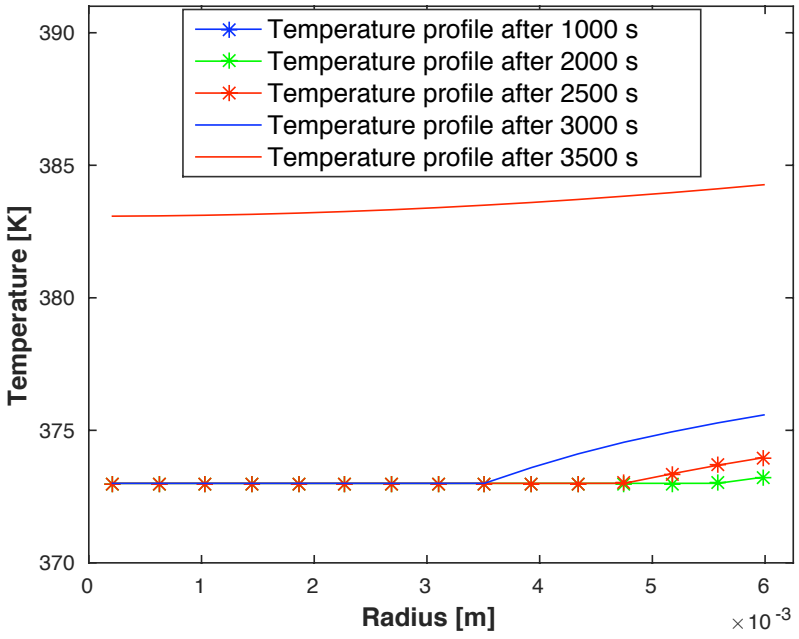

Figure 5.29: *Simulation results of the RPM for spatial profiles of temperature inside a particle from inlet layer of the bed during fixed-bed drying of wood particles.* $T_{drying} = 150°C$

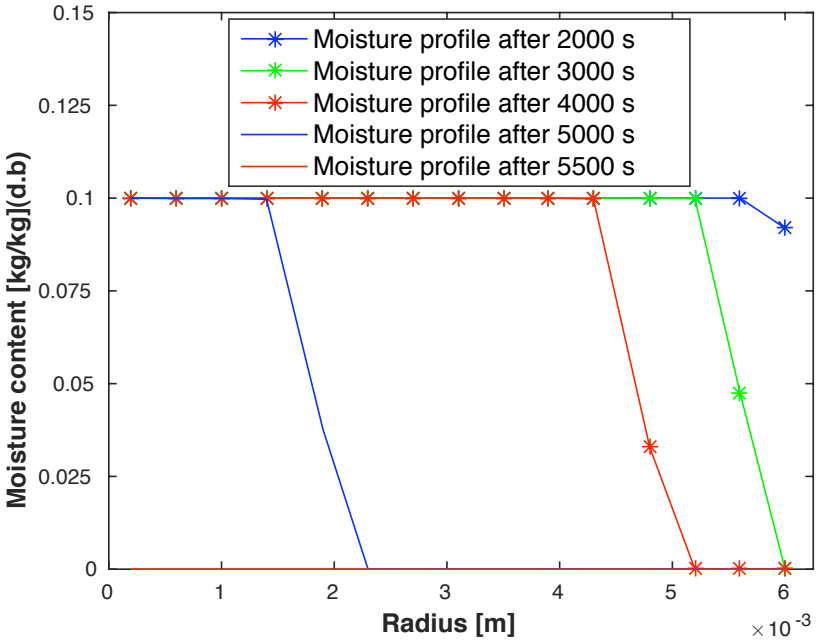

Figure 5.30: *Simulation results of the RPM for spatial profiles of moisture inside a particle from middle layer of the bed during fixed-bed drying of wood particles.* $T_{drying} = 150°C$

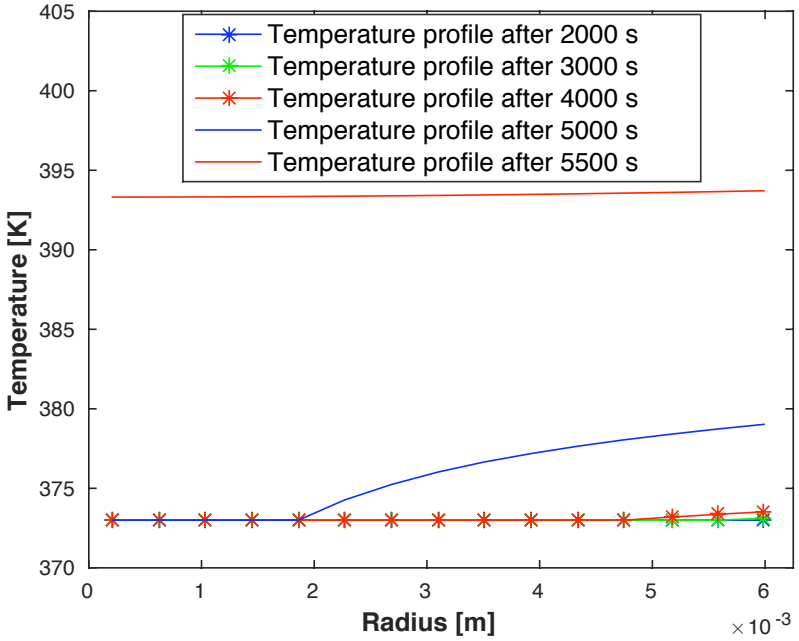

Figure 5.31: *Simulation results of the RPM for spatial profiles of temperature inside a particle from middle layer of the bed during fixed-bed drying of wood particles.* $T_{drying} = 150°C$

5.2.2 Fixed-bed drying of lignite particles

As already mentioned in this chapter, single particle drying experiments for two kinds of lignite particles were done by Zhang and You ([102]). They also carried out the fixed-bed drying experiments with these kinds of lignite particles and compared the data with their simulation results of the DPM [104]. In this section, the simulation results of the HQCM and the RPM are compared with the experimental data and the simulation results of the DPM from [104]. The input parameters for single particle simulation are the same as Tab. 5.7. The input parameters used for the simulation of the bed of lignite particles are given in Tab. 5.9. Fig. 5.32 to Fig. 5.35 show the comparison between the results of weight loss for the fixed-bed drying of two kinds of the lignite particles with two different heights of the bed; 250 mm and 500 mm. Similar to the fixed-bed drying of wood particles, the simulation results of the RPM show very good agreement with the experimental data as well as the simulation results of the DPM. But against the acceptable predictions of the HQCM for wood drying under mentioned conditions, the simulation results of the HQCM can poorly express the drying behavior of the coarse lignite particles with rather thick bed size.

By conducting the grid-independence study for the HQCM, 32 grid points are considered for the bed with $H_{bed} = 250mm$ and 64 grid points for the bed with $H_{bed} = 500mm$. The grid-independence study is done for the grid points of the particle scale of the RPM. 8 grid points inside the particles are used for the simulation by the RPM where 8 and 16 representative particles are selected along the height of the beds; 250 mm and 500 mm, respectively. Almost linear behavior of the results of the HQCM is an evident of neglecting the transport phenomena inside the particles. It can be seen that not considering the transport phenomena inside the particles can lead to a significant error in prediction of drying process of thermally thick particles. Both types of studied lignite particles have rather high moisture content, then the free water, water vapor and bound water are existing inside the particles and their internal heat and mass transport control the drying process. Under moderate heating conditions, the transport of free water by convection and the water vapor by convection and diffusion are important in controling the drying process. In the case of wood drying in the previous section, only the diffusion of water vapor has been dominant because of low moisture content but in the case of lignite particles, with rather bigger size and thicker bed, the heat and mass transport inside the particle domain are more important.

The difference between the results of the HQCM with the other data is related to the mass exchange from the particle domain to the interstitial gas phase. Despite the fact that the heat and mass transfer inside the particles play the role as

Table 5.9: *Model inputs for simulation of fixed-bed drying of lignite particles based on experiments of Zhang & You ([104])*

Parameter	Correlation/Value	Unit	Reference
	Reactor scale		
ϵ_{bed}	0.4	(-)	[104]
$D_{z,v}$	1.165×10^{-5}	$(m^2 s^{-1})$	[104]
Λ_z	0.0279	$(W m^{-1} K^{-1})$	[104]
	Interface		
α	$\frac{(2+1.1Re^{0.6}Pr^{1/3})\mu_g}{d_p}$	$(W m^{-2} K^{-1})$	[117]
β	$\frac{(2+1.1Re^{0.6}Sc^{1/3})D_g}{d_p}$	$(m s^{-1})$	[117]

internal resistances for the RPM but the convection flux from the particles to the interstitial gas phase which is not considered in the HQCM, causes higher drying rate in the RPM. This convection term is not taken into account in the HQCM because there is no physical meaning for it based on the assumptions of this method. The deviation of simulation results of the RPM from the DPM's results can be partially related to the convective coefficients of heat and mass transfer between the particles and the interstitial gas phase used in the RPM (Tab. 5.9). Wakao's correlations are used for calculation of the convective coefficients of heat and mass transfer in the simulation by the RPM. It should be noted that the convective coefficients of heat and mass transfer between the particles and the interstitial gas phase were not reported for the solution of the DPM in the study of [104]. However, the differences between the results of the RPM and the DPM are mainly related to the mass transport coefficients inside the particles used in the RPM of this thesis different with the values used in the DPM by Zhang and You [104]. Nevertheless, the difference between the results of the RPM and the DPM is naturally expectable because more simplifications are applied in the RPM in comparison to the DPM.

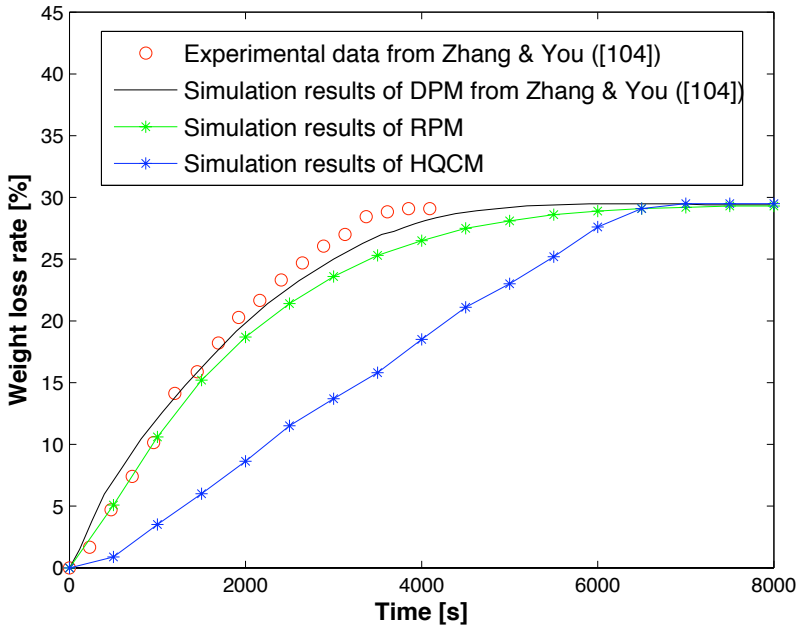

Figure 5.32: *Comparison of simulation results with experimental data for fixed-bed drying of Hailaer lignite particles; evolution of weight loss.* $T_g = 428K$, $V_g = 0.6m/s$, $H_{bed} = 250mm$

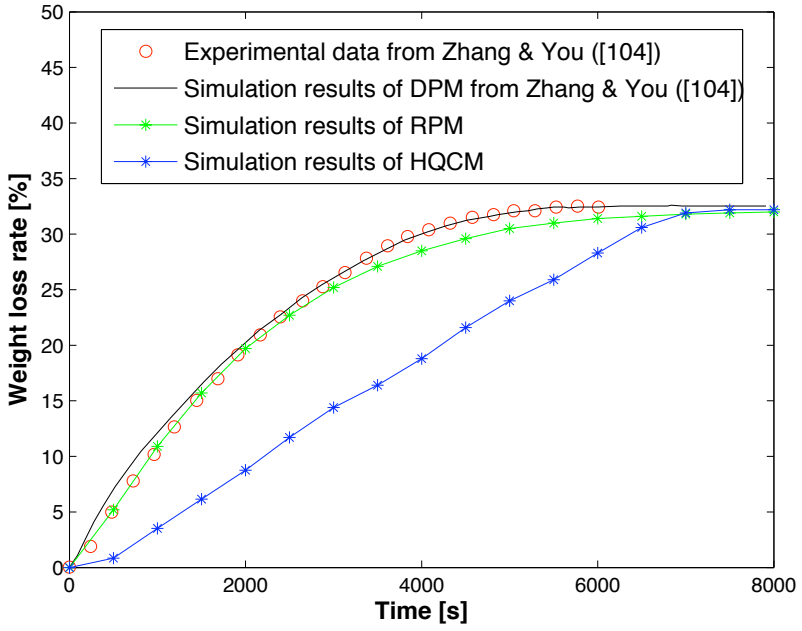

Figure 5.33: *Comparison of simulation results with experimental data for fixed-bed drying of Huolinhe lignite particles; evolution of weight loss.* $T_g = 428K$, $V_g = 0.6m/s$, $H_{bed} = 250mm$

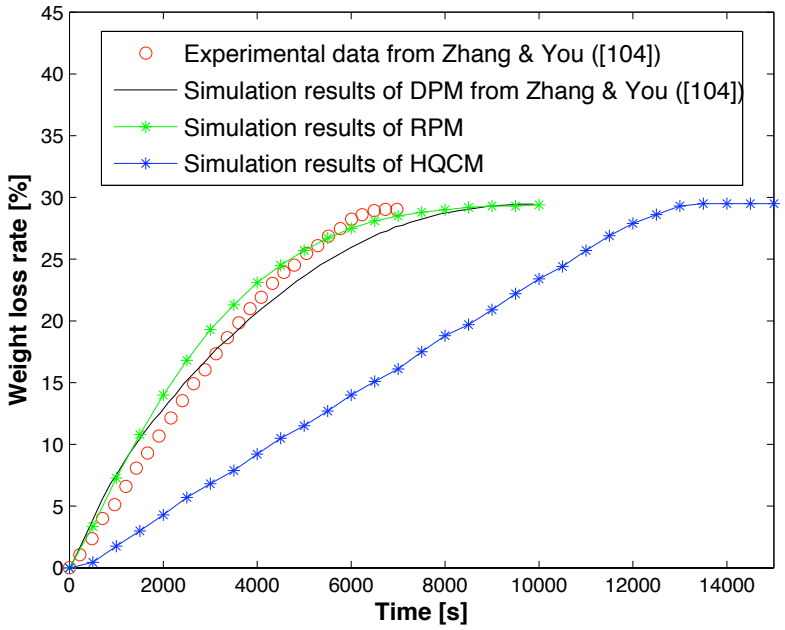

Figure 5.34: *Comparison of simulation results with experimental data for fixed-bed drying of Hailaer lignite particles; evolution of weight loss.* $T_g = 428K$, $V_g = 0.6m/s$, $H_{bed} = 500mm$

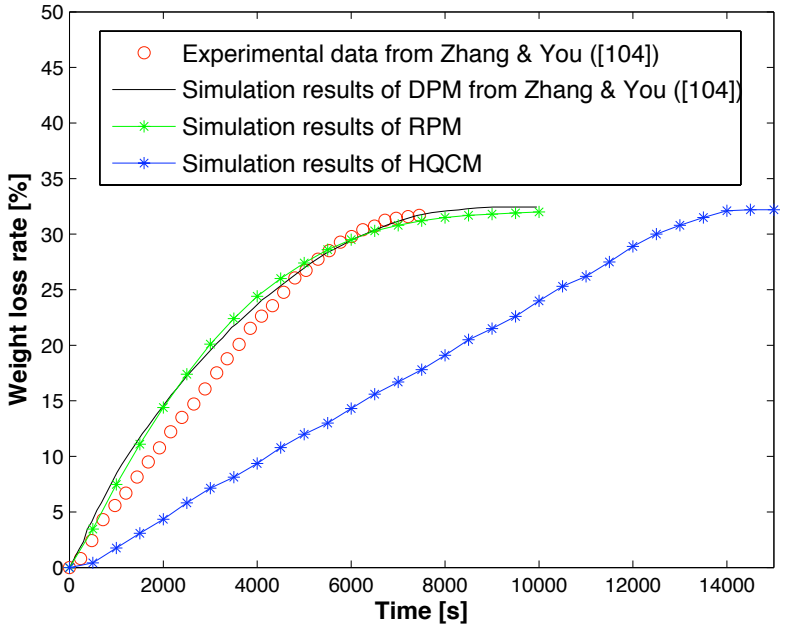

Figure 5.35: *Comparison of simulation results with experimental data for fixed-bed drying of Huolinhe lignite particles; evolution of weight loss.* $T_g = 428K$, $V_g = 0.6m/s$, $H_{bed} = 500mm$

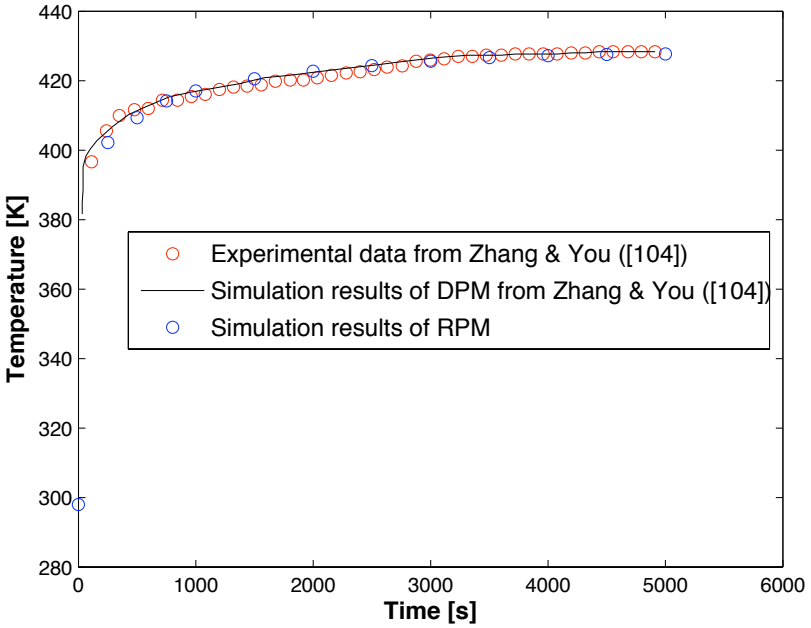

Figure 5.36: *Comparison of simulation results with experimental data for fixed-bed drying of Hailaer lignite particles; evolution of gas temperature at* $H = 100mm$ *of the bed.* $T_g = 428K$, $V_g = 1.5m/s$, $H_{bed} = 500mm$

5.2.2.1 Evolution of gas temperature in the bed during fixed-bed drying

Fig. 5.36 to Fig. 5.38 show the evolution of gas temperature at different heights inside the bed during the fixed-bed drying of Hailaer lignite particles. The simulation results are compared with the experiments done under the conditions of $H_{bed} = 500mm$, $T_g = 428K$ and $V_g = 1.5m/s$. The simulation results of the RPM are in a good agreement with the experimental data as well as the simulation results of the DPM. The gas temperature in the layer close to the inlet port are higher than the layer far from the inlet. This shows that the heat of drying gas is absorbed by the wet particles in different layers which causes the gas temperature varies significantly along the height of the bed. The accurate predictions of the distribution of gas temperature along the height of the bed is important in designing the reactors for thermo-chemical conversion processes.

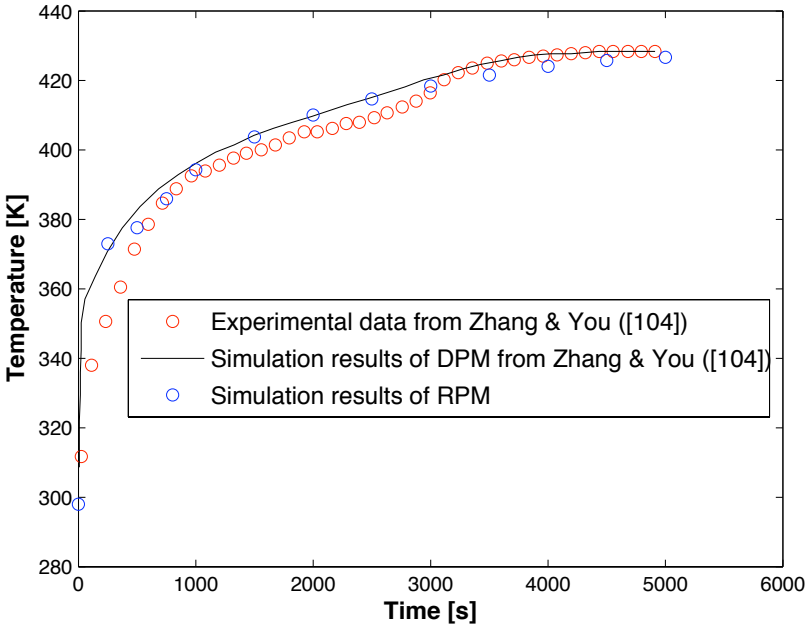

Figure 5.37: *Comparison of simulation results with experimental data for fixed-bed drying of Hailaer lignite particles; evolution of gas temperature at* $H = 300mm$ *of the bed.* $T_g = 428K$, $V_g = 1.5m/s$, $H_{bed} = 500mm$

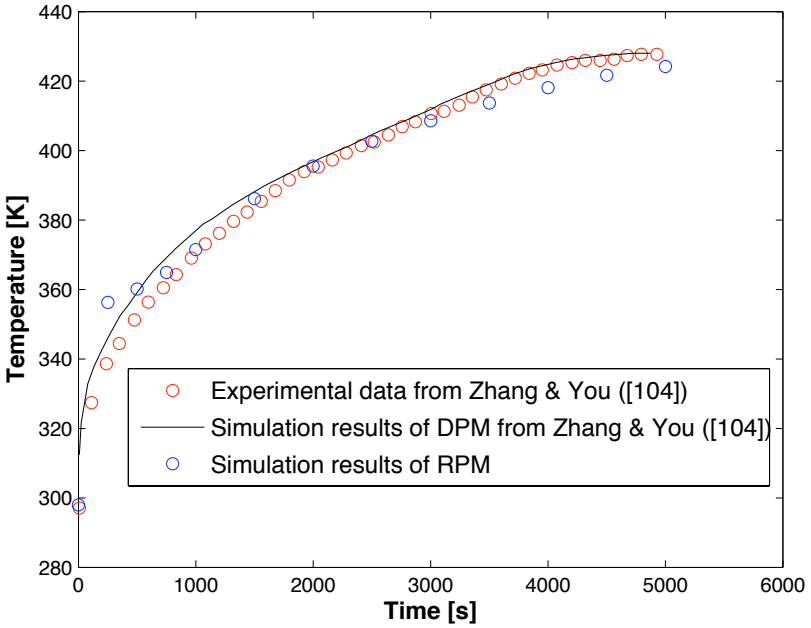

Figure 5.38: *Comparison of simulation results with experimental data for fixed-bed drying of Hailaer lignite particles; evolution of gas temperature at outlet of the bed.* $T_g = 428K$, $V_g = 1.5m/s$, $H_{bed} = 500mm$

5.2.2.2 Intra-particle profiles of moisture and temperature during fixed-bed drying of lignite particles

The simulation results of the RPM for the intra-particle moisture and temperature of Hailaer lignite particles at different layers of the bed during the fixed-bed drying are shown in Fig. 5.39 to Fig. 5.42. The simulations are performed under the conditions of $H_{bed} = 500mm$, $T_g = 428K$ and $V_g = 0.6m/s$. Against the wood drying in the previous section, there are significant gradients in the temperature as well as the moisture profiles of the lignite particles at both inlet and middle layers in the bed. The temperature differences inside the particle reach up to 40 K and the moisture content has a gradient from 30% to zero inside the particles. Averaging such significant gradients of the moisture and temperature inside the particle domain, which is done by the HQCM, gives a wrong evaluation of the drying behaviour of the bed. It has been seen that the predictions of the HQCM are very inaccurate particularly for the thicker bed.

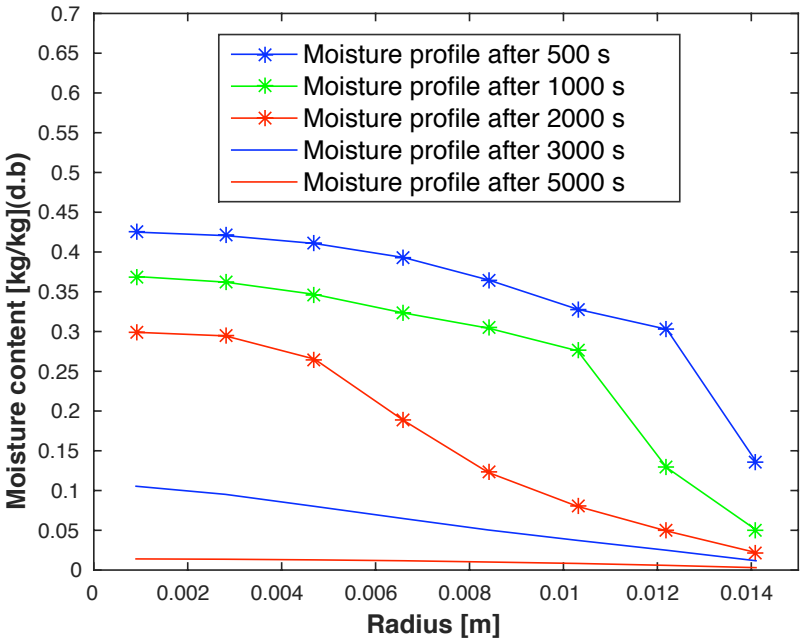

Figure 5.39: *Simulation results of the RPM for spatial profiles of moisture inside a particle from inlet layer of the bed during fixed-bed drying of Hailaer lignite particles.* $T_g = 428K$, $V_g = 0.6m/s$, $H_{bed} = 500mm$

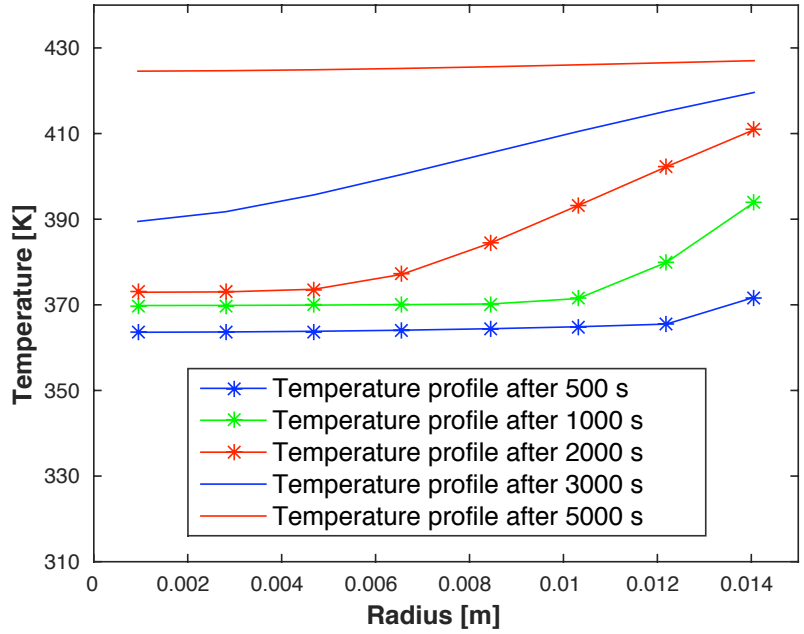

Figure 5.40: *Simulation results of the RPM for spatial profiles of temperature inside a particle from inlet layer of the bed during fixed-bed drying of Hailaer lignite particles.* $T_g = 428K$, $V_g = 0.6m/s$, $H_{bed} = 500mm$

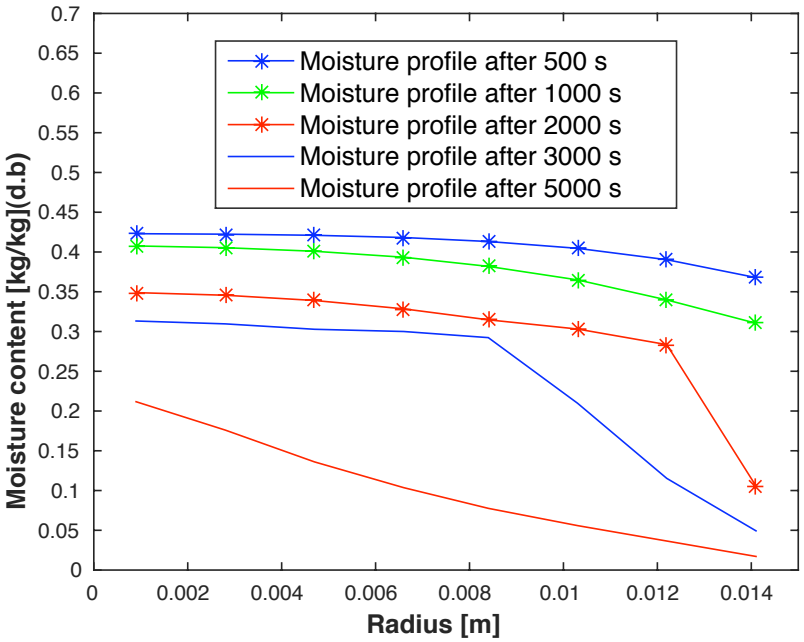

Figure 5.41: *Simulation results of the RPM for spatial profiles of moisture inside a particle from middle layer of the bed during fixed-bed drying of Hailaer lignite particles.* $T_g = 428K$, $V_g = 0.6m/s$, $H_{bed} = 500mm$

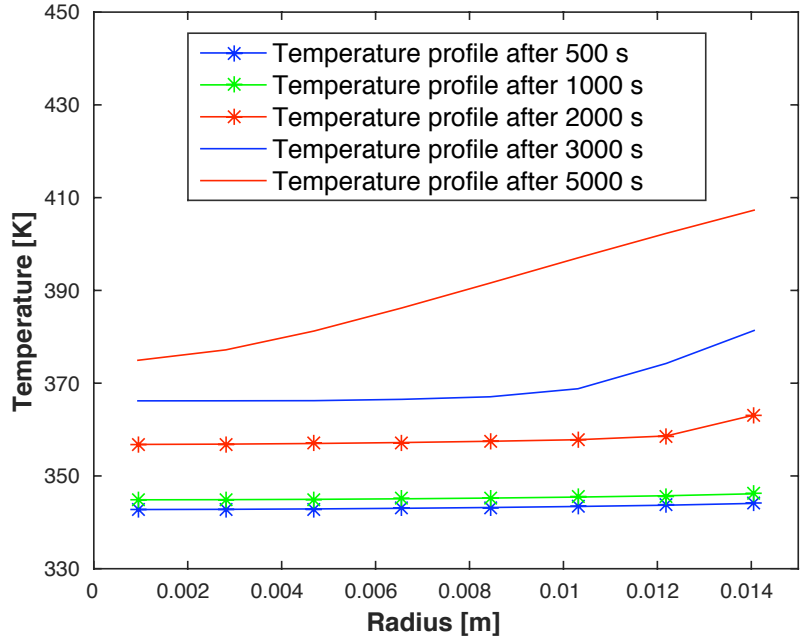

Figure 5.42: *Simulation results of the RPM for spatial profiles of temperature inside a particle from middle layer of the bed during fixed-bed drying of Hailaer lignite particles.* $T_g = 428K$, $V_g = 0.6m/s$, $H_{bed} = 500mm$

Table 5.10: *Share of parallel computing on reduction of running time of fixed-bed drying simulation*

Model	Execution time (s)		Speedup factor (-)
	Single CPU core	8 CPU cores	
RPM	15480	8820	1.755
HQCM	15960	9840	1.622

5.2.3 Parallel computing

In this section, the share of parallel computing on the reduction of the computational time of both the HQCM and the RPM is evaluated. As a case study, the fixed-bed drying of Hailaer lignite particles under the conditions of $H_{bed} = 500mm$, $T_g = 428K$ and $V_g = 0.6m/s$ is considered to be simulated with the final simulation time of 10000 s. Tab. 5.10 shows the execution times of the HQCM as well as the RPM and also the speedup factor of parallel computing. The simulations are done for two cases; with single CPU core and with 8 CPU cores. The speedup factor of the parallel computing that is the ratio of the execution time on a single processor to that on multiprocessors for this case study is 1.75 and 1.62 for the RPM and the HQCM, respectively. Thanks to parallel computing, the computational time for the RPM reduced to lower than the real time of the process. The results have been computed in the EVUR institute's cluster by the machine with two Quad-Core AMD Opteron(tm) Processors 2354.

5.2.4 Concluding remarks

Fixed-bed drying of wood and lignite particles have been simulated by the HQCM and the RPM under different drying conditions. Numerical simulations by the HQCM have been done using a fractional-step algorithm solving the equations of the interstitial gas phase at the reactor scale and employing the LIMEX solver for solving the equations of the solid phase. For the simulation by the RPM, at the reactor scale also the same solution method (fractional-step algorithm) has been used but for the particle model coupled to the reactor scale, an iterative solution method has been employed.

The drying experiments of a quite thin bed of rather small wood particles with two inlet gas temperatures have been considered as case studies. The simulation results of the HQCM and the RPM have been compared with these experimental data and the simulation results of the DPM from the literature. Both the HQCM and the RPM have shown acceptable agreement with the data from the literature,

although the results from the RPM have been more accurate. In contrary to these wood experiments, for the drying of lignite particles with bigger size of particles (2.5 times bigger than wood particles) and the beds with higher heights (2.5 and 5 times bigger than the bed of wood particles) the results are different. The fixed-bed drying experiments of two kinds of lignite particles under different conditions (different kinds of the lignite particle as well as different values of inlet gas velocity and the height of bed) have been used as benchmarks for the simulation. Overall, It has been shown that the HQCM is not able to predict the drying behavior of such coarse particles properly. Particularly, for the higher height of the bed ($H_{bed} = 500mm$) the HQCM predictions have big deviations from the experimental data. While the simulation results of the RPM have showed very good agreement with the experimental data and the simulation results of the DPM, under different drying conditions. The RPM predictions for intra-particle profiles of moisture and temperature have been acceptable too. The intra-particle profiles of the variables involved in drying process play important role in controlling this process and it has been shown that neglecting this fact by the HQCM led to remarkable errors in the results.

The share of the parallel computing have been shown by running the codes for two cases of single CPU core and 8 CPU cores, for the HQCM and the RPM. It have been shown that by parallel computing using MPI approach on 8 processors, the computational time could be improved to 75% for the RPM and 62% for the HQCM, in comparison to the case with single processor.

Chapter 6

Conclusions

The major objectives of this work have been achieving higher accuracy in modeling of the fixed-bed drying of thermally thick porous particles by using a multi-scale model and also reducing the computational time by optimization of the numerical procedure. To this end, a multi-scale model has been developed for fixed-bed drying of hygroscopic porous particles, with the accuracy competitive with the DPM without that much computational cost as the DPM. This multi-scale method has been named Representative Particle Model (RPM) after how it correlates the particle scale to the reactor scale. In this model, a particle model is solved as a representative of other particles in a spesific solution segment by assuming that the other particles from that segment will behave the same as this representative particle. In this way the number of particles needed to be solved decreases to the number of representative particles over the solution domain. Furthermore, a heterogeneous quasi-continuous model (HQCM) has been developed to highlight the effect of neglecting intra-particle phenomena, qualitatively as well as quantitatively.

A comprehensive particle model has been developed base on Whitaker model for coupling to the RPM. In addition to using LIMEX solver for this particle model, an iterative model has been developed which solves each phenomenon in the drying process of the particle separately through a suitable numerical method. The importance of the model parameter for wood particle drying has been evaluated by the sensitivity analysis. The gas intrinsic permeability, effective diffusivity of water vapor and capillary pressure have been known as the most significant parameters affecting the model output that must be correctly determined to have reliable predictions from the drying model. The prediction capability of the drying particle model solved by two solution methods has been examined by wood as well as lignite drying under different conditions. The simulation results has shown very good agreement with the experimental data and the simulation results from the literature. It has

been shown that the intra-particle gradients of moisture and temperature has been remarkable for a coarse solid particle under high-temperature drying.

A fractional-step algorithm has been used for solving the equations of the interstitial gas phase in the bed. The equations governing on the solid phase in the HQCM have been solved by LIMEX solver. For the RPM the solutions from the reactor scale done by the same fractional-step algorithm have been coupled to the solutions from a comprehensive particle model solved by an iterative solution method. The equations of these two phases (scales) are coupled through a two-way coupling at the interface of the phases (scales). The fixed-bed drying of different materials, wood and lignite particles, have been simulated by the HQCM and the RPM under different drying conditions. The simulation results have been compared with the experimental data and the simulation results of the DPM for fixed-bed drying of wood and lignite particles with different values of inlet gas temperature, inlet gas velocity, initial moisture content, size of the particle as well as the porosity and height of the bed. The simulation results of the RPM have shown very good agreement with the experimental data for almost all cases of studied fixed-bed drying. But for drying of the rather thick bed filled by coarse particles, that is more close to the industrial cases, there are remarkable deviations in the simulation results of the HQCM in comparison to the experimental data,. It has been shown that there are up to two times mispredicting the drying time of the bed, in the simulation results of the HQCM.

For optimization of the computational time, in addition to using an efficient iterative solution method for the particle model coupled to the reactor model, A code using the parallel computing has been employed for the solution at the reactor scale. By using parallel computing via MPI approach on 8 CPU cores, the computational time of the RPM and the HQCM have reduced by speedup factor of 1.755 and 1.622, respectively.

Finally, A multi-scale model has been developed that is able to describe and predict the fixed-bed drying of hygroscopic solid fuel particles with high moisture content properly; reasonably accurate and computationally efficient. The computational time of the RPM for simulation of the fixed-bed drying of porous particles has been less than the real time of the process.

6.1 Future work

Some further works are suggested for improving different aspects of mathematical modeling, numerical procedure and also experimentation and application of the presented models:

Shrinkage has not been considered in this study because it is not critical for drying process however in order to coupling this process to the others processes of thermo-chemical conversion, the shrinkage is suggested to be included in the models of particle and reactor scales. For approaching to the practical state and predicting the drying process under different conditions, the models should be extended to a two-dimensional or three-dimensional models. The drying models should be coupled to the other thermo-chemical conversion processes such as pyrolysis and gasification. Since the simulation results of the RPM for the fixed-bed drying of fuel particles are quite accurate therefore by employing this model the problem of poor modeling of drying process during thermo-chemical processes can be solved.

The parallel computing has been used for the solution of reactor scale, it is suggested to investigate the implementation of the parallel computing for the particle scale too. Using the CFD tools which are able to parallel computing such as Ansys CFX are recommended for the reactor scale to evaluate the efficiency of different schemes of parallel computing. The sensitivity analysis of the model parameters has been done at particle scale, the same is suggested to be done for the fixed-bed drying.

At laboratory scale, very good data of lignite and wood drying have been presented however the prediction capability of the RPM is suggested to be examined for an industrial case of fixed-bed drying.

Appendix A

Correlations for model coefficients of wood drying

Table A.1: *Specific heat capacity of pine wood*

Empirical correlation	Species	Reference
$C_p = \frac{4185\,M+4.85\,T+1113}{1+M}$	Softwood	Perre et al. [10] Perre & Turner [47], [58]
$C_p = \frac{0.0022}{1+M}(T)^2+\frac{3.32\,M+2.95}{1+M}(T)+\frac{4057\,M+526}{1+M}$	Scotspine	Deliiski [112]
$C_p = \frac{C_{pw}M+1710}{1+M}$	Scotspine	Pozgaj et al. [112]
$C_p = -9.12 \cdot 10^{-2} + 4.4 \cdot 10^{-3}T$	Spruce pine	Koch [118]
$C_p = \frac{C_{pw}M+1357}{1+M}$	Scotspine	Krzysik [112]

Table A.2: *Effective thermal conductivity of pine wood in transverse direction*

Empirical correlation	Species	Reference
$k_T = 0.142 + 0.46\,M$ $k_R = 2\,k_T$ $k_{\text{eff}} = 1.5\,(0.142 + 0.46\,M)$	Softwood	Perre & Turner [47]
$k_{\text{eff}} = \frac{\langle \rho_{SD} \rangle}{1000}(0.4 + 0.5\,M) + 0.024$	Southern pine	Stanish et al. [57]
$k_T = 0.1989 + 0.8314 \cdot 10^{-4}(T - 273)$ $k_R = 0.1990 + 0.8393 \cdot 10^{-4}(T - 273)$ $k_{\text{eff}} = 0.17681 + 0.83535 \cdot 10^{-4}(T - 273) +$ $0.2765\,M$	Scotspine	Olek et al. [112]
$k_T = 0.15894 + 0.47048 \cdot 10^{-3}(T - 273)$ $k_R = 0.14749 + 0.43657 \cdot 10^{-3}(T - 273)$ $k_{\text{eff}} = 0.131075 + 0.453525 \cdot 10^{-3}(T - 273) +$ $0.2765\,M$	Scotspine	Deliisky [112]
$k_{\text{eff}} = (0.129 - 0.049M) \cdot (0.986 + 2.695M) \cdot$ $[1 + 0.001(2.05 + 4\,M)(T - 273)]$ If $(M > 0.4)$ $k_{\text{eff}} = (0.0932 - 0.0065\,M) \cdot (0.986 + 2.695\,M) \cdot$ $[1 + 0.00365(T - 273)]$ If $(M \leq 0.4)$	Softwood	Perre & Degiovanni [59]
$k_{\text{eff}} = 6 \cdot 10^4 \langle \rho_{SD} \rangle \frac{1+M}{1+0.15} - 0.166$ If $(M > M_{\text{fsp}})$ $k_{\text{eff}} = 6 \cdot 10^4 \langle \rho_{SD} \rangle \frac{1+M}{1+0.44\,M} - 0.166$ If $(M \leq M_{\text{fsp}})$	Pine	Bonneau & Puiggali [42]

Table A.3: *Bound water diffusivity in pine wood in transverse direction*

Empirical correlation	Species	Reference
$D_{\text{bw}} = \exp(-9.9 + 9.8 M_{\text{bw}} - \frac{4300}{T})$	Softwood	Perre & Degiovanni [59]
$D_{\text{bw}} = \exp(-30.39 + 5.46\,M + 2.54 \cdot 10^{-2} T)$	Scotspine	Hukka [119]
$D_{\text{bw}} = \frac{1}{\langle \rho_{SD} \rangle} \exp[(\frac{-2590.1}{T} + 11.954)\,M - \frac{1046.63}{T} - 12.35]$	Pine	Bonneau & Puiggali [42]
$D_{\text{bw}} = \exp(-12.81 + 10.89 M_{\text{bw}} - \frac{4300}{T})$	Softwood	Perre & Turner [110]

Table A.4: *Effective diffusivity of water vapor in pine wood in transverse direction*

Empirical correlation	Species	Reference
$D_v^{\text{eff}} = \epsilon^6 D_{v-a}$	Pine	Bonneau & Puiggali [42]
$D_v^{\text{eff}} = \frac{0.05\epsilon}{1.37} D_{v-a}$	Southern pine	Fernandez & Howell [14]
$D_v^{\text{eff}} = 0.05\epsilon^2 D_{v-a}$	Southern pine	Stanish et al. [57]
$D_v^{\text{eff}} = 10^{-3} D_{v-a}$	Softwood	Perre et al. [10]
$D_{v-a} = [1.192 \cdot 10^{-4}(\frac{T^{1.75}}{P})]$		

Table A.5: *Gas relative permeability in pine wood in transverse direction*

Empirical correlation	Species	Reference
$\mathbf{K}_{rg} = 1 + (2S - 3)S^2$	Softwood	Perre et al. [10]
$\mathbf{K}_{rg} = (\frac{1-S}{1-S_{irr}})^3$	Pine	Couture et al. [43]
$\mathbf{K}_{rg} = (1 - S)^3$	Pine	Couture et al. [43]
$\mathbf{K}_{rg} = 0.95(1 - \frac{M_{\text{fw}}}{M_{cr}})^2 + 0.05$ If $(0 < M_{\text{fw}} < M_{cr})$ $\mathbf{K}_{rg} = 0.05\frac{M_{sat}-M_{\text{fw}}}{M_{sat}-M_{cr}}$ If $(M_{cr} < M_{\text{fw}} < M_{sat})$	Softwood	Perre & Degiovanni [59]
$S_{irr} = 0.07, M_{sat} = 1.33, M_{cr} = 0.8$		

Table A.6: *Capillary pressure in pine wood in transverse direction*

Empirical correlation	Species	Reference
$P_c = exp(16.348 - 0.3909\,M -$ $17.761\,M^2 + 21.228\,M^3 - 7.0789\,M^4)$	Red pine	Tremblay et al. [113]
$P_c = 8.4 \cdot 10^4 S^{-0.63}$	Southern pine	Spolek & Plumb [120]
$P_c = 101325[1.937(S)exp(-3.785S) +$ $(0.093(1-S)S^{-1.4}] \cdot 1 - 2.79 \cdot 10^{-3}(T-273))$	Pine	Bonneau & Puiggali [42]
$P_c = 1.364 \cdot 10^5 \sigma(T)(M_{fw} + 1.2 \cdot 10^{-4})^{-0.63}$	Softwood	Perre & Degiovanni [59]
$P_c = \sigma(T)[\frac{3150}{S+10^{-4}} - \frac{1047+3.368\langle\rho_{SD}\rangle}{1.02-S} +$ $149.8\langle\rho_{SD}\rangle(1 - S) + 52350 + 168.4\langle\rho_{SD}\rangle -$ $\frac{3150}{1+10^{-4}}]$	Softwood	Perre & Turner [111]
$\sigma(T) = (1.28 \cdot 10^2 - 0.185T)10^{-3}$		

Table A.7: *Liquid relative permeability in pine wood in transverse direction*

Empirical correlation	Species	Reference
$\mathbf{K}_{rl} = 0.95(\frac{M_{\text{fw}}}{M_{cr}})^2$ If $(0 < M_{\text{fw}} < M_{cr})$ $\mathbf{K}_{rl} = 0.05\frac{M_{\text{fw}}-M_{cr}}{M_{sat}-M_{cr}} + 0.95$ If $(M_{cr} < M_{\text{fw}} < M_{sat})$	Softwood	Perre & Degiovanni [59]
$\mathbf{K}_{rl} = S^3$	Softwood	Perre et al. [10]
$\mathbf{K}_{rl} = (\frac{S-Sirr}{1-S_{irr}})^3$	Pine	Couture et al. [43]
$\mathbf{K}_{rl} = S^{0.5}[1 - (1 - S^{\frac{1}{m}})^m]^2$	Pine	Kang & Chung [55]
$S_{irr} = 0.07, M_{sat} = 1.33, M_{cr} = 0.8$ $m = (1 - \frac{1}{1.921})$		

Nomenclature

Latin symbols

A	pre-exponential factor	$[s^{-1}]$
A	area	[m^2]
C_p	specific heat capacity at constant pressure	$[Jkg^{-1}K^{-1}]$
D	mass dispersion / diffusivity	$[m^2s^{-1}]$
D_i^{eff}	effective diffusivity of component i in gas mixture	$[m^2s^{-1}]$
d_p	particle diameter	[m]
d_{por}	pore diameter	[m]
E	activation energy	$[Jmol^{-1}]$
F	friction terms in momentum equation	$[kgm^{-2}s^{-2}]$
f_1	first friction factor	$[kgm^{-3}s^{-1}]$
f_2	second friction factor	$[kgm^{-4}]$
G	conductance	$[WK^{-1}]$
H	convective and viscous terms in the momentum equation	$[kgm^{-2}s^{-2}]$
H	length of the control volume / height of bed	[m]
$h(M_{\text{bw}}, T)$	relative humidity	
k	thermal conductivity	$[Wm^{-1}K^{-1}]$
K_o	phase change rate constant	$[s^{-1}]$
$\mathbf{K}$	intrinsic permeability	$[m^2]$
$\mathbf{K}_r$	relative permeability	[-]
M	molecular weight	$[kgmol^{-1}]$
M	dry-basis moisture content	$[kgkg^{-1}]$
M_{fw}	dry-basis moisture content of free water	$[kgkg^{-1}]$
M_{bw}	dry-basis moisture content of bound water	$[kgkg^{-1}]$
M_{cr}	critical moisture content	$[kgkg^{-1}]$

M_{irr}	irreducible moisture content	$[kgkg^{-1}]$
M_{fsp}	moisture content at fiber saturation point	$[kgkg^{-1}]$
M_{sat}	saturated moisture content	$[kgkg^{-1}]$
$M_{\max}$	maximum possible value for moisture content	$[kgkg^{-1}]$
n	unit normal vector with direction out of surface	
Nu	Nusselt number	[-]
P	pressure	$[Nm^{-2}]$
P_c	capillary pressure	$[Nm^{-2}]$
$\langle P_g \rangle^g$	pressure in the gas phase	$[Nm^{-2}]$
Pr	Prandtl number	[-]
$\langle P_w \rangle^w$	pressure in free water	$[Nm^{-2}]$
r_p	radius of particle	[m]
R	universal gas constant	(=8.3144 $[Jmol^{-1}K^{-1}]$)
Re	Reynolds number	[-]
S	saturation	[%]
s	surface to volume ratio of the particle	$[m^{-1}]$
t	time	[s]
T	temperature	$[^\circ C]$ or [K]
$\mathbf{v}$	general vectorial velocity	$[ms^{-1}]$
V, v	superficial velocity	$[ms^{-1}]$
w_z	reactor axial velocity	$[ms^{-1}]$
Y	mass fraction	[-]
z	axial coordinate of the reactor	[m]
$\langle V_i \rangle$	superficial velocity vector of component i	$[ms^{-1}]$
$\triangle\, h$	latent heat of vaporization	$[Jkg^{-1}]$
$\triangle\, h_{\text{sorp}}$	differential heat of sorption	$[Jkg^{-1}]$

Greek symbols

α	heat transfer coefficient	$[Wm^{-2}K^{-1}]$
β	mass transfer coefficient	$[ms^{-1}]$
ϵ	volume fraction	
Λ	thermal dispersion	$[Wm^{-1}K^{-1}]$

μ	dynamic viscosity	$[kgm^{-1}s^{-1}]$
$\langle\rho_\gamma\rangle$	phase averaged density of phase γ	$[kgm^{-3}]$
$\langle\rho_i\rangle^\gamma$	intrinsic density of component or phase i in phase γ	$[kgm^{-3}]$
ϕ	general variable	
Ω	volume	$[\mathrm{m}^3]$
Ω_γ	volume of phase γ	$[m^3]$
$\langle\dot{\omega}_i\rangle$	phase change rate of component i in phase γ	$[kgm^{-3}s^{-1}]$
ζ	Stefan correction	$[kgm^{-3}]$

Subscripts

0	initial value
a	air
atm	atmosphere
bc	boundary condition
b , bed	bed
bw	bound water
cr	critical
eff	effective
equ	equilibrium
fw	free water
fsp	fiber saturation point
g	gas mixture phase
i	component or phase i
$init$	initial
irr	irreducible
l	liquid free water phase
s	solid
sat	saturated state
SD	solid dry wood
$surf$	external surface of particle
v	water vapor
w	water
γ	phase γ
∞	ambient

Bibliography

[1] Energy, transport and environment indicators, 2013th Edition, European Union, 2013. doi:10.2785/4663.

[2] European commission, eurostat: Consumption of energy (2013).
URL http://ec.europa.eu/eurostat/statistics-explained/index.php/Consumption_of_energy#

[3] W. Ge, W. Wang, N. Yang, J. Li, M. Kwauk, F. Chen, J. Chen, X. Fang, L. Guo, X. He, X. Liu, Y. Liu, B. Lu, J. Wang, J. Wang, L. Wang, X. Wang, Q. Xiong, M. Xu, L. Deng, Y. Han, C. Hou, L. Hua, W. Huang, B. Li, C. Li, F. Li, Y. Ren, J. Xu, N. Zhang, Y. Zhang, G. Zhou, G. Zhou, Meso-scale oriented simulation towards virtual process engineering (vpe)-the {EMMS} paradigm, Chemical Engineering Science 66 (19) (2011) 4426 – 4458, multiscale Simulation. doi:http://dx.doi.org/10.1016/j.ces.2011.05.029.

[4] J. Li, W. Ge, W. Wang, N. Yang, X. Liu, L. Wang, X. He, X. Wang, J. Wang, M. Kwauk, From Multiscale Modeling to Meso-Science: A Chemical Engineering Perspective, Springer Publishing Company, Incorporated, 2013.

[5] R. Helmig, J. Niessner, B. Flemisch, M. Wolff, J. Fritz, Efficient modeling of flow and transport in porous media using multiphysics and multiscale approaches, in: W. Freeden, M. Nashed, T. Sonar (Eds.), Handbook of Geomathematics, Springer Berlin Heidelberg, 2010, pp. 417–457. doi:10.1007/978-3-642-01546-5_15.

[6] I. Schüßler, D. Bräkow, K. Treppe, B. Salomo, T. Zschunke, Schwachstellenanalyse an bhkw-vergaseranlagen, TU Dresden / HS Zittau/Görlitz (2009).

[7] A. S. Mujumdar, Handbook of Industrial Drying, CRC Press; 3 edition, 2006.

[8] T. Kudra, A. S. Mujumdar, Advanced Drying Technologies, CRC Press; 2 edition, 2009.

[9] S. B. Nasrallah, P. Perre, Detailed study of a model of heat and mass transfer during convective drying of porous media, International Journal of Heat and Mass Transfer 31 (5) (1988) 957–967. doi:10.1016/0017-9310(88)90084-1.

[10] P. Perre, M. Moser, M. Martin, Advances in transport phenomena during convective drying with superheated steam and moist air, International Journal of Heat and Mass Transfer 36 (11) (1993) 2725–2746. doi:10.1016/0017-9310(93)90093-L.

[11] C. Fyhr, A. Rasmuson, Mathematical model of steam drying of wood chips and other hygroscopic porous media, AIChE Journal 42 (9) (1996) 2491–2502. doi:10.1002/aic.690420909.

[12] C. D. Blasi, Multi-phase moisture transfer in the high-temperature drying of wood particles, Chemical Engineering Science 53 (2) (1998) 353 – 366. doi:10.1016/S0009-2509(97)00197-8.

[13] T. H. Vu, Influence of pore size distribution on drying behaviour of porous media by a continuous model, Ph.D. thesis (2006).

[14] M. L. Fernandeza, J. R. Howella, Convectwe drying model of southern pine, Drying Technology 15 (10) (1997) 2343–2375. doi:10.1080/07373939708917365.

[15] C. Jianmin, D. Fangtian, Classification and comparison of wood drying models, Journal of Northeast Forestry University 4 (2) (1993) 112–117. doi:10.1007/BF02843082.

[16] P. Perre, How to get a relevant material model for wood dring simulation?, in: Advances in drying of Wood, 1999.

[17] N. Koumoutsakos, Modelling radio frequency/vacuum drying of wood, Ph.D. thesis, The University of British Columbia (2001).

[18] C. Di Blasi, Simultaneous heat, mass and momentum transfer during biomass drying, in: A. Bridgwater, D. Boocock (Eds.), Developments in Thermochemical Biomass Conversion, Springer Netherlands, 1997, pp. 117–131. doi:10.1007/978-94-009-1559-6_9.

[19] B. Moghtaderi, B. Z. Dlugogorski, E. M. Kennedy, D. F. Fletcher, Effects of the structural properties of solid fuels on their re-ignition characteristics, Fire and Materials 22 (4) (1998) 155–165. doi:10.1002/(SICI)1099-1018(1998070)22:4<155::AID-FAM651>3.0.CO;2-F.

[20] J. Larfeldt, B. Leckner, M. C. Melaaen, Modelling and measurements of the pyrolysis of large wood particles, Fuel 79 (13) (2000) 1637–1643.

[21] J. C. Wurzenberger, S. Wallner, H. Raupenstrauch, J. G. Khinast, Thermal conversion of biomass: Comprehensive reactor and particle modeling, Aiche Journal 48 (10) (2002) 2398–2411. doi:10.1002/aic.690481029.

[22] M. Bellais, Modelling of the pyrolysis of large wood particles, Ph.D. thesis, KTH - Royal Institute of Technology (2007).

[23] M. Jalili, A. Anca-Couce, N. Zobel, F. Behrendt, Calculation of evaporation rate in drying section of fixed-bed gasifiers, in: 21st European Biomass Conference and Exhibition, Copenhagen, 2013, pp. 879 – 886. doi:10.5071/21stEUBCE2013-2CV.3.53.

[24] P. K. Agarwal, W. E. Genetti, Y. Y. Lee, Coupled drying and devolatilization of wet coal in fluidized beds, Chemical Engineering Science 41 (9) (1986) 2373 – 2383. doi:http://dx.doi.org/10.1016/0009-2509(86)85087-4.

[25] S. Alves, J. Figueiredo, A model for pyrolysis of wet wood, Chemical Engineering Science 44 (12) (1989) 2861–2869. doi:10.1016/0009-2509(89)85096-1.

[26] J. Saastamoinen, J.-R. Richard, Simultaneous drying and pyrolysis of solid fuel particles, Combustion and Flame 106 (3) (1996) 288 – 300. doi:http://dx.doi.org/10.1016/0010-2180(96)00001-6.

[27] R. Bilbao, J. Mastral, J. Ceamanos, M. Aldea, Modelling of the pyrolysis of wet wood, Journal of Analytical and Applied Pyrolysis 36 (1) (1996) 81 – 97. doi:http://dx.doi.org/10.1016/0165-2370(95)00918-3.

[28] G. Palchonok, Heat and mass transfer to a single particle in fluidized bed, Ph.D. thesis, Chalmers University of Technology (1998).

[29] L. F. de Diego, F. García-Labiano, A. Abad, P. Gayán, J. Adánez, Modeling of the devolatilization of nonspherical wet pine wood particles in fluidized

beds, Industrial & Engineering Chemistry Research 41 (15) (2002) 3642–3650. doi:10.1021/ie0201922.

[30] R. Bilbao, J. F. Mastral, J. A. Lana, J. Ceamanos, M. E. Aldea, M. Betrán, A model for the prediction of the thermal degradation and ignition of wood under constant and variable heat flux, Journal of Analytical and Applied Pyrolysis 62 (1) (2002) 63 – 82. doi:http://dx.doi.org/10.1016/S0165-2370(00)00214-X.

[31] M. L. Janssens, Modeling of the thermal degradation of structural wood members exposed to fire, Fire and Materials 28 (2-4) (2004) 199–207. doi:10.1002/fam.848.

[32] B. Peters, E. Schroder, C. Bruch, T. Nussbaumer, Measurements and particle resolved modelling of heat-up and drying of a packed bed, Biomass and Bioenergy 23 (4) (2002) 291 – 306. doi:http://dx.doi.org/10.1016/S0961-9534(02)00052-1.

[33] U. Sand, Dynamics of wood particle pyrolysis applied to gas-solids fluidisation, Ph.D. thesis, Mälardalen University (2005).

[34] A. H. Mahmoudi, F. Hoffmann, B. Peters, Application of {XDEM} as a novel approach to predict drying of a packed bed, International Journal of Thermal Sciences 75 (0) (2014) 65 – 75. doi:http://dx.doi.org/10.1016/j.ijthermalsci.2013.07.016.

[35] W. C. R. Chan, M. Kelbon, B. B. Krieger, Modeling and experimental verification of physical and chemical processes during pyrolysis of a large biomass particle, Fuel 64 (11) (1985) 1505–1513.

[36] B. Krieger-Brockett, D. Glaister, Wood devolatilization - sensitivity to feed properties and process variables, in: A. Bridgwater, J. Kuester (Eds.), Research in Thermochemical Biomass Conversion, Springer Netherlands, 1988, pp. 127–142. doi:10.1007/978-94-009-2737-7_10.

[37] D. Shrestha, S. Cramer, R. White, Time-temperature profile across a lumber section exposed to pyrolytic temperatures, Fire and Materials 18 (4) (1994) 211–220. doi:10.1002/fam.810180404.

[38] K. M. Bryden, K. W. Ragland, C. J. Rutland, Modeling thermally thick pyrolysis of wood, Biomass & Bioenergy 22 (1) (2002) 41–53. doi:10.1016/S0961-9534(01)00060-5.

[39] C. D. Blasi, C. Branca, S. Sparano, B. L. Mantia, Drying characteristics of wood cylinders for conditions pertinent to fixed-bed countercurrent gasification, Biomass and Bioenergy 25 (1) (2003) 45 – 58. doi:http://dx.doi.org/10.1016/S0961-9534(02)00180-0.

[40] S. Whitaker, Simultaneous heat, mass, and momentum transfer in porous media: A theory of drying, Advances in Heat Transfer 13 (1977) 119–203.

[41] N. Ouelhazi, G. Arnaud, J. Fohr, A two-dimensional study of wood plank drying. the effect of gaseous pressure below boiling point, Transport in Porous Media 7 (1) (1992) 39–61. doi:10.1007/BF00617316.

[42] P. Bonneau, J.-R. Puiggali, Influence of heartwood-sapwood proportions on the drying kinetics of a board, Wood Science and Technology 28 (1) (1993) 67–85. doi:10.1007/BF00193878.

[43] F. Couture, W. Jomaa, J.-R. Puiggali, Relative permeability relations: A key factor for a drying model, Transport in Porous Media 23 (3) (1996) 303–335. doi:10.1007/BF00167101.

[44] M. C. Melaaen, Numerical analysis of heat and mass transfer in drying and pyrolysis of porous media, Numerical Heat Transfer, Part A: Applications 29 (4) (1996) 331–355. doi:10.1080/10407789608913796.

[45] M. G. Gronli, A theoretical and experimental study of the thermal degradation of biomass, Ph.D. thesis, The Norwegian University of Science and Technology (1996).

[46] Z. Zhang, S. Yang, D. Liu, Mechanism and mathematical model of heat and mass transfer during convective drying of porous materials, Heat Transfer-Asian Research 28 (5) (1999) 337–351. doi:10.1002/(SICI)1523-1496(1999)28:5<337::AID-HTJ1>3.0.CO;2-9.

[47] P. Perre, I. W. Turner, A 3-d version of transpore: a comprehensive heat and mass transfer computational model for simulating the drying of porous media, International Journal of Heat and Mass Transfer 42 (24) (1999) 4501–4521. doi:10.1016/S0017-9310(99)00098-8.

[48] M. Jalili, A. Anca-Couce, N. Zobel, On the uncertainty of a mathematical model for drying of a wood particle, Energy & Fuels 27 (11) (2013) 6705–6717. doi:10.1021/ef401156s.

[49] A. Halder, A. Dhall, A. K. Datta, Modeling transport in porous media with phase change: Applications to food processing, J. Heat Transfer 133.

[50] C. D. Blasi, C. Branca, S. Sparano, B. L. Mantia, Drying characteristics of wood cylinders for conditions pertinent to fixed-bed countercurrent gasification, Biomass and Bioenergy 25 (2003) 45–58.

[51] P. Perre, A. Karimi, Fluid migration in two species of beech (fagus silvatica and fagus orientalis): A percolation model able to account for macroscopic measurements and anatomical observations, Maderas. Ciencia y tecnologgy 4 (2002) 50–68.

[52] P. Perre, E. Agoua, Mass transfer in wood: Identification of structural parameters from diffusivity and permeability measurements, Journal of Porous Media 13 (11) (2010) 1017–1024.

[53] A. Redman, H. Bailleres, I. Turner, P. Perre, Mass transfer properties (permeability and mass diffusivity) of four australian hardwood species, BioResources 7 (3).

[54] T. Tanaka, Y. Kawai, M. Sadanari, S. Shida, T. Tsuchimoto, Air permeability of sugi (Cryptomeria japonica) wood in the three directions, Maderas. Ciencia y tecnología 17 (2015) 17 – 28.

[55] W. Kang, W. Chung, Liquid water diffusivity of wood from the capillary pressure-moisture relation, Journal of Wood Science 55 (2) (2009) 91–99. doi:10.1007/s10086-008-1009-x.

[56] L. J. Bao Fucheng, A. Stavros, On the permeability of main wood species in china, Holzforschung 53 (1999) 350–354.

[57] M. A. Stanish, G. S. Schajer, F. Kayihan, A mathematical model of drying for hygroscopic porous media, AIChE Journal 32 (8) (1986) 1301–1311. doi:10.1002/aic.690320808.

[58] P. Perre, I. W. Turner, A dual-scale model for describing drier and porous medium interactions, AIChE Journal 52 (9) (2006) 3109–3117. doi:10.1002/aic.10918.

[59] P. Perre, A. Degiovanni, Simulation par volumes finis des transferts couplés en milieux poreux anisotropes: séchage du bois à basse et à haute température, International Journal of Heat and Mass Transfer 33 (11) (1990) 2463–2478. doi:10.1016/0017-9310(90)90004-E.

[60] N. Lemcoff, S. Pereira Duarte, M. O.M., Heat transfer in packed beds, Reviews in Chemical Engineering 6.

[61] P. Borman, J. Borkink, K. Westerterp, Heat transport in a wall heated tubular packed bed reactor at elevated pressures and temperatures, Chemical Engineering Communications 114 (1) (1992) 17–47. doi:10.1080/00986449208936014.

[62] B. Koning, Heat and mass transport in tubular packed bed reactors at reacting and non-reacting conditions, Ph.D. thesis, University of Twente (2002).

[63] M. Wesenberg, Gas heated steam reformer modelling, Ph.D. thesis, Norwegian University of Science and Technology (2006).

[64] H. Delmas, G. Froment, A simulation model accounting for structural radial nonuniformities in fixed bed reactors, Chemical Engineering Science 43 (8) (1988) 2281 – 2287. doi:http://dx.doi.org/10.1016/0009-2509(88)87116-1.

[65] E. Tsotsas, E.-U. Schlunder, Heat transfer in packed beds with fluid flow: remarks on the meaning and the calculation of a heat transfer coefficient at the wall, Chemical Engineering Science 45 (4) (1990) 819 – 837. doi:http://dx.doi.org/10.1016/0009-2509(90)85005-X.

[66] D. Vortmeyer, E. Haidegger, Discrimination of three approaches to evaluate heat fluxes for wall-cooled fixed bed chemical reactors, Chemical Engineering Science 46 (10) (1991) 2651 – 2660. doi:http://dx.doi.org/10.1016/0009-2509(91)80058-7.

[67] M. Winterberg, E. Tsotsas, A. Krischke, D. Vortmeyer, A simple and coherent set of coefficients for modelling of heat and mass transport with and without

chemical reaction in tubes filled with spheres, Chemical Engineering Science 55 (5) (2000) 967 – 979. doi:http://dx.doi.org/10.1016/S0009-2509(99)00379-6.

[68] M. Winterberg, E. Tsotsas, Correlations for effective heat transport coefficients in beds packed with cylindrical particles, Chemical Engineering Science 55 (23) (2000) 5937 – 5943. doi:http://dx.doi.org/10.1016/S0009-2509(00)00198-6.

[69] E. Tsotsas, Heat and Mass Transfer in Packed Bed with Fluid Flow. VDI Heat Atlas, Springer-Verlag, 2010.

[70] B. Peters, C. Bruch, A flexible and stable numerical method for simulating the thermal decomposition of wood particles, Chemosphere 42 (5-7) (2001) 481–490.

[71] B. Peters, Measurements and application of a discrete particle model (dpm) to simulate combustion of a packed bed of individual fuel particles, Combustion and Flame 131 (1-2) (2002) 132–146. doi:10.1016/S0010-2180(02)00393-0.

[72] B. Peters, E. Schroder, C. Bruch, Measurements and particle resolved modelling of the thermo- and fluid dynamics of a packed bed, Journal of Analytical and Applied Pyrolysis 70 (2) (2003) 211–231. doi:10.1016/S0165-2370(02)00133-X.

[73] B. Peters, C. Bruch, Drying and pyrolysis of wood particles: experiments and simulation, Journal of Analytical and Applied Pyrolysis 70 (2) (2003) 233–250. doi:10.1016/S0165-2370(02)00134-1.

[74] B. Peters, Validation of a numerical approach to model pyrolysis of biomass and assessment of kinetic data, Fuel 90 (6) (2011) 2301–2314. doi:10.1016/j.fuel.2011.02.003.

[75] R. Wijngaarden, K. Westerterp, Do the effective heat conductivity and the heat transfer coefficient at the wall inside a packed bed depend on a chemical reaction? weaknesses and applicability of current models, Chemical Engineering Science 44 (8) (1989) 1653 – 1663. doi:http://dx.doi.org/10.1016/0009-2509(89)80008-9.

[76] H. Martin, M. Nilles, Radiale waermeleitung in durchstromten schuttungsrohren, Chemie Ingenieur Technik 65 (12) (1993) 1468–1477. doi:10.1002/cite.330651206.

[77] J. Papageorgiou, G. Froment, Simulation models accounting for radial voidage profiles in fixed-bed reactors, Chemical Engineering Science 50 (19) (1995) 3043 – 3056. doi:http://dx.doi.org/10.1016/0009-2509(95)00138-U.

[78] O. R. Derkx, A. G. Dixon, Effect of the wall nusselt number on the simulation of catalytic fixed bed reactors, Catalysis Today 35 (4) (1997) 435 – 442. doi:http://dx.doi.org/10.1016/S0920-5861(96)00210-6.

[79] D. B. Ingham, I. Pop, Transport Phenomena in Porous Media, 1st Edition, Vol. II, Pergamon, 2002.

[80] J. Kuipers, K. V. Duin, F. V. Beckum, W. V. Swaaij, A numerical model of gas-fluidized beds, Chemical Engineering Science 47 (8) (1992) 1913 – 1924. doi:http://dx.doi.org/10.1016/0009-2509(92)80309-Z.

[81] S. Becker, E. Laurien, Three-dimensional numerical simulation of flow and heat transport in high-temperature nuclear reactors, Nuclear Engineering and Design 222 (2003) 189 – 201, hTR-2002 1st international topical meeting on High Temperature reactor technology. doi:http://dx.doi.org/10.1016/S0029-5493(03)00011-6.

[82] C. du Toit, P. Rousseau, G. Greyvenstein, W. Landman, A systems {CFD} model of a packed bed high temperature gas-cooled nuclear reactor, International Journal of Thermal Sciences 45 (1) (2006) 70 – 85. doi:http://dx.doi.org/10.1016/j.ijthermalsci.2005.04.010.

[83] C. J. Visser, Modelling heat and mass flow through packed pebble beds: a heterogeneous volume-averaged approach, Master's thesis, University of Pretoria (2007).

[84] S. Ergun, Fluid flow through packed columns, Chemical Engineering Progress 48 (2) (1952) 89–94.

[85] A. Iordanidis, Mathematical modeling of catalytic fixed bed reactors, Ph.D. thesis, University of Twente (2002).

[86] E. E. Dieterich, Systematische bilanzierung und modulare simulation verfahrenstechnischer apparate, Ph.D. thesis, University of Stuttgart (1998).

[87] F. Chejne, J. Hernandez, W. Florez, A. Hill, Modelling and simulation of time-dependent coal combustion processes in stacks, Fuel 79 (8) (2000) 987 – 997. doi:http://dx.doi.org/10.1016/S0016-2361(99)00224-0.

[88] J. C. Wurzenberger, A combined packed bed and single particle model applied to biomass combustion, Ph.D. thesis, Technischen Universitaet Graz (2001).

[89] N. Zobel, The representative particle model, Ph.D. thesis, Technischen Universitaet Berlin (2007).

[90] J. Porteiro, J. Collazo, D. Patino, E. Granada, J. C. M. Gonzalez, J. L. Miguez, Numerical modeling of a biomass pellet domestic boiler, Energy & Fuels 23 (1) (2009) 1067–1075. doi:10.1021/ef8008458.

[91] A. Anca-Couce, N. Zobel, H. A. Jakobsen, Multi-scale modeling of fixed-bed thermo-chemical processes of biomass with the representative particle model: Application to pyrolysis, Fuel 103 (0) (2013) 773 – 782. doi:http://dx.doi.org/10.1016/j.fuel.2012.05.063.

[92] A. Anca-Couce, Multi-scale approach to describe fixed-bed thermo-chemical processes of biomass, Ph.D. thesis, Technischen Universitaet Berlin (2012).

[93] A. J. Slavin, V. Arcas, C. A. Greenhalgh, E. R. Irvine, D. B. Marshall, Theoretical model for the thermal conductivity of a packed bed of solid spheroids in the presence of a static gas, with no adjustable parameters except at low pressure and temperature, International Journal of Heat and Mass Transfer 45 (20) (2002) 4151–4161. doi:10.1016/S0017-9310(02)00117-5.

[94] A. Anca-Couce, N. Zobel, Numerical analysis of a biomass pyrolysis particle model: Solution method optimized for the coupling to reactor models, Fuel 97 (2012) 80–88.

[95] H. A. Jakobsen, H. Lindborg, V. Handeland, A numerical study of the interactions between viscous flow, transport and kinetics in fixed bed reactors, Computers & Chemical Engineering 26 (3) (2002) 333–357. doi:10.1016/S0098-1354(01)00758-X.

[96] P. Deuflhard, E. Hairer, J. Zugck, One-step and extrapolation methods for differential-algebraic systems, Numerische Mathematik 51 (5) (1987) 501–516.

[97] M. G. Wolfinger, Modellierung der thermischen umsetzung nichtisothermer holzpartikel in inerter und reaktiver atmosphaere, Ph.D. thesis, Technischen Universitaet Graz (2001).

[98] B. Wilmes, Modellierung und simulation der vergasung eines holzpartikels unter verwendung detaillierter reaktionsmechanismen, Ph.D. thesis, Technischen Universitaet Berlin (2007).

[99] F. Mermoud, F. Golfier, S. Salvador, L. Van de Steene, J. L. Dirion, Experimental and numerical study of steam gasification of a single charcoal particle, Combustion and Flame 145 (1-2) (2006) 59–79. doi:10.1016/j.combustflame.2005.12.004.

[100] C. DiBlasi, Heat, momentum and mass transport through a shrinking biomass particle exposed to thermal radiation, Chemical Engineering Science 51 (7) (1996) 1121–1132.

[101] B. Moghtaderi, The state-of-the-art in pyrolysis modelling of lignocellulosic solid fuels, Fire and Materials 30 (1) (2006) 1–34. doi:10.1002/fam.891.

[102] K. Zhang, C. You, Experimental and numerical investigation of convective drying of single coarse lignite particles, Energy & Fuels 24 (12) (2010) 6428–6436. doi:10.1021/ef101198k.

[103] H. Lindborg, V. Eide, S. Unger, S. T. Henriksen, H. A. Jakobsen, Parallelization and performance optimization of a dynamic pde fixed bed reactor model for practical applications, Computers & Chemical Engineering 28 (9) (2004) 1585–1597. doi:10.1016/j.compchemeng.2003.12.009.

[104] K. Zhang, C. You, Experimental and numerical investigation of lignite particle drying in a fixed bed, Energy & Fuels 25 (9) (2011) 4014–4023. doi:10.1021/ef200759t.

[105] Wood Handbook : Wood as an Engineering Material, Forest Products Society: Madison, US (WI), 2010.

[106] J. Siau, Transport Processes in Wood, Springer-Verlag New York, LLC, 1984.

[107] K. Raznjevic, Handbook of Thermodynamic Tables and Charts, Hemisphere Publishing Corporation, 1976.

[108] J. H. Ferziger, M. Peric, Computational Methods for Fluid Dynamics, Springer ; 3rd edition, 2001.

[109] P. Deuflhard, E. Hairer, J. Zugck, One-step and extrapolation methods for differential-algebraic systems, Numerische Mathematik 51 (1987) 501–516.

[110] P. Perre, I. W. Turner, Determination of the material property variations across the growth ring of softwood for use in a heterogeneous drying model. part 2. use of homogenisation to predict bound liquid diffusivity and thermal conductivity, Holzforschung 55 (2001) 417–425.

[111] P. Perre, I. W. Turner, Determination of the material property variations across the growth ring of softwood for use in a heterogeneous drying model part 1. capillary pressure,tracheid model and absolute permeability, Holzforschung 55 (2001) 318–323.

[112] W. Olek, J. Weres, R. Guzenda, Effects of thermal conductivity data on accuracy of modeling heat transfer in wood, Holzforschung 57 (2003) 317–325.

[113] C. Tremblay, A. Cloutier, Y. Fortin, Moisture content-water potential relationship of red pine sapwood above the fiber saturation point and determination of the effective pore size distribution, Wood Science and Technology 30 (1996) 361–371.

[114] F. Brun, D. Wallach, D. Makowski, J. W. Jones, Working with Dynamic Crop Models: Evaluation, Analysis, Parameterization, and Applications, Elsevier Science; 1st edition, 2006.

[115] O. Plumb, G. Spolek, B. Olmstead, Heat and mass transfer in wood during drying, International Journal of Heat and Mass Transfer 28 (9) (1985) 1669–1678. doi:10.1016/0017-9310(85)90141-3.

[116] A. Saltelli, M. Ratto, T. Andres, F. Campolongo, J. Cariboni, D. Gatelli, M. Saisana, S. Tarantola, Global Sensitivity Analysis: The Primer, Wiley-Interscience; 1st edition, 2008.

[117] N. Wakao, S. Kaguei, Heat and Mass Transfer in Packed Beds, Studies in Cybernetics, Gordon and Breach Science Publishers, 1982.

[118] P. Koch, Specific heat of ovendry spruce pine wood and bark, Wood Science 1 (2) (1969) 203–214.

[119] A. Hukka, The effective diffusion coefficient and mass transfer coefficient of nordic softwoods as calculated from direct drying experiments, Holzforschung 53 (1999) 534–540.

[120] G. Spolek, O. Plumb, Capillary pressure in softwoods, Wood Science and Technology 15 (3) (1981) 189–199. doi:10.1007/BF00353471.

ISBN 978-3-945682-07-4